Self-Spacing Algorithms for Continuous Descent Approaches

Alexander in 't Veld

Self-Spacing Algorithms for
Continuous Descent Approaches

Summary

Self-Spacing Algorithms for Continuous Descent Approaches

Alexander in 't Veld

The focus in aircraft noise regulations has shifted from technical measures, such as the development of quieter engines, to operational measures. These can be political such as the imposition of night curfews, or putting a cap on the yearly number of flights at a particular airport, but can also be procedural in the form of noise abatement flight procedures. As a result, research efforts have increased in the area of flight procedures that generate less noise impact on the environment. In addition, the environmental impact of gaseous emissions has become an increasingly important aspect of these research efforts.

Research into noise abatement has naturally centered on airport arrival and departure procedures, as sound only becomes noise when it is experienced negatively by people on the ground, i.e., during those phases of a flight that are operated on, or close to, the ground. Research has resulted in a number of effective noise abatement departure procedures that have been adopted by the International Civil Aviation Organization (ICAO). Noise abatement for arrival procedures has proven to be more difficult to achieve, however, as noise-effective procedures

generally showed to be difficult to implement in a high traffic density environment.

This thesis focuses on aircraft arrival procedures. When looking at the optimal arrival profile, noise impact can be mitigated through:

- reducing the noise at the source, and

- increasing the distance to the receiver.

From a procedural point of view, the reduction of source noise can be accomplished by selecting low thrust settings and by delaying the deployment of the landing gear and lift generating devices, as these increase airframe noise. Increasing the distance between noise source and receiver is usually addressed in the procedure design by avoiding overflying cities and towns, but also by eliminating level flight segments at low altitudes, effectively increasing the average altitude of the flight. Extended research efforts to design the optimal noise abatement approach procedure indicate that a Continuous Descent Approach (CDA) without any level flight segments achieves the greatest reduction in noise impact.

Most of the work in this thesis investigates the Three-Degree Decelerating Approach (TDDA), which is a particular implementation of a continuous descent approach. This type of approach is flown at idle-thrust, following a relatively steep, three degree trajectory to the runway. The result is a procedure where the aircraft is decelerating, aiming to be configured for landing no sooner than at a stabilization point close to the runway, maintaining idle-thrust up to that point, controlling airspeed only by the timing of subsequent flap and landing gear selections.

The problem with this and similar idle-thrust approach procedures is that different aircraft exhibit varying speed profiles, due to differences in aircraft aerodynamic performance, the aircraft's mass and the control strategy of the flight crew. These factors combined make the task of safely spacing and separating the aircraft converging to a runway very difficult for air traffic controllers. As a result, controllers have to increase the minimum spacing of approaching aircraft, thereby greatly reducing the number of aircraft that can land on a runway in an hour.

Typically, aircraft will be gradually decelerating to reach their final approach speed close to the runway, presenting the controller with a string of aircraft that are all catching up to the aircraft directly in front of them. This leaves the controller with the undesirable task of assessing whether the final spacing between any pair of aircraft will still match the minimum separation criteria. This stands in sharp contrast to current practice where aircraft receive speed, heading and altitude instructions from ATC, resulting in less optimal approach trajectories in terms of noise and emissions, but also in a situation where a human controller can manage high volumes of traffic.

Two obvious strategies to solve this issue are 1) to develop a tool to support the controller in closely spacing decelerating aircraft, and/or 2) to develop a tool to allow the flight crew to manage their relative spacing to their preceding aircraft in the arrival flow.

This thesis explores the possibilities of introducing closely spaced decelerating continuous descent approaches by addressing the problem from the flight deck, although realistically, a future scenario incorporating these kind of advanced continuous descent approaches will probably see advancements both in the controller work station and on the flight deck.

For this research it is assumed that some form of data-link is available to enable the exchange of information between aircraft and ATC, and among aircraft. This is in line with SESAR's notion of system wide information management (SWIM) being part of future ATM. The exact form of this data-link is of no importance to the research presented here, but generally it is assumed that aircraft are equipped with Automatic Dependent Surveillance - Broadcast (ADS-B). Two possible scenarios are investigated; one is a form of *self-spacing* where aircraft are required to control their deceleration in such a way that the minimum safe distance to the aircraft in front is not violated. The other is a slightly different scenario where air traffic control issues the aircraft with a *Required Time of Arrival (RTA)* at the runway, making the flight crew responsible for arriving at the assigned time. In both these scenarios, the flight crew becomes responsible for meeting an ATC requirement, based on the hypothesis that the flight crew has the best information on and control over their flight track and speed profile.

Distance-based self-spacing requires the ability to accurately estimate the trajectory of the lead aircraft as well as the own trajectory. It turns out that trajectory prediction of sufficient accuracy requires detailed knowledge of the lift-drag polar in all aircraft configurations as well as a good estimate of the current operating mass of the aircraft. It is feasible to have this information available for the own aircraft, but having this information up-to-date for every possible preceding aircraft is harder to achieve. In this thesis, good results were obtained by extrapolating a set of lead aircraft ground speed, position and altitude data which are assumed to be available through ADS-B. In order to get a workable solution, knowledge about the lead aircraft's final approach speed and the altitude where he aims to have achieved that speed are also necessary, both of which are conveniently assumed to be available as part of the 'intent information' broadcast through ADS-B.

Based on these estimates of the own trajectory and the lead aircraft, an algorithm was developed that constantly optimizes the appropriate times to close the power levers, select the gear down and select the flaps in such a way that the aircraft flies the TDDA while maintaining a safe separation behind the lead aircraft. Monte Carlo simulations show that this algorithm is robust against errors in the wind estimation, aircraft mass estimate and accuracy of the drag-coefficient. Errors in the estimates of the headwind component of up to ± 20 kts, estimate errors of

aircraft mass of $\pm 10\%$ and errors in the drag-coefficient of $\pm 10\%$ showed no loss of separation at all and only a slight degradation of the noise impact due to the early re-application of thrust on short final of ± 0.3 NM before the normal reference point.

A cockpit interface was then developed that uses the flap schedule algorithm to drive cues on the primary flight display and the navigation display to inform the flight crew when to select the next configuration and to show how the current and final predicted spacing is developing. This display was tested in the SIMONA research simulator and in actual flight using the Cessna Citation II laboratory aircraft operated by TU Delft and NLR, to investigate the usefulness of this display and the feasibility of the whole self-spacing scenario. It was found that most pilots are capable of performing the TDDA without help from the developed display, as long as the aircraft were correctly spaced to begin with and the lead aircraft behaved nominally. However, in non-nominal cases, managing both the TDDA and achieving the correct spacing generally proved to be too difficult for pilots. In those cases, the use of the flight deck display improved performance drastically, while achieving a reduction in pilot workload, proving the feasibility of distance based self-spacing.

The main advantage of the alternative to distance-based spacing, i.e., time based self-separation, is that no on-board knowledge of the lead aircraft is required. Separation is assured just by meeting a required time of arrival (RTA), as issued by ATC. The flap scheduling algorithm was modified to combine flying the TDDA while trying to meet the RTA. Piloted simulator experiments showed similar results as for the distance-based case. Pilots performed better with the display, especially in situations where large errors were introduced into the wind predictions, or the RTA was chosen to be only barely achievable. In all cases, the use of the augmented displays showed a significant reduction in pilot workload, as compared to the runs without augmented displays.

Now that both distance-based and time based solutions have proven to be feasible, a comparison was conducted to assess the effects on landing runway capacity. Up to this point only combinations of two aircraft had been studied and no information was yet available on the behavior and stability of a chain of multiple aircraft. Monte Carlo simulations were performed with random mixes of five different aircraft types, operating at masses varying from maximum take-off mass to dry operating mass, flying a TDDA in chains of eight aircraft. Pilot behavior was varied, as were the wind profiles and the initial spacing error.

In the distance-based scenario, each aircraft in the stream is reacting to the behavior of its preceding aircraft, which could lead to string instability effects. These effects were not found however, during the Monte Carlo simulation. Time based separation has the advantage that string instability effects are not possible as there is no direct interaction between aircraft. In terms of capacity both methods

were able to achieve around 39 aircraft per hour on a single runway, or about 90% of the theoretical maximum capacity for the same combination of aircraft. Distance-based spacing performed slightly better, because any increase in spacing is absorbed by the chain as the algorithm aims for the minimum separation. In the case of time based spacing this loss of capacity goes uncorrected as the RTAs are not updated during the run. On the other hand, this aspect of time based separation means that no action will be taken by the flight crew when the preceding aircraft is unexpectedly decelerating too soon and separation could be violated. In this case a controller or an airborne separation assurance system should intervene, while in the distance-based scenario this situation will be clearly displayed and automatically reacted upon by the flap scheduling algorithm.

In conclusion, both distance-based and time based self-separation scenarios were shown to be a feasible solution to the capacity problem. Self-separation relieves the air traffic controller of the spacing task during the approach, reducing the controller's workload while maintaining current runway throughput numbers. However, both scenarios still require a proper set-up by ATC. For distance-based spacing, the required initial spacing on final approach is dependent on the combination of aircraft types and mass. The same holds when determining the required times of arrival of subsequent aircraft. Research is ongoing on how ATC can be supported in the task of determining the proper initial spacing or required arrival time, but this is beyond the scope of this thesis. The results indicate that runway throughput numbers comparable to current levels are possible, while maintaining stability in the string of arriving aircraft.

It is clear that the next problem to solve is the correct initial spacing of aircraft before they begin the approach procedure, which needs to be optimized for each aircraft combination. Although it is unlikely the TDDA as presented in this work will be implemented in its current form, the results presented in this thesis will be useful in the future development of advanced arrival procedures within the scope of the SESAR and NextGen program.

Abbreviations and Symbols

Δsep_{safe}	maximum deviation from required safe separation
$h@V_{APP}$	altitude at which V_{APP} is reached
h_R	height at the reference point R
h_{APP}	target reference altitude
h_{TCB}	thrust cut-back altitude
$N\&T$	Noise & Traffic (optimization)
NO	Noise-Only (optimization)
R	Reference point
V_{APP}	Final Approach Speed
V_{APP}	final approach speed
LNAV	Lateral Navigation
RNAV	Area Navigation
SESAR	Single European Sky ATM Research
VNAV	Vertical Navigation
ACARS	Aircraft Communication and Reporting System
ACDA	Advanced CDA
ADS-B	Automatic Dependant Surveillance - Broadcast
AMDAR	Aircraft Meteorological Data Relay
ANAP	advanced noise abatement procedure
ARMA	Auto-Regressive Moving-Average model
ATC	Air Traffic Control
AWPA	AMDAR wind prediction algorithm
BADA	Base of Aircraft DAta
CDA	Continuous Descent Approach

CDTI	Cockpit Display of Traffic Information
ETA	Estimated Time of Arrival
FAA	Federal Aviation Administration
FAST	Final Approach Spacing Tool
FMC	Flight Management Computer
FMS	Flight Management System
GPS	Global Positioning System
IAS	Indicated Air Speed
ICAO	International Civil Aviation Organization
ILS	Instrument Landing System
IRU	Inertial Reference Unit
LPLDA	Low Power Low Drag Approach
LVNL	Luchtverkeerleiding Nederland
MCP	Mode Control Panel
MLS	Microwave Landing System
MLW	Maximum Landing Weight
NASA	National Aeronautics and Space Administration
ND	Navigation Display
NM	Nautical Mile
OEW	Operating Empty Weight
PBL	Planetary Boundary Layer
PFD	Primary Flight Display
RMS	Root Mean Squared
RTA	Required Time of Arrival
SARA	Speed And Route Advisor
SSR	Secondary Surveillance Radar
SWIM	system wide information management
TBO	Trajectory Based Operations
TCAS	Traffic Alert and Collision Avoidance System
TCB	thrust cutback
TDDA	Three-Degree Decelerating Approach
TLX	NASA Task Load indeX
TMA	Terminal Maneuvering Area
TSD	Time-Space Diagram
VHF	Very High Frequency

Contents

7 Self-spacing in High-Density Arrival Streams   133

List of Figures

List of Tables

1

Introduction

1-1 Historic background

When the first jet airliners started operations in the early 1960s and travel by air became more commonplace, the noise that accompanied these early, low by-pass ratio jet aircraft turned out to be a hindrance to people. In September 1968 in Buenos Aires, the Assembly of the International Civil Aviation Organization (ICAO) recognized the need to address 'noise in the vicinity of aerodromes' and adopted the first resolution on this matter, which was further elaborated in 1969 during a special meeting in Montreal.[1,2]

During this meeting it was decided to develop standards for aircraft noise certification and the first design aspects of noise abatement departure and arrival procedures were discussed. Also guidance on land-use planning around airports was published. This was further elaborated by the Commission on Aircraft Noise (CAN) which ultimately led to the publication of ICAO Annex 16, which was adopted in 1972.[1,2,7]

Initially, the focus on aircraft noise reduction lay squarely on the production of quieter engines. Aircraft are certified based on the maximum sound levels they produce during different flight phases and in different aircraft configurations. As time progresses, the regulations are amended and new aircraft have to meet more and more stringent noise certification standards, ultimately resulting in quieter aircraft.[1,2,7]

The phasing out of older, noisier aircraft (so-called 'Chapter 2' aircraft) has now almost been completed at most airports in Europe and the United States. As can be seen in Figure 1-1, the noise levels of jet-powered aircraft have reduced some 50% over the last 50 years, but the point of diminishing returns has been reached. Unless a completely different form of propulsion is introduced in aviation, the noise levels produced by future generations of aircraft can not be expected to be significantly lower than current levels.
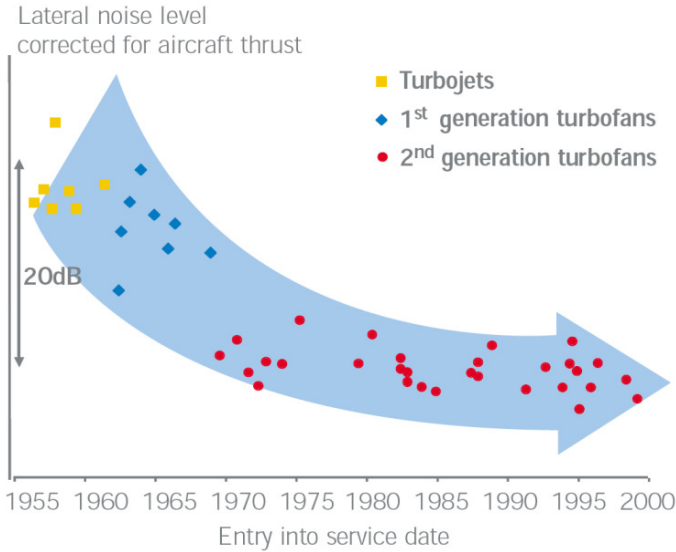
Figure 1-1: Historical progress in jet-powered aircraft noise reduction. [source: www.iata.org]

1-2 Aircraft noise mitigation

The 2001 ICAO convention realized that to further reduce noise impact levels, or at least maintain the current levels while accommodating air traffic growth, a shift of the research focus towards other means of reducing aircraft noise impact was required.[4,8] During this conference the concept of a 'balanced approach to noise management' was introduced, indicating four areas where noise mitigation measures can be taken:

1. Reduction of source noise,

2. Land use policies,

3. Operating restrictions, and

4. Noise abatement flight procedures.

As the name implies, the idea is to combine all these aspects in noise mitigation efforts. Land-use planning is most useful in the development of new airports, where certain areas can be designated for residential or industrial use in such a way that the noise impacted areas are not used for housing.

Operating restrictions are quite common, and these consist of e.g., restricting the number of movements of chapter 2 aircraft, or closing the airport at night.

Maintain positive rate of climb. Accelerate smoothly to en-route climb speed.
Retract flaps/slats on schedule.

900 m ⊢(3000 ft)

Climb at V_2 + 10 to 20 kt
Maintain reduced power
Maintain flaps/slats in the take-off
configuration

240 m ⊢(800 ft) ⊢ Initiate power reduction at or above 800 ft

Take-off thrust V_2 + 10 to 20 kt

(a) NADP 1

Transition to en-route climb speed

900 m ⊢(3000 ft)

Not before 800 ft and while maintaining a
positive rate of climb, accelerate towards V_{ZF} and reduce
power with the initiation of the first flap/slat retraction
or
when flaps/slats are retracted and while maintaining
a positive rate of climb, reduce power and climb at
V_{ZF} + 10 to 20 kt

240 m ⊢(800 ft)

Take-off thrust V_2 + 10 to 20 kt

(b) NADP 2

Figure 1-2: ICAO noise abatement departure procedures. [Source: PANS-OPS[5]]

Since operating restrictions and land use policies are necessarily specific solutions, driven by local constraints, this thesis focuses on the more generic noise abatement procedures that are more widely applicable.

1-3   Noise abatement procedures

When discussing noise abatement procedures, generally a distinction is made between arrival procedures and departure procedures.

The development of noise abatement departure procedures has led to the adaptation by ICAO of a limited number of procedures that are generally considered optimal. As modern aircraft are able to climb quite steeply, the strategy is to gain altitude as quickly as possible and thus increase the distance from the receiver over the shortest possible distance. Although noise of departing aircraft has by no means been eliminated, due to the fact that aircraft gain altitude so quickly, the noise impact is limited to a relatively compact area close to the airport. So, despite the fact that the departure is the phase of flight where the highest engine thrust is used and thus the highest levels of source noise are generated it is the *approach* phase that has the highest noise impact.[5,8]

Figure 1-2 shows the two basic variants of noise abatement departure procedures (NADP) as published by ICAO.[5] Variant one features a delayed flap/slat retraction which alleviates the noise impact close to the airport. Variant 2 has an earlier flap retraction schedule, which reduces the noise footprint distant from the airport. Depending on the local situation, either procedure 1 or 2 is warranted.

As explained above, the greatest problem of aircraft noise lies with arriving aircraft. When aircraft start the arrival procedure, they typically follow a number of step-down descents and level decelerations to arrive in level flight at an altitude of 2,000-3,000 ft above ground level, slowed down and configured for the final approach. The final descent to the runway usually starts some 6 to 10 NM from the
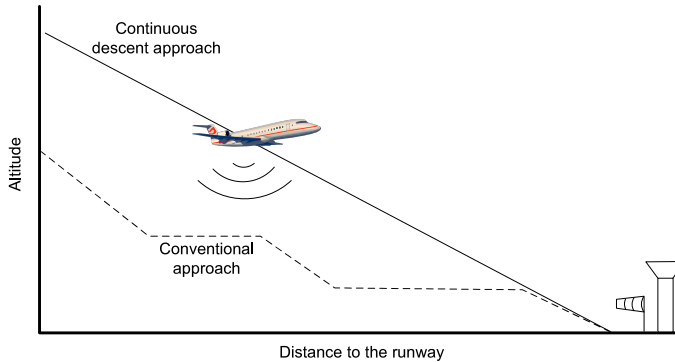
Figure 1-3: Inherent noise benefits of continuous descent over conventional approach procedures due to less time spent at lower altitudes and the elimination of level segments.

runway. Operating in this manner allows for a safe and stabilized approach to the runway, but the relatively low level flight segments with aircraft's lift-generating devices deployed also generate drag and increase airframe noise. Furthermore, to overcome this drag, the aircraft fly at relatively high power settings, adding to engine noise.

With these observations in mind, most research efforts have focused on optimizing arrival flight trajectories in such a way that a *continuous descent* was possible, eliminating level flight segments. This way the average altitude and thus distance from the noise source is increased, as illustrated in Figure 1-3. Furthermore, the continuously descending flight path can be executed at lower thrust levels, further reducing the noise impact of the aircraft.[6, 12, 14, 15, 18, 20–22]

Although different procedures yield different results, the results in terms of noise impact for most of these procedures are comparable. Figure 1-4 illustrates the reduction of the noise footprint of a single aircraft when executing a Three-Degree Decelerating Approach, which will be discussed later, compared to the same aircraft flying a conventional ILS approach from 2,000 ft.

1-3-1   Engine emissions

The lower required thrust settings of continuous descent approaches lead to lower fuel consumption, improving the efficiency of the flight. Furthermore, jet engines are less efficient at low altitude and the fact that the average altitude of the aircraft is higher than during a conventional approach further reduces fuel consumption.

Unfortunately, lower fuel consumption does not necessarily reduce the exhaust emissions. The primary products of combustion, water (H_2O) and carbon-dioxide (CO_2) reduce with selected engine thrust, as does the emission of NO_x, as can be
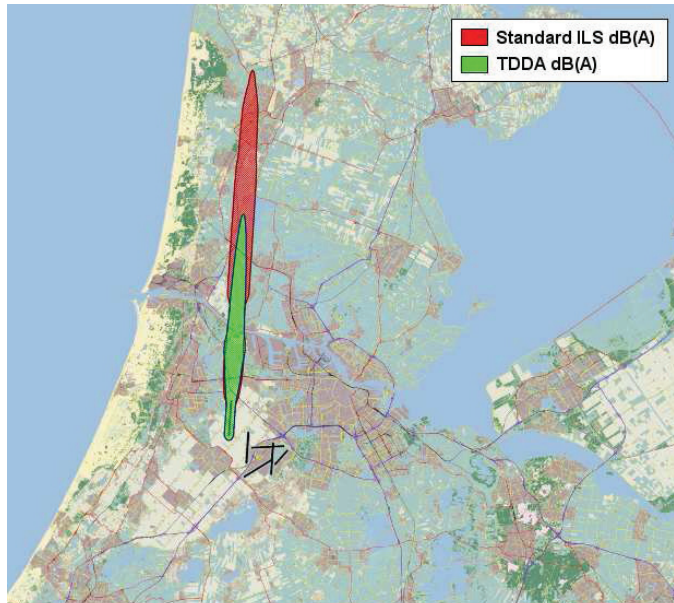
Figure 1-4: Calculated noise contour for a single ILS approach from 2,000 ft and a Three-Degree Decelerating Approach from 7,000 ft.

seen in Figure 1-5. At lower thrust settings, however, the combustion process takes place at lower temperatures, which reduces the efficiency of the process and increases the amount of soot and carbon-monoxide (CO) in the exhaust gasses.

1-4 Air traffic control

Although the various noise abatement approach procedures discussed so far proved to be successful in greatly reducing the noise impact of individual aircraft, the implementation of these procedures proved to be difficult in the current air traffic control environment.[6,12,20] Due to the fact that different aircraft show greatly varying deceleration behavior, depending on aircraft type, operating mass and pilot strategy, it becomes increasingly difficult for an air traffic controller to predict the behavior of an individual aircraft.

In the current air traffic management environment, the air traffic controller is responsible for establishing a safe and efficient flow of traffic. As departing traffic generally has a radiating pattern with the departure runway as source, assuring separation between aircraft is generally less difficult than for arriving traffic which exhibits a converging pattern. Different strategies can be deployed by the controller to assure a safe traffic flow. In general, controllers will try to harmonize the flow of traffic by issuing speed, altitude and heading instructions to generate a flow of
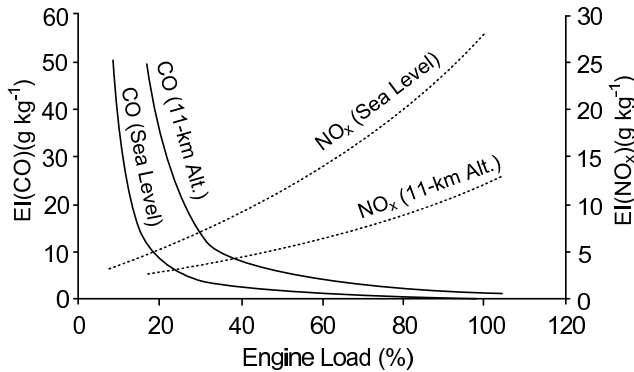
Figure 1-5: Emission index of a turbofan engine for CO and NO$_x$.[Source: IPCC[19]]

more or less equally behaving aircraft lining up for the landing runway.

When introducing continuous descent approaches, the associated individual descent and speed profiles make the controller's task more difficult. E.g., when Amsterdam Airport Schiphol implemented the RNAV-night transitions, a reduction of landing runway capacity of approximately 50% was experienced.[16,17] Because the predictability of the arriving aircraft was reduced, controllers had to increase the spacing to assure safe separation.

The Continuous Descent Approaches at London's Heathrow Airport work around this by issuing speed and heading instructions and informing pilots of the number of track miles to the runway. The absence of level flight segments means that these are technically Continuous Descent Approaches (CDA), but at constant speeds and different lateral paths, these procedures are far from optimal from a noise impact perspective.

For the purpose of this thesis the latter will be referred to as *vectored CDAs* and the former as RNAV-*CDAs* as these have prescribed ground tracks. One could argue that spreading the ground tracks distributes the noise, and lowers the peak cumulative noise footprint. However, current development in air traffic management moves towards optimized 4-D trajectories.

In Europe, the program for Single European Sky ATM Research (SESAR) defines so-called *business trajectories*, which will be the optimal trajectory for the aircraft involved, but also optimized for noise abatement, fuel consumption and other traffic.[9] In the United States, the Federal Aviation Administration (FAA) is working on a similar concept, defining Trajectory Based Operations (TBO) in its NextGen program.[10] In both programs, the notion of a vectored CDA is difficult if not impossible to reconcile with an optimal descent profile, instead opting for the development of the RNAV-CDA.

This thesis will therefore only address the RNAV-CDA, and aims to develop various strategies to cope with the profile uncertainty and subsequent arrival spacing
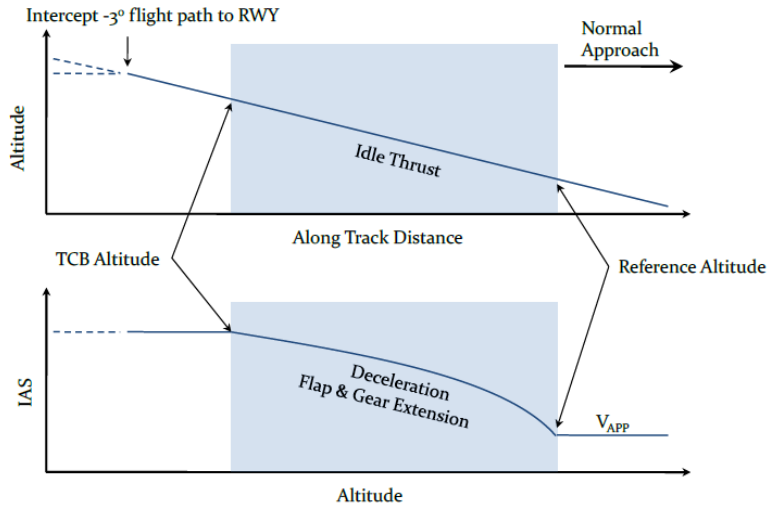
Figure 1-6: Three-Degree Decelerating Approach (TDDA) Procedure.

problems associated with these procedures.

1-4-1   Three-Degree Decelerating Approach

Examining the various continuous descent procedures, the noise benefits turn out to be mostly the result of the increase in the distance from the ground, compared to conventional approach procedures. Also, elimination of level segments, introducing a *continuous descent* in some form, requires less thrust which reduces engine noise and fuel consumption.[19]

The Three-Degree Decelerating Approach (TDDA) mainly used in this research is a good example of this principle. The TDDA was originally designed to offer the maximum possible noise reduction, at the cost of all else.[11,20] It is an idle thrust, steep approach without any level segments, see Figure 1-6. Since both the lateral and vertical paths are fixed in the TDDA, the only means to control the deceleration rate available to the flight crew is the timing of the flap and landing gear deployment. Since the last part of the approach is flown at idle thrust, the speed-profile is highly non-linear, making it especially difficult for controllers to predict the behavior of the aircraft during the last few miles before the runway threshold.

This thesis does not aim to optimize procedure design to further mitigate noise impact. Instead it is assumed that the TDDA is a representative CDA and as such it is considered sufficiently noise effective. The focus of this research lies on the algorithm designs to allow robust implementation of the TDDA while minimizing capacity loss in varying wind conditions.

(a) B747 following B737.   (b) B737 following B747
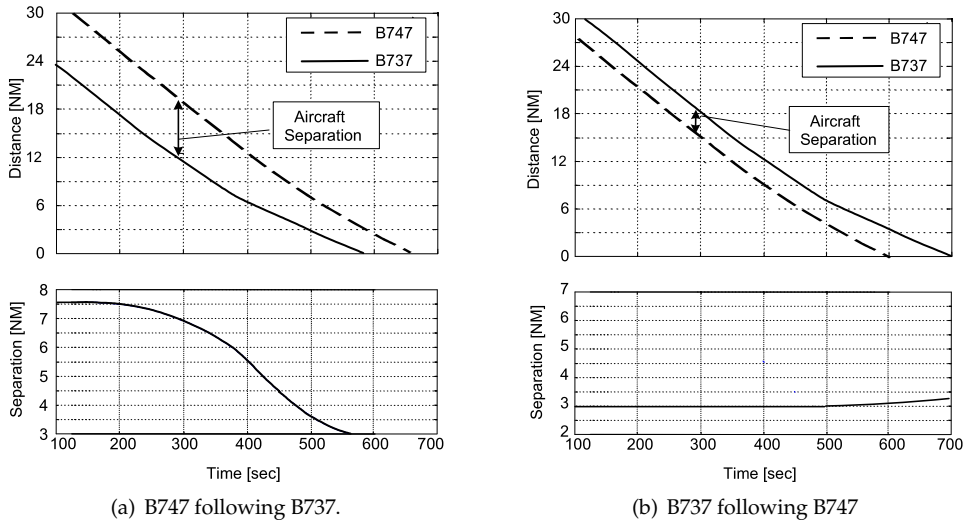
Figure 1-7: Evolution of the in-trail spacing during the TDDA.

1-5   Self-spacing scenarios

Figure 1-7 shows an example of how the in-trail distance evolves between a Boeing 737 and a Boeing 747 during a TDDA. Due to the difference in deceleration characteristics the initial separation needs to be 7.5 NM in order to end up at 2.5 NM at the runway threshold when the B747 is following the B737, but the spacing is more or less constant when the B737 follows the B747. This is a typical illustration of the difficulties encountered when spacing and sequencing traffic for a CDA.

The required initial spacing for any pair of aircraft is mostly dependent on the encountered wind profile and on the drag-characteristics and actual mass of the aircraft involved. Since two of these parameters are readily available on board of the aircraft, a possible solution would be to transfer the spacing task from the controller to the flight crew.

Two self-spacing strategies will be presented to show that it is indeed possible to consistently have aircraft arriving fully configured for landing at a safe distance behind the preceding aircraft. This way runway capacity can be maintained while each aircraft can fly its own individual speed profile.

1-5-1   Distance based self-spacing

In the distance based self-spacing scenario, each aircraft monitors the distance to its predecessor in the arrival stream. As has been shown in previous research,[13] maintaining a constant distance or a constant time behind the lead aircraft only

works for aircraft that exhibit largely the same dynamic properties. The distance based concept presented in this thesis uses a trajectory prediction algorithm that assumes the availability of aircraft status information through some form of data link such as ADS-B as proposed in FAA's NextGen program.[3,10] Also, in SESAR's future ATM scenario the notion of System Wide Information Management (SWIM) is introduced, so in this thesis it is assumed that necessary information is available through an (airborne) network.[9]

The position information is used to construct a descent profile of the lead aircraft which is compared with the own predicted profile. The algorithm assures that the minimum distance between the predicted profiles is maintained. This means that it is entirely possible for the algorithm to start increasing the deceleration of the own aircraft, when the aircraft are still 10 NM apart.

1-5-2   Time based spacing

In this scenario, it is assumed that air traffic control has the means to compare the future trajectories of the aircraft in the arrival stream and issues each aircraft a Required Time of Arrival (RTA) at the runway threshold. Instead of controlling the in-trail distance, aircraft are expected to meet the RTA with a predetermined degree of accuracy. It will be shown that safe separation can be assured by merely having aircraft adhere to their RTA.

The obvious advantage of this form of spacing is that no knowledge of the dynamics of the preceding aircraft is required on board the own aircraft. An algorithm was designed to meet this time-goal while still satisfying the goals of the TDDA.

1-5-3   Scope

Both the distance based and the time based scenarios require a proper set-up by ATC. The initial spacing needs to be correct and the issued RTAs need to be within the controllability range of the aircraft. Current development in this research is focused on developing tools for the air traffic controller to help sequence, space and monitor aircraft for idle-thrust CDAs. These developments are outside the scope of this thesis, however. Here it is assumed that the initial spacing is taken care of and the RTA are correctly calculated.

1-6   Performance metrics

In order to draw any conclusion about the performance of the developed algorithms, a number performance metrics have been identified.

First of all, combining the self-spacing task with the execution of a TDDA must be possible. In order to assess this the altitude at which thrust is re-applied is measured as an indicator for the effectiveness of the TDDA as noise abatement procedure. Earlier thrust application means a degradation of the noise performance. Furthermore, the actual in-trail distance achieved is a measure of the success of the self-spacing task. The aim is to finish the procedure at the minimum safe separation, as this generates the highest runway throughput. A larger in-trail spacing constitutes a capacity loss, but a smaller spacing indicates a loss of separation and will result in the in-trail aircraft having to perform a missed approach.

After it is established that the algorithms work in principle, a sensitivity analysis will be performed to investigate the robustness of the solution. This will provide an indication on whether implementation of the procedure is feasible under realistic operational uncertainties.

Another aspect that needs attention is the additional workload for the flight crew. During piloted experiments an assessment of the overall workload needs to be performed to verify that the introduction of the self-spaced TDDA does not result in unacceptable workload levels.

Finally, it needs to be investigated how the achievable landing runway throughput levels compare to the current traffic levels experienced at major airports.

> Summarizing, the goal of this thesis is to develop the algorithms and the pilot support systems necessary to allow self-spaced TDDAs to be flown in realistic wind conditions. The performance of the time based and distance based algorithms is compared, both in terms of flight crew workload and the accuracy with which the procedure can be flown.

1-7   Thesis outline

This thesis consists of a number of publications on different aspects of this research. The way in which these papers are related is illustrated in Figure 1-8 and explained below.

In the concept of self-spacing it is necessary to have a good estimate of the speed- and altitude profiles of the leading aircraft. In **Chapter 2** a trajectory prediction algorithm is introduced that is based on ADS-B position reports and aircraft intent information. This algorithm stands at the very basis of the work presented in the rest of the chapters.

Chapter 3 presents a pilot support interface that was developed to assist the flight crew in flying a TDDA, while simultaneously controlling the spacing with the lead aircraft. Tests of this interface in the fixed-base human-machine interface laboratory of the Control and Simulation section, showed that, while experienced airline pilots
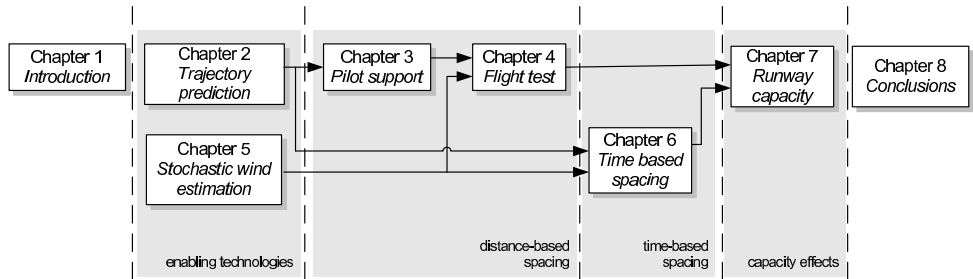
Figure 1-8: Thesis structure.

are well capable of flying accurate TDDAs as long as the lead aircraft follows its nominal flight path, nevertheless help from the displays was a necessity when the lead aircraft showed non-nominal behavior.

All research up to this point has been done in the simulator in a no-wind scenario, so in **Chapter 4** a simple logarithmic wind-estimator is incorporated in the simulation. The experiment described in Chapter 3 was repeated both in the SIMONA six-degrees-of-freedom research flight simulator and in the Cessna Citation II laboratory aircraft. These test results showed that the simulation results were valid, but also that a better wind estimator was needed.

Wind behavior can be elegantly described using a simple logarithmic model. However, although this produces results that are acceptable on a large scale, the TDDA support system requires a more accurate, high-resolution wind profile estimate. Actual wind measurements show a much more random pattern than the logarithmic model would predict. **Chapter 5** presents a stochastic wind estimator that uses the data broadcast from nearby aircraft to construct an accurate wind profile that can be used for precision trajectory prediction.

Chapter 6 introduces the concept of *time based* self-spacing. The results of a simulator experiment are presented where pilots were instructed to fly TDDAs while trying to arrive at the runway as close as possible to the Required Time of Arrival. To add to the realism, the wind-estimator from Chapter 5 is used. Furthermore, realistic curved approach trajectories had to be flown, based on the current night regime arrival procedures of Amsterdam Schiphol Airport.

Chapter 7 presents the results of an extended series of Monte Carlo simulations that were performed to compare the dynamic behavior of both distance based and time based self-spacing concepts. The simulations were set up using realistic fleet mixes of medium and heavy aircraft at different operating masses. Arrival string stability issues were studied as well as runway landing capacity numbers.

Chapter 8 discusses the results and draws conclusions on whether the research goals as stated in this section were met. Based on the findings areas that require further investigation are identified and possible future developments discussed.

References

[1] Resolutions Adopted by the Assembly and Index to Documentation, 16th Session of the Assembly. Technical Report Doc 8779/A16-RES, International Civil Aviation Organization (ICAO), Buenos Aires, Argentina, Sep 1968.

[2] ICAO News Release, Major Progress Made towards Solution to Aircraft Noise Problems. Montreal, Canada, Nov 24 1969.

[3] Minimum Aviation System Performance Standards for Automatic Dependent Surveillance Broadcast (ADS-B). Technical Report RTCA/DO-242, RTCA, Inc., Washington DC, USA, Feb 1998.

[4] Resolutions Adopted by the Assembly and Index to Documentation, 33rd Session of the Assembly. Technical report, International Civil Aviation Organization (ICAO), Montreal, Canada, Sep 25 - Oct 5 2001.

[5] Procedures for Air Navigation Services - Aircraft Operations, Volume 1 - Flight Procedures. Technical Report Doc 8168-Ops/611, International Civil Aviation Organization (ICAO), Oct 2006.

[6] Sourdine II, Final Report. Technical Report D9-1, National Aerospace Laboratory (NLR), Aug 31 2006.

[7] Annex 16 to the Convention on International Civil Aviation: Environmental Protection, Volume 1 - Aircraft Noise. Technical Report AN16-1, International Civil Aviation Organization (ICAO), Jul 2008.

[8] Guidance on the Balanced Approach to Aircraft Noise Management. Technical Report Doc 9829-AN/451, Second Edition, International Civil Aviation Organization (ICAO), 2008.

[9] SESAR Master Plan-Deliverable 5. Technical Report DLM-0710-001-02-00, SESAR Consortium, Apr 2008.

[10] FAA's NextGen Implementation Plan. Technical report, Federal Aviation Administration (FAA), Mar 2010.

[11] J.-P. Clarke. *A Systems Analysis Methodology for Developing Single Event Noise Abatement Procedures*. Sc.D. Dissertation, Massachusetts Institute of Technology, Cambridge (MA), USA, 1997.

[12] R. A. Coppenbarger, R. W. Mead, and D.N. Sweet. Field Evaluation of the Tailored Arrivals Concept for Datalink-Enabled Continuous Descent Approaches. In *AIAA Aviation Technology, Integration and Operations Conference (ATIO)*, number AIAA-2007-7778, Belfast, Northern Ireland, Sep 18-20 2007.

[13] J. C. M. de Groot, M. Mulder, and M. M. van Paassen. Distance-Based Self-Spacing in Arrival Streams. In *Proceedings of the AIAA Guidance, Navigation, and Control Conference*, number 2005-6275, San Francisco (CA), USA, Aug 15-18 2005.

[14] J. L. de Prins, K. F. M. Schippers, M. Mulder, M. M. van Paassen, A. C. in 't Veld, and J.-P. Clarke. Enhanced Self-Spacing Algorithm for Three-Degree Decelerating Approaches. *AIAA Journal of Guidance, Control & Dynamics*, 30(5):576–590, Mar-Apr 2007.

[15] E. Dinges. Determining the Environmental Benefit of Implementing Continuous Descent Approach Procedures. In *7th USA/Europe Air Traffic Management R&D Seminar (ATM 2007)*, Barcelona, Spain, July 2-5 2007.

[16] L. J. J. Erkelens. Research on Noise Abatement Procedures. Technical Report NLR TP 98066, National Aerospace Laboratory (NLR), Amsterdam, The Netherlands, Feb 1998.

[17] L. J. J. Erkelens. Development of Noise Abatement Procedures in The Netherlands. Technical Report NLR TP 99386, National Aerospace Laboratory (NLR), Amsterdam, The Netherlands, Nov 1999.

[18] N. T. Ho and J.-P. Clarke. Mitigating Operational Aircraft Noise Impact by Leveraging on Automation Capability. In *Proceedings of the AIAA Aircraft, Technology, Integration and Operations Forum*, number AIAA 2001-5239, pages 1–8, Los Angeles (CA), USA, Oct 16-18 2001.

[19] J. E. Penner, D. H. Lister, D. J. Griggs, D. J. Dokken, and M. McFarland. Aviation and the Global Atmosphere. Technical report, Intergovernmental Panel on Climate Change (IPCC), Cambridge, UK, Jun 1999.

[20] L. Ren, J.-P. Clarke, and N. T. Ho. Achieving Low Approach Noise without Sacrifying Capacity. In *22nd Digital Avionics Systems Conference*, number AIAA-2001-5239, pages 1–9, Indianapolis (IN), USA, Oct 12-16 2003.

[21] I. Wilson and F. Hafner. Benefit Assessment of Using Continuous Descent Approaches at Atlanta. In *Digital Avionics Systems Conference*, volume 1, pages 2.B.2– 2.1–7, Washington DC, USA, Oct 30-Nov 3 2005.

[22] F. J. M. Wubben and J. J. Bussink. Environmental Benefits of Continuous Descent Approaches at Schiphol Airport Compared with Conventional Approach Procedures. Technical Report NLR-TP-2000-275, National Aerospace Laboratory (NLR), Amsterdam, The Netherlands, May 2000.

2

Trajectory Prediction

Trajectory Prediction for Self Separation During Decelerating Approaches in a Data-link Environment

A.C. in 't Veld and J.-P. Clarke

2-1 Abstract

Previous research on aircraft noise abatement has resulted in a few promising flight procedures, such as the $3°$ decelerating approach (TDDA), that reduce the noise impact of aircraft operations on the community. The TDDA procedure incorporates an approach flown at a constant glide path angle with idle thrust resulting in a significant reduction of the noise footprint. The primary difficulty with decelerating approaches however is that different types of aircraft have different rates of deceleration. Thus, air traffic controllers are unable to estimate the separation between two consecutive aircraft that is necessary at the beginning of the approach to insure safe in trail separation throughout the entire procedure, and they add a buffer to the required separation to compensate for this uncertainty. Actual implementation of a similar procedure at Amsterdam Schiphol airport and London Heathrow has shown a reduction of airport landing capacity of nearly 50%. One way to minimize the noise impact while maximizing aircraft throughput might be to delegate the task of separating the aircraft during the approach to the pilot, i.e. to instruct the pilot to maintain a certain separation from the preceding aircraft while the controller assumes a monitoring role. New airborne surveillance equipment such automatic dependant surveillance broadcast (ADS-B) will increase the level of traffic information available in the cockpit, in particular the ground- and

air-vectors of all aircraft in the vicinity will be available to the flight management system (FMS). This paper discusses how this information can be used to predict the trajectory of the preceding aircraft and how this information when combined with an own aircraft trajectory calculation can be used for self-separation purposes.

2-2   Introduction

The impact of aircraft noise on residential communities near airports is an increasing impediment to the expansion of airports around the world. This is particularly true in Europe where the impact of airport noise on the community has reached the point where it threatens to limit and in some cases actually does restrict airport capacity growth.

It has been shown that improvements are possible particularly in the approach phase of a flight.[1,2,4,5] In the terminal maneuvering area (TMA) the current practice is to slow aircraft down and have them descent to low altitudes of 2,000 to 3,000 feet relatively far from the runway to sequence them for final approach. Due to the low speeds, aircraft typically fly with their flaps partial extended, which means they have to use higher thrust settings to offset the flap-induced drag. The combination of slow speeds and low altitudes are very detrimental to the aircraft noise impact. Thus, significant reductions in aircraft approach noise are possible if the aircraft stay at higher altitudes and fly faster as long as possible. With these observations in mind several advanced noise abatement procedures (ANAPs) have been developed. Examples include the $3°$ decelerating approach (TDDA), the continuous descent approach (CDA), the advanced CDA (ACDA) and the low power low drag approach (LPLDA) . The features common to all these procedures are that the aircraft descend to the runway at low or idle thrust, with no level flight segments thus significantly reducing the noise impact on the community.

In this paper it is assumed that the aircraft are flying the TDDA, which requires the aircraft to descend from 7,000 feet and follow a three degree glide-path to the runway at idle thrust. The aircraft start out at a speed of 250 knots and decelerate as they descend to the runway due to aerodynamic drag, all the while optimizing the moments of flap selection in order to reach the final approach speed at 1,000 feet above the runway. At the 1,000 feet point thrust is then added to maintain the final approach speed and the aircraft then continues for a normal flare and touchdown.

One key issue with the TDDA is that air traffic controllers (ATC) find it very difficult to space consecutive aircraft during a decelerating approach. Actual implementation of the CDA at Amsterdam's Schiphol airport has resulted in a reduction in landing capacity of nearly 50%, thus limiting use of this procedure to the low traffic density hours of the night.[4,5] The problem lies in the fact that different aircraft will have different deceleration characteristics, which makes it very hard for controllers to estimate the initial separation necessary to ensure safe separation throughout the entire procedure. As can be seen in Figures 2-2 and 2-3, for the case of a Boeing 747
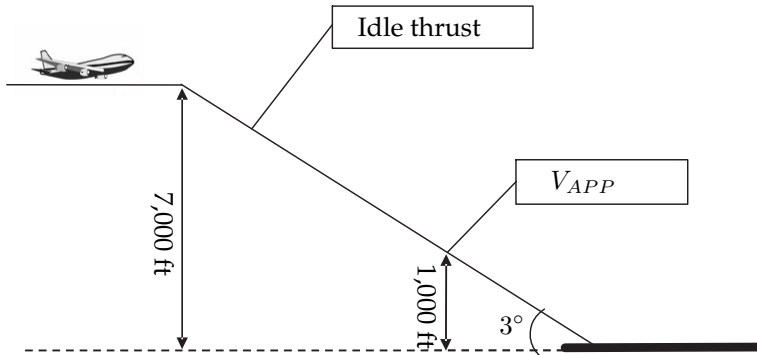
Figure 2-1: The Three-Degree Decelerating Approach.
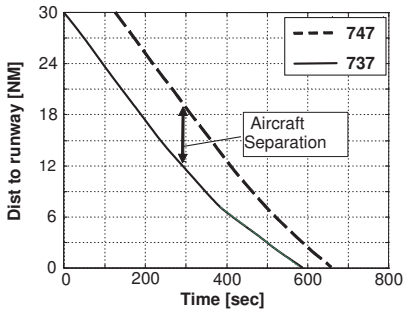
Figure 2-2: Distance profiles of a B747 following a B737 on a TDDA.
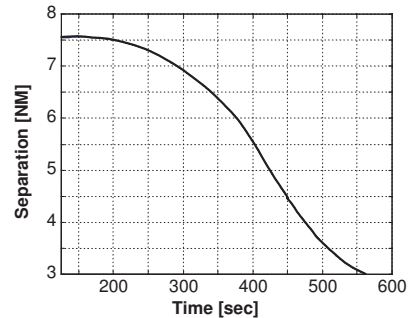
Figure 2-3: Separation trend during the TDDA.

following a Boeing 737, the initial separation needs to be 7.5 NM in order to still have the minimum 2.5 NM at the end of the procedure.[6]

Furthermore, since the separation is constantly changing, it is virtually impossible for the controller to assess whether the aircraft are deviating from their respective profiles, let alone issue commands to control their trajectories.

2-3   Proposed scenario

In order to solve the capacity problems of decelerating approaches, a new scenario has been proposed in which ATC spaces and sequences the aircraft to set them up for the TDDA with the help of a dedicated tool such as the final approach spacing tool (FAST) developed by NASA.[3,8,9] When the aircraft is cleared for the TDDA, the spacing task is then transferred to the pilot. While ATC will retain overall re-
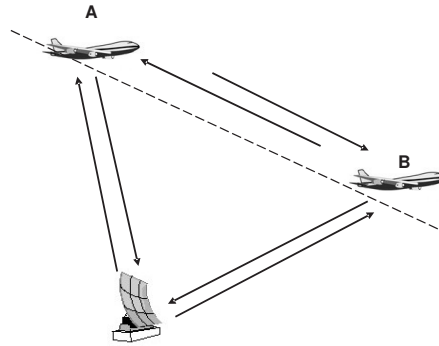
Figure 2-4: Data flows during in-trail self separation.

sponsibility for aircraft separation and will thus have the authority to intervene when necessary, the pilot will have the primary task of ensuring adequate separation during the approach. Thus, the controller who might be responsible for several decelerating aircraft in his airspace is relieved of the complicated controlling task and only has to intervene when aircraft do not conform to their respective trajectories. New tools that monitor the trajectory of the decelerating aircraft would have to be available to assist the controller in his monitoring task. Also, the pilot would need a tool to help him control his spacing.

2-3-1 ADS-B

One key input to any separation prediction tool is accurate trajectory information about other aircraft. With the introduction of automatic surveillance broadcast (ADS-B) a whole new wealth of traffic information will become available in the cockpit. Each aircraft broadcasts its state vector and the on-board receiver receives the state vectors of all aircraft in the vicinity, which can then be used for cockpit display of traffic information (CDTI). Also, ATC will have access to the information through its own dedicated receivers. According to the current specifications ADS-B will provide state-vector information with a one-second update rate in the terminal area.[10] Besides accurate position and identification information, this state vector will include the ground- and air-vector and intent information of the broadcasting aircraft.

2-4 Algorithm

In order to asses the future trend of the separation between the own aircraft and the preceding aircraft, the pilot needs a tool that is able to accurately predict own

aircraft trajectory as well as the trajectory of the leading aircraft. Comparison of these two trajectories then yields the separation trend. Previous research has shown that it is possible to predict own aircraft trajectory with adequate accuracy using a relatively simple aerodynamic model of the aircraft.[7] However, using such a model to predict the future trajectory of the preceding aircraft during the TDDA would require an elaborate database of aerodynamic data for all common airliners. To circumvent the need for such a database, we have developed an algorithm that would predict the future speed- and position-profile based on ADS-B data alone.

2-4-1   Wind model

Since wind can significantly influence the trajectories of aircraft, accurate wind data is required for accurate trajectory prediction. It is assumed that very accurate wind data will be available in the cockpit as each ADS-B equipped aircraft will be transmitting its ground- and air-vector. Combining these two vectors yields the wind-vector, so each aircraft that has completed the TDDA procedure will essentially have broadcast a complete wind profile for the approach path. Every consecutive aircraft will update this profile, so a very accurate average wind profile will thus be available to the separation algorithm. With enough data even a trend in the wind profile could be incorporated into the calculations.

In order to test the robustness of the algorithm under realistic wind conditions, a wind model was introduced to the simulations, consisting of a basic aerodynamic boundary layer model. White noise variations were added to this model to capture the uncertainties of turbulence. All the simulations were run under two conditions; a no wind scenario and a scenario where the wind model was introduced. In the latter case the prediction algorithm had knowledge of the nominal wind profile, but not of the white noise variations.

2-5   Least Square Estimate

In order to make the prediction, the algorithm looks at the history of the position and speed information, fits a polynomial to this data using a least square error fit and then extrapolates this polynomial to the point where the speed profile passes V_{ref} or the distance profile passes the point where the $3°$ glide-path descends below an altitude of 1,000 feet. This process is repeated during the procedure at a 25 second interval to continuously update the predicted trajectory.

Figure 2-5 and Figure 2-6 show that in the no wind case the fit is quite good, but much less so when wind is added to the scenario. In both figures the bottom curve is the actual profile as flown by the aircraft. As the extrapolations are made closer to the end of the procedure they tend to get more accurate which is to be expected since accumulative errors have less time to grow. Furthermore the changes in deceleration characteristics brought on by the selection of flaps tend to be less pronounced when the extrapolation is carried out over a shorter time interval.
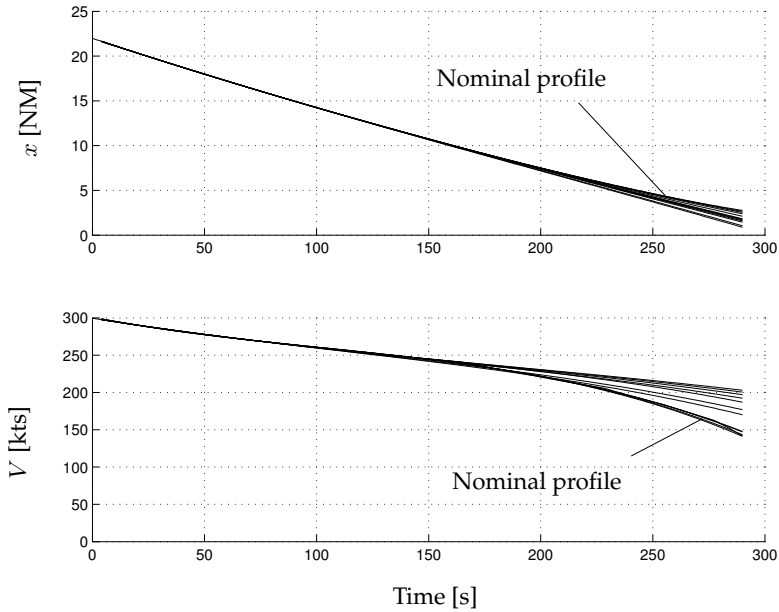
Figure 2-5: Least square error approximations of the position and speed profiles in zero wind conditions.
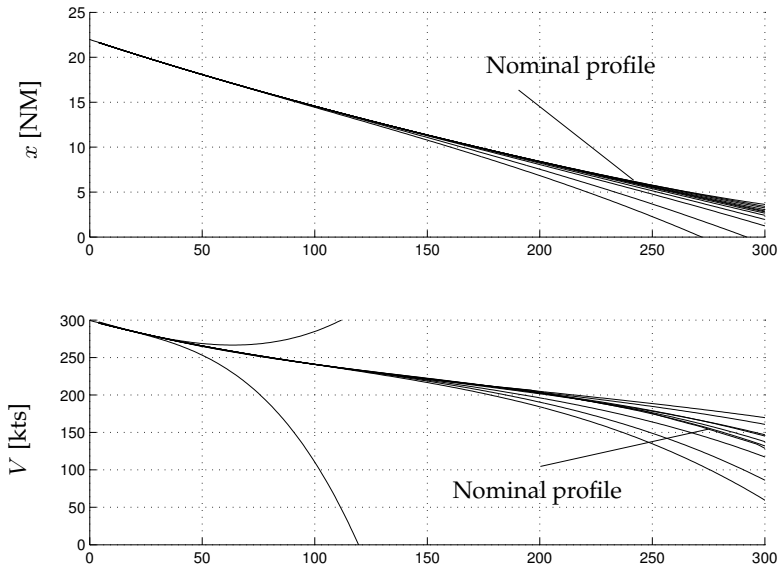
Figure 2-6: Least square error approximations of the position and speed profiles in the presence of wind and turbulence.
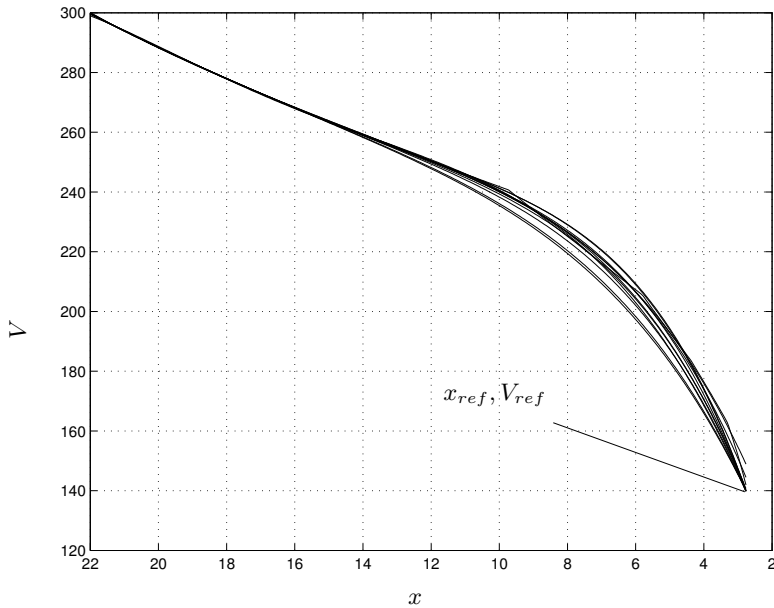
Figure 2-7: Least square error approximations of the position and speed profiles in the presence of wind and turbulence.

2-6   Intent information

One of the major advantages of ADS-B over current surveillance systems is that it allows aircraft to broadcast their intent information. During the TDDA this information could consist of the final approach speed V_{ref} the pilot is aiming for and at what altitude he intents to have achieved that speed. This information can be utilized by the prediction algorithm to get more accurate results.

As can be seen in Figure 2-7, the intent information can be treated as an extra data point in the xV-plane, when speed is plotted against position. In other words, the intent information forms an end constraint for the prediction. Using the earlier described least square error extrapolation algorithm this curve now can be approximated resulting in an expression for V as a function of x.

$$\left.\begin{array}{l} V_g = f(x) \\ V_g = \dot{x} \end{array}\right\} \dot{x} = f(x) \tag{2-1}$$

Realizing that the ground speed V is the time derivative of the position x, the resulting differential equation can be solved and expressions for x and V in the time domain can be obtained.

As can be seen in Figure 2-8 and Figure 2-9 this produces far more accurate results than the method used earlier. As Figure 2-9 shows however, the scenario with wind
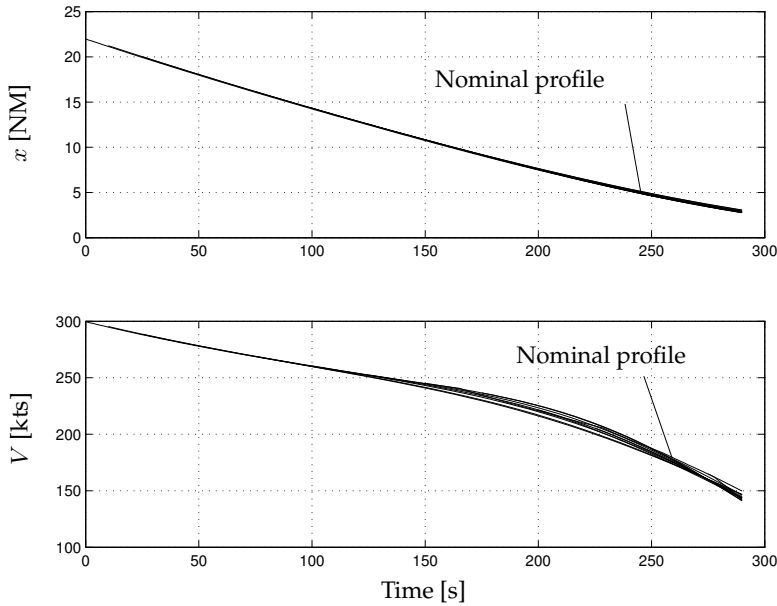
Figure 2-8: Least square error approximations with end constraint information in zero wind conditions.

requires an initial integration period before predictions become accurate enough. This may be seen by the fact that the first two approximations in Figure 2-9, at $t = 10sec$ and $t = 25sec$, are not usable, but from $t = 50sec$ and on there are enough data points to get an accurate prediction.

2-7   Accuracy

The actual error in the prediction and the initial integration time varies with wind conditions, the number of data-points available and the length of the time interval over which the extrapolation is carried out. The error is reduced when the amplitude of the white noise disturbance on the wind profile is reduced, when the time interval gets shorter and when the number of data-points is increased.

When an aircraft is flying the TDDA this translates into the prediction getting increasingly more accurate as the separation is decreasing. When the aircraft are about 75 seconds into the approach, the prediction error of the position of the leading aircraft is of the order of 0.1 NM, and the speed error is of the order of 5 knots. Since the aircraft are initially spaced 2 minutes apart, by the time the second aircraft reaches the point where thrust is reduced, accurate predictions are already available.
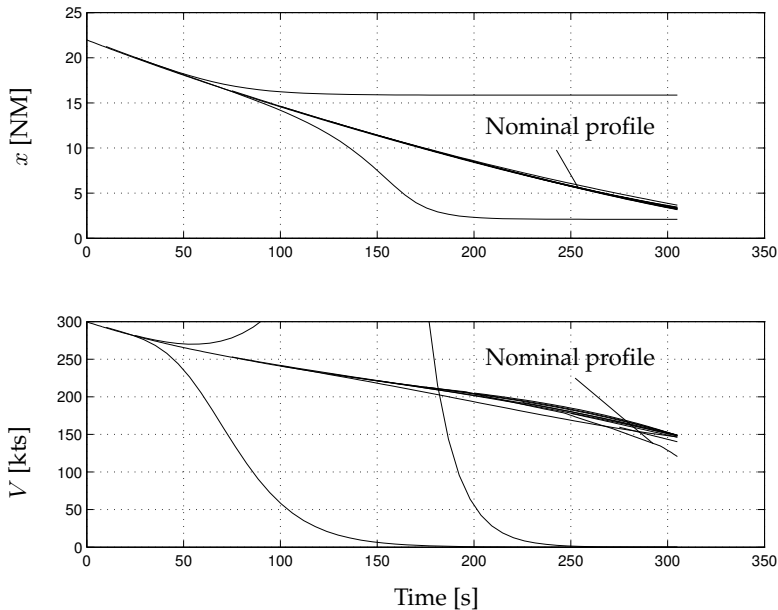
Figure 2-9: Least square error approximations with end constraint information in wind and turbulence conditions.

2-8   Conclusions and future research

Although aircraft noise impact on residential communities near airports can be significantly reduced by the application of advanced noise abatement procedures, runway capacity problems have restricted the implementation of these procedures to the lower traffic density hours. The main problem lies with the inability of air traffic controllers to separate aircraft that are decelerating at significantly different rates. A proposed scenario has the pilot control his own separation during the final approach with the controller monitoring his performance, thus relieving the controller from the task of controlling the spacing between several decelerating aircraft. The pilot on the other hand needs to be given a tool to assist him with his new task. Such a tool needs to be driven by an algorithm that can successfully assess the future trend of the in-trail separation, for which an accurate prediction of the future trajectory of the preceding aircraft is essential. Simulation results indicate that such a prediction based on ADS-B data alone is possible, but to get usable results the intent information available in the state vector must be utilized. The resulting algorithm is robust to variability in the wind profile.

Further research is ongoing to investigate how the separation information is best presented to the pilot to support the self-separation task. The best way to incorporate this information in an automated TDDA is also being investigated.

References

[1] J.-P. Clarke. Systems Analysis of Noise Abatement Procedures Enabled by Advanced Flight Guidance Technology. *Journal of Aircraft*, 37, no. 2(AIAA 97-0490), Mar-Apr 2000.

[2] J.-P. Clarke and R. J. Hansman. A Systems Analysis Methodology for Developing Single Event Noise Abatement Procedures. Technical Report ASL-97-1, MIT - Aeronautical Systems Laboratory, Cambridge (MA), USA, Jan 1997.

[3] T. J. Davis, K. J. Krzeczowski, and C. Bergh. The Final Approach Spacing Tool. In *13th IFAC Symposium on Automatic Control in Aerospace*, Palo Alto (CA), USA, Sep 1994.

[4] L. J. J. Erkelens. Research on Noise Abatement Procedures. Technical Report NLR TP 98066, National Aerospace Laboratory (NLR), Amsterdam, The Netherlands, Feb 1998.

[5] L. J. J. Erkelens. Development of Noise Abatement Procedures in The Netherlands. Technical Report NLR TP 99386, National Aerospace Laboratory (NLR), Amsterdam, The Netherlands, Nov 1999.

[6] N. T. Ho and J.-P. Clarke. Mitigating Operational Aircraft Noise Impact by Leveraging on Automation Capability. In *AIAA 1st Aircraft, Technology Integration, and Operations Forum (ATIO)*, number AIAA-2001-5239, Cambridge, UK, 2001.

[7] M. F. Koeslag. Advanced Continuous Approaches, an Algorithm Design for the Flight Management System. Technical Report NLR-TR-2001-359, National Aerospace Laboratory (NLR), Amsterdam, The Netherlands, Mar 1999.

[8] K. K. Lee and T. J. Davis. The Development of the Final Approach Spacing Tool (FAST): A Cooperative Controller-Engineer Design Approach. *Journal of Control Engineering Practice*, 4(8):1161–1168, Aug 1996.

[9] C. Quinn and J. E. Robertson III. A Human Factors Evaluation of Active Final Approach Spacing Tool Concepts. In *3rd USA/Europe Air Traffic Management R&D Seminar*, Napoli, Italy, Jun 2000.

[10] RTCA, Inc., Washington, USA. *Minimum Aviation System Performance Standards for Automatic Dependent Surveillance Broadcast (ADS-B)*, Feb 1998.

3

Pilot Support Interface

3-1 Abstract

Previous research on aircraft noise abatement has resulted in some promising flight procedures to mitigate noise impact, such as the three-degree decelerating approach (TDDA). A problem with decelerating approaches, however, is that they typically lead to increased spacing, which in turn results in a significant reduction of runway landing capacity. A possible solution to this problem might be to delegate the task of separating the aircraft during the approach to the pilot. To aid the pilot, an algorithm has been developed that predicts the trajectory of the preceding aircraft and optimizes the flap schedule based on this prediction. Off-line simulations indicate that using this system runway throughput numbers of up to 98% of the capacity of a conventional instrument landing system (ILS) approach can be achieved.[18] To assess practical implementation issues and to investigate pilot appreciation, a piloted experiment was conducted, for which a pilot support interface has been developed that presents the future separation information in an intuitive fashion. The experiment showed that it is indeed possible for pilots to perform the spacing task while flying a TDDA. The pilot support interface significantly reduces pilot workload when compared to a baseline display. Also the effects of off-nominal lead pilot behavior on pilot performance are reduced by the use of online flap schedule optimization and separation prediction.

The impact of aircraft noise on residential communities near major airports is an impediment to the expansion of airports around the world. At a number of airports the impact of airport noise on the community has reached the point where it threatens to and in some cases actually does restrict airport capacity growth. Current practice for aircraft approaching an airport for landing is to slowdown and descend to low altitudes between 2,000 and 3,000 ft relatively far from the runway to sequence for final approach. Due to the low speeds, aircraft typically fly with the flaps partially extended, requiring higher thrust settings to offset the flap-induced drag. This mode of operation is very detrimental to the aircraft noise impact. Thus, significant noise reductions seem possible if the aircraft would stay at higher altitudes and keep the speed up as long as possible.

With these observations in mind, several advanced noise abatement procedures (ANAPs) have been developed. Examples include the three-degree decelerating approach (TDDA), the (advanced) continuous descent approach ((A)CDA) and the low-power-low-drag approach.[2,3,7,8,13] The features common to all these procedures are that the aircraft descend to the runway at low or idle thrust with no level flight segments, thus significantly reducing the noise impact on the community.

Although successful in reducing noise, runway capacity problems have restricted the implementation of the noise abatement procedures to the lower traffic density hours. The main problem lies with the inability of air traffic controllers to separate aircraft that are decelerating at significantly different rates. The major contributors to the variability of the aircraft trajectories are the aerodynamic properties of the aircraft type, the current flight mass, pilot intent, and the wind conditions. Controllers typically start applying larger separations between aircraft to compensate for these uncertainties, resulting in fewer aircraft being handled per hour.[7,13]

On board the aircraft, knowledge about the aircraft's aerodynamic properties, current flight mass, and pilot intent is readily available. Hence, smaller separation distances seem possible when the spacing task is delegated to the pilot, relieving the controller from the task of controlling the spacing between several decelerating aircraft. Before the separation task can be transferred to the flight deck, two items need to be addressed. Although the necessary information is in itself available on the flight deck, this information needs to be integrated first to be able to accurately predict the approach trajectory and speed profile to allow the flight crew to consistently and predictably fly the decelerating approach in varying operational conditions. Furthermore, support must be given to the pilots to be able to perform the self-separation task. For the self-spacing task, cockpit displays are needed that exceed the capabilities of current airborne collision avoidance systems.

This article describes the design and evaluation of a pilot support interface that
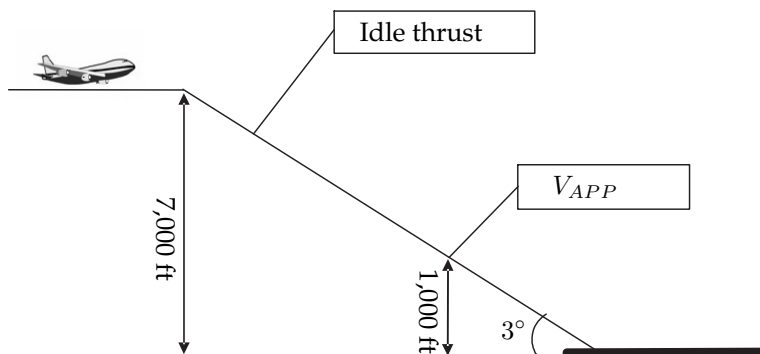
Figure 3-1: The Three-Degree Decelerating approach

helps the crew in conducting a self-spacing decelerating approach. First, one of the most promising ANAPs, the TDDA, is discussed along with the problems accompanying its implementation, followed by a description of the algorithms needed to drive a pilot support system. Finally, the design of the piloted experiment is explained, followed by the results of that experiment.

3-2 The Three-Degree Decelerating Approach

3-2-1 Description of the procedure

The key differences between the TDDA and a standard instrument landing system (ILS) approach are the higher intercept altitude and the fact that the TDDA is flown at idle power. A TDDA, illustrated in Figure 3-1, requires pilots to control their aircraft along a three-degree glide path to the runway at idle thrust, from an initial altitude of, for example, 7,000 ft. This is much higher than the typical 2,000 to 3,000 ft of normal ILS glide slope intercept, resulting in significant noise benefit both by increasing the distance between the noise source and observers on the ground and by reduced engine noise.

The TDDA is one of the most promising ANAPs because consistent speed and distance profiles can be flown by optimizing the speeds at which the next stage of flaps are deployed and the landing gear is lowered.[14] Furthermore, this procedure in itself need not reduce runway capacity significantly, as recent off-line studies have shown. Here, a representative mix of Boeing 737 and Boeing 747 aircraft was simulated flying TDDAs, and taking into account the operational uncertainties, runway capacity losses were limited to a 2% reduction compared to the theoretical maximum using conventional procedures, retaining a major noise reduction.[18]

The aircraft begins with a speed of 250 kt and decelerates as it descends to the runway. The aerodynamic drag determines the deceleration, and the selection of flap

and landing gear positions is used to control the aerodynamic drag. The flap extension schedule is optimized so that the aircraft reaches the final approach speed at 1,000 ft above the runway. At this point, thrust is added to maintain the final approach speed (V_{app}) and for the remainder of the trajectory to the runway, the aircraft flies a stabilized approach, with a constant speed, attitude, and power setting, leading to a normal flare and touchdown. The choice of 1,000 ft as the final altitude is motivated by the fact that it is standard operating procedure to be configured and stabilized no later than at 1,000 ft. Also previous research has shown that continuing at idle thrust below 1,000 ft has very little effect on the further reduction of the noise impact on residential areas.[3,7]

The aircraft begins with a speed of 250 knots and decelerates as it descends to the runway. The aerodynamic drag determines the deceleration, and the selection of flap and landing gear positions is used to control the aerodynamic drag. The flap extension schedule is optimized, so that the aircraft reaches the final approach speed at 1,000 feet above the runway. At this point, thrust is added to maintain the final approach speed (V_{app}) and for the remainder of the trajectory to the runway, the aircraft flies a stabilized approach, with a constant speed, attitude and power setting, leading to a normal flare and touchdown. The choice of 1,000 feet as the final altitude is motivated by the fact that it is standard operating procedure to be configured and stabilized no later than at 1,000 feet. Also previous research has shown that continuing at idle thrust below 1,000 feet has very little effect on the further reduction of the noise impact on residential aereas.[3,7]

3-2-2   The problem of separation

The key issue with the TDDA and other ANAPs is that air traffic controllers find it very difficult to space consecutive aircraft during a decelerating approach. Actual implementation of the CDA at Amsterdam's Schiphol Airport has resulted in a reduction in landing capacity of nearly 50%, thus limiting use of this procedure to the low-traffic-density hours of the night.[7,8] As mentioned earlier, the problem lies in the fact that different aircraft will have different deceleration characteristics, which makes it very hard for controllers to estimate the initial separation necessary to ensure safe separation throughout the entire procedure. Furthermore, for the procedure to be effective, the air traffic controller must not interfere with the aircraft trajectory during the decelerating part of the approach. As can be seen in Figure 3-2, for the case of a Boeing 747 following a Boeing 737, the initial separation needs to be 7.5 nm to preserve the minimum 2.5 nm at the end of the procedure.[10] Furthermore, because the separation is constantly changing, it is virtually impossible for the controller to assess whether the aircraft are deviating from their profiles, let alone issue commands to control their trajectories.
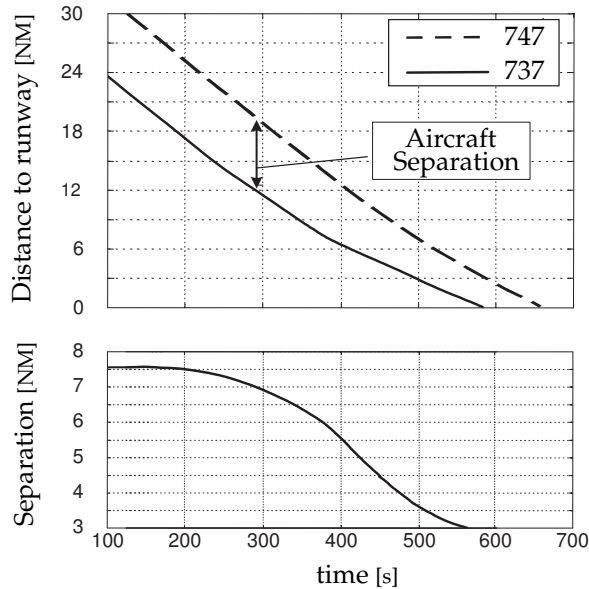
Figure 3-2: Distance profiles and separation history of a B747 following a B737 on a TDDA.

3-2-3   Delegating the separation task to the pilot

To solve the capacity problems of decelerating approaches, a new scenario has been proposed in which air traffic control spaces and sequences the aircraft to set them up for the TDDA at a certain altitude and still at a constant speed. Dedicated tools such as the Final Approach Spacing Tool and the Advanced Terminal Area Approach Spacing Tool, both developed by the National Aeronautics and Space Administration (NASA) , would be employed to support the pilots and air traffic controllers in their task.[4,5,15–17]   When an aircraft is cleared for the TDDA, the spacing task is then transferred to the pilot. Although air traffic control will retain overall responsibility for aircraft separation and will thus have the authority to intervene when necessary, the pilot will have the primary task of ensuring adequate separation from the preceding aircraft during the approach. Thus, the controller who might be responsible for several decelerating aircraft in his or her airspace is relieved of the complicated controlling task and only has to intervene when aircraft do not conform to their respective trajectories.

It is clear that when introducing this concept, new tools that monitor the trajectory of the decelerating aircraft would have to be available to assist the controller in the monitoring task. However, this article focuses on the pilot support system necessary to help pilots control the spacing and speed profile.
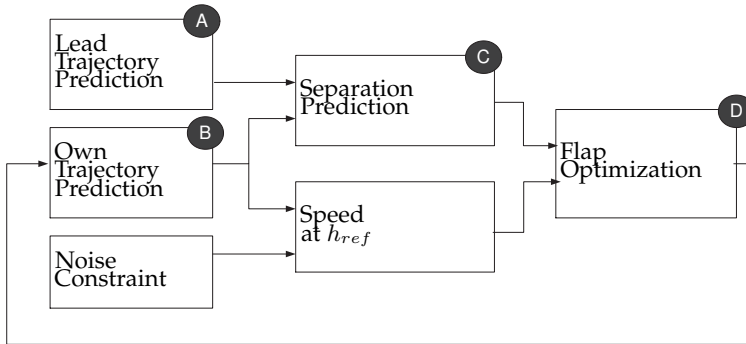
Figure 3-3: Structure of the flap scheduler algorithm.

3-3   Algorithm design

Figure 3-3 shows the structure of the algorithm that drives the pilot support system. First the trajectory of the lead aircraft is predicted (**A**), which is then compared to the prediction of the own trajectory (**B**), yielding the future separation trend (**C**). Next the predicted own speed profile is analyzed and compared with the TDDA requirements. If the separation is predicted to be less than the minimum safe separation (i.e., 2.5 nm in the case of a Boeing 747 trailing a Boeing 737), the flap speeds are adjusted to slow down earlier and increase the separation. This process is iterated until the separation is no longer compromised (**D**). When separation is not a factor, the flap schedule is optimized by the algorithm to make sure that the TDDA profile is followed and V_{app} is reached at the reference height h_{ref}.

Each element of the algorithm (**A**, **B**, **C**, **D**) will be treated in more detail below.

3-3-1   Block A: Lead trajectory prediction algorithm

To assess the future trend of the separation between the own aircraft and the preceding aircraft, the flap scheduler needs to accurately predict the own aircraft trajectory as well as the trajectory of the leading aircraft. Comparison of these two trajectories then yields the separation trend. As shown later, the own trajectory is predicted using a simple aerodynamic model taking the current flap schedule into account. However, using such a model to predict the future trajectory of the preceding aircraft during the TDDA would require an elaborate database of aerodynamic data for all common airliners. To circumvent the need for such a database, the algorithm treats the preceding aircraft as a 'black box', predicting the future speed and position profile based on secondary radar data,[11] such as can be acquired using a system like the Automatic Dependent Surveillance-Broadcast (ADS-B).

Enabling technology: ADS-B   One key input to any separation prediction tool is accurate trajectory information about other aircraft.With the introduction of ADS-B a new wealth of traffic information will become available to the pilot. Each aircraft broadcasts its state vector and the on-board receiver receives the state vectors of all aircraft in the vicinity, which can then be used for cockpit display of traffic information (CDTI). Also, air traffic control will have access to the information through its own dedicated receivers. According to the current specifications, ADS-B will provide state-vector information with a 1-sec update rate in the terminal area (according to the standards set by the Radio Technical Commission for Aeronautics[1]). Besides accurate position and identification information, this state vector will include the ground and air vector and intent information of the broadcasting aircraft. During the TDDA the intent information could consist of the final approach speed Vapp the pilot is aiming for and at what altitude he or she intends to have achieved that speed. As shown later, this information can be used by the separation prediction algorithm.

Data collection and fitting   As the lead aircraft is approaching the runway, decelerating and aiming to reach its V_{app} at 1,000 ft, it is broadcasting its state vector every second. These data are received on board the ownship and stored in the flight management system. The trajectory prediction algorithm then fits a third-order polynomial through the collected position and velocity data using a leastsquare-error fit. Because sole extrapolation of a higher order polynomial would lead to unpredictable results, the intent information is used as an extra data point to help the data-fitting process. The intent information is used as follows: Assuming the intent information consists of the final approach speed V_{app} of the lead aircraft and altitude h_{ref} at which the pilot wants to have achieved that speed, it still is not clear at which time the lead expects to reach href. In other words, the data still lack a constraint in the time domain. To work around this problem, first the lead aircraft's V_{app} (indicated airspeed) is corrected for altitude and (predicted) wind to get an estimated $V_{g_{ref}}$ (ground speed). Then the lead's h_{ref} is combined with the glide path angle γ of the ILS to yield x_{ref}.

It is clear from Figure 3-4, where ground speed is plotted against position, that the intent information now forms an extra data point in the xV-plane. When a leastsquare-error curve is fitted to this data set, an expression for Vg as a function of x can now be obtained. Realizing that the $V_{g_{ref}}$ ground speed V_g is the time derivative of the position x, the resulting ordinary differential equation can be solved and expressions for x and V_g in the time domain can be obtained:

$$\left. \begin{array}{l} V_g = f(x) \\ V_g = \dot{x} \end{array} \right\} \dot{x} = f(x) \qquad (3\text{-}1)$$
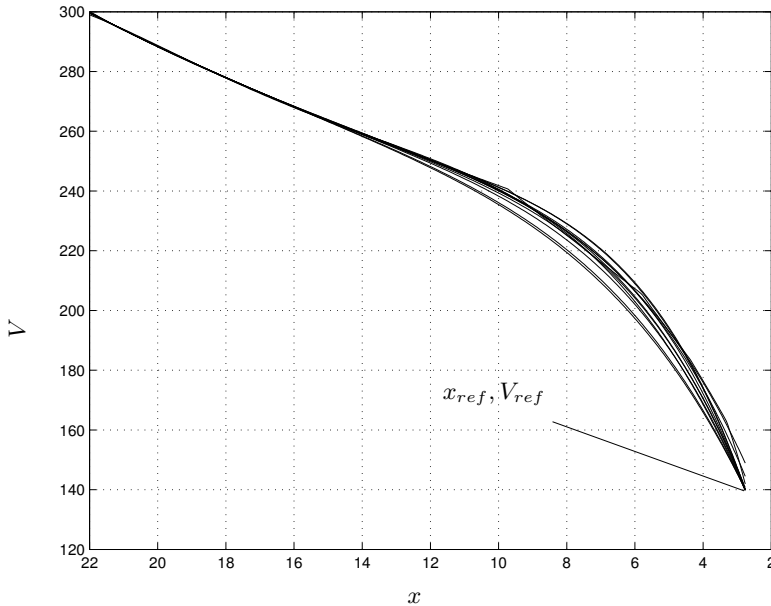
Figure 3-4: Least square error approximations of the position and speed profiles in the presence of wind and turbulence.

Accuracy   The actual error in the prediction varies with wind conditions, the number of data points available, and the length of the time interval over which the extrapolation is carried out. The error is reduced when the amplitude of the white noise disturbance on the wind profile is reduced and when the time interval gets shorter.

When an aircraft is flying the TDDA, this translates into the favorable condition that the prediction gets increasingly accurate as the separation is becoming smaller. When the aircraft are about 75 sec into the approach, the prediction error of the position of the leading aircraft is on the order of 0.1 nm, and the speed error is of the order of 5 kt. Because the aircraft are initially spaced 2 min apart, by the time the ownship reaches the point where thrust is reduced, accurate predictions are already available.

3-3-2   Block B: Own trajectory prediction

Aerodynamic model   Because the ownship trajectory prediction will be used for the optimization of the flap schedule later on, the prediction will need to reflect the effect of changes in the flap schedule. Because of this, a simple aerodynamic model is used for the ownship trajectory prediction, as described by Koeslag.[14] The model is a center of gravity model that only considers the forces along the flight path and

perpendicular to it:

$$\Sigma F_Z : 0 = L - mg\cos\gamma$$
$$\Sigma F_X : m\ddot{x} = T - D + mg\sin\gamma$$

(3-2)

The lift and drag coefficients are known for the ownship, as are the thrust coefficients, and these can be used to find the acceleration $\ddot{x}$. The resulting acceleration along the flight path $\ddot{x}$ is then integrated in time to yield the predicted speed and distance profiles. A more elaborate treatment of this method can be found in.[6]

3-3-3 Block C: Separation trend prediction

Now that predictions for both the lead trajectory and the own trajectory are available, a separation trend is readily derived by superpositioning the two distance profiles. The minimum predicted separation is then determined by locating the minimum value of the separation trend.

3-3-4 Block D: Flap schedule optimization algorithms

To assist the pilot in the timing of the flap selections, a flap schedule optimization algorithm has been developed[12,14] that runs onboard the aircraft and calculates at what speed each flap setting should be selected to arrive at the 1,000 ft point at V_{app}; refer also to Figure 3-3. This flap scheduler works in one of two modes.

In *capture mode*, the algorithm calculates the altitude at which the thrust should be set to flight-idle so that the runway can be reached using the nominal flap schedule. The corresponding altitude is the thrust-cut altitude. Descending below this altitude causes the flap scheduler to switch to hold mode.

In *hold mode*, the flap scheduling algorithm predicts the own speed profile based on the current speed and the current flap schedule. When the difference between the predicted V_{app} is more than 2 kt, the flap schedule is adjusted and the model is run again. This process is repeated until the predicted speed difference is less than 2 kt.

Self-spacing constraint   The flap scheduler as presented so far does not, however, provide a means to aid the pilot in his self-spacing task. Therefore the algorithm has been extended to account for the minimum safe separation constraint. The scheduler optimizes the flap speeds as before, but now also checks whether the predicted own profile will put the ownship too close to the preceding aircraft. When it turns out that this will be the case, the flap schedule is adjusted until a safe separation can be assured during the whole approach.

The consequence of such an adjustment is, of course, that the aircraft will deviate from the optimal speed profile for the TDDA and therefore it is inevitable that V_{app}

will be reached at a higher altitude, thus decreasing the noise benefits of the procedure. As shown later, the experiment results indicate that the increase in altitude will typically be less than 500 ft, so an increase in the produced noise will most likely be almost negligible. Only in extreme cases, when the aircraft are sequenced much too close, will the altitude at which Vapp is reached increase to higher values, but typically not above 2,500 ft. In these extreme cases the noise impact during the last 2,000 ft would be comparable to a standard ILS approach, so the noise benefits would still be worthwhile.

3-4   Pilot support interface design

After the flap schedule has been optimized, the information has to be presented to the pilot in a meaningful way. To do so, a number of displays were designed with the following ideas in mind: First, the display should enhance the situation awareness of the pilot in such away that he or she not only knows where he or she is in relation to the other planes in the vicinity, but also where he or she will be in the future. Furthermore, the display should support the pilot in his or her task of accurately flying the TDDA profile with only flap and gear timing to control his or her speed. Finally, the display should depart as little as possible from current display formats to facilitate pilot acceptance, so a modification of an existing display becomes more feasible.

3-4-1   TDDA support

Thrust cue   As explained in the previous sections, the first critical pilot action is the thrust cutback. The altitude at which this should occur as calculated by the algorithm is presented by a bug on the altitude tape of the primary flight display (PFD) in the form of the letter 'T', as represented in Figure 3-5. The thrust cutback altitude is recalculated every second, updated for the current situation, and presented in numerical format underneath the altitude tape. In order to provide a stable cue, the thrust cut-back altitude is no longer updated when the aircraft has descended to within 500 feet of its value.

Flap cue   In order to inform the pilot when to select the next stage of flaps a cue was added to the speed tape of the PFD). This cue consists of the letter F and a pointer (see Figure 3-5). In doing so, the pilot has an intuitive display of the difference between his or her current speed and the optimal speed for his or her next stage of flaps, which in turn give the pilot an indication of the time left before his or her next required action without the need for displaying the numerical value of the flap speed.
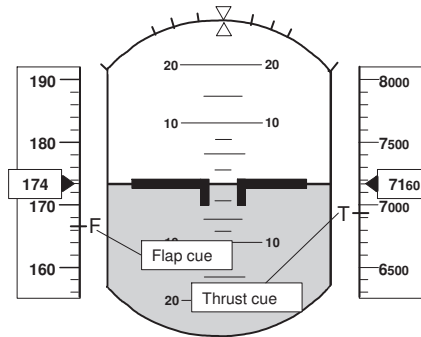
Figure 3-5: Primary Flight Display with thrust cut-back cue 'T' and flap cue 'F'.

Annunciators   The flap speeds can only be varied over a limited range, each speed limited by the maximum structural flap speed and the minimum maneuvering speed. It is possible that all the flap speeds have been set at their maximum value by the flap scheduling algorithm, but the aircraft is still predicted to either end up too close behind the lead aircraft, or faster than V_{app} at 1,000 ft. When this situation occurs, an amber 'add drag' annunciator illuminates on the PFD to indicate to the pilot that the algorithm has run out of ideas and that the TDDA goals are probably not going to be met unless the pilot increases the drag by other means (e.g., by using the speed brakes).

On the other hand, when the pilot has reduced too early and even delaying all the flap selections to the lowest possible speeds will not stretch the glide sufficiently, an amber 'add thrust' message appears, indicating that the aircraft will reach V_{app} when still above 1,000 ft. In this case the pilot can either accept the noise penalty later on, or add thrust to reduce deceleration, increasing the noise generated at the current point of the flight path.

In both cases, the annunciator will disappear and the algorithm will resume scheduling as soon as the pilot has corrected the situation by use of speed brakes or thrust levers, respectively. At this point the pilot can stow the speed brakes and continue the approach at idle thrust and be certain to complete the TDDA satisfactorily.

Cockpit Display of Traffic Information   The navigation display is enhanced with information on the aircraft in the vicinity (cockpit display of traffic information [CDTI]), adhering as much as possible to the standard symbology of the traffic alert and collision avoidance system (TCAS), as can be seen in Figure 3-6 where the solid diamond shape represents the lead aircraft with the relative altitude and trend displayed, in this case 1,200 ft below the ownship and descending as indicated by the arrow. However, because here the symbology is driven by ADS-B, the bearing and range information is far more accurate than current TCAS can provide.[1]
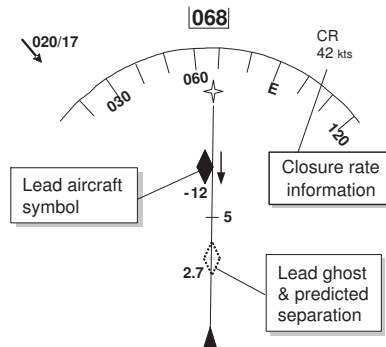
Figure 3-6: Navigation Display with lead (solid) and ghost symbol (dashed).

Ghost symbol   In addition to the standard TCAS symbology, information about the future separation is displayed on the navigation display (ND) as a so-called ghost of the lead aircraft (see Figure 3-6). This ghost consists of a dashed traffic symbol that is projected at a distance from the ownship symbol, equal to the minimum predicted separation during the entire approach. Next to the ghost the numeric value of the predicted separation over the reference point is displayed. When the predicted separation over the reference point is less than the minimum safe separation of 2.5 nm, the symbol will change from white to amber to indicate to the pilot that the minimum separation will be violated when no action is taken. When the actual separation is being violated, the symbol of the actual aircraft will also turn into a red square, just as is the case with conventional TCAS displays.

The ghost provides the pilot with a preview on the minimum separation reached during the procedure and provides feedback on his or her control actions. Also, the ghost offers a way to cross-check the performance of the flap scheduling algorithm driving the flap cues.

Closure rate information   Because of the unconventional nature of the scenario, having two aircraft relatively close to one another at significantly different speeds, the display further departs from standard TCAS symbology by offering a readout of the closure rate; that is, the difference in ground speed of the two aircraft. This is done because the closure rate can be a good clue to the pilot on how the situation is developing, a clue not so easily derived visually from the closing of the symbols on the ND, because of the scale of the display. The closure rate information is presented in the upper right corner of the ND using the symbol 'CR' plus the closure rate in knots.

3-5   Experiment

To test the self-spacing scenario and to assess the operational uncertainties of self-separation in a realistic fashion, a piloted experiment was conducted to determine the effects of different scenarios on pilot performance, workload, and situation awareness and how these ultimately reflect on runway capacity numbers. Another measurement of the experiment was the feedback from the pilots on the display design and their appreciation of the self-spacing concept.

3-5-1   Method

Participants and instructions   Ten professional airline pilots, all men, were invited to participate in the experiment, 6 of whom had many years of experience on the Boeing 747. After a thorough briefing on the displays and the procedure, they were asked to manually fly a TDDA in a Boeing 747, following a conventional straight-in ILS glide path with the engines running at flight idle, following a Boeing 737. Pilot performance was scored based on how accurately the TDDA profile was followed and how close to the minimum safe separation the approach was finished. The minimum safe separation was set to 2.5 nm and as a measure for TDDA performance throttle inputs and flap deflections were measured.

Table 3-1: The five pilot support interfaces that were tested in the experiment.

Display	Flap Cues	CDTI
1 (base-line)	Fixed	TCAS + CR
2	Noise optimized	TCAS + CR
3	Noise+Traff.opt.	TCAS + CR
4	Noise optimized	Lead ghosting
5	Noise+Traff.opt	Lead ghosting

Apparatus   The experiment was conducted in the Human-Machine Interaction Laboratory of the faculty of Aerospace Engineering of Delft University. This laboratory consists of a fixed-base simulator that has two 18-in. LCD screens on which the PFD, ND, and mode control panel of a Boeing 747-400 were projected. Furthermore the simulator has a hydraulic side-stick and rudder pedals. Because the goal of this experiment was to determine the performance of pilots during instrument flight conditions, no outside visual information was shown.

Aircraft and weather model   As no Boeing 747-400 model was available, the aircraft flown was a Boeing 747-200, simulated through a realistic nonlinear model. Although this meant a B747-200 model was flown using a B747-400 flight deck

setup, the pilots indicated that the characteristics of the two models were similar enough to not pose a distraction. The aircraft was flown with the yaw-damper engaged to improve lateral stability. At the beginning of each run the aircraft was controlled by autopilot (fly level at 7,000 ft) and autothrottle (fly at 250 kt IAS). At the start of each measurement run, these systems both had to be deactivated by the pilot. The weather model was set to ICAO International Standard Atmosphere conditions and zero wind.

Independent variables   Two independent variables were defined. First of all, different combinations of the display elements were tested, resulting in five pilot support interfaces, listed in Table 3-1: (1) the baseline interface; that is, a standard TCAS display augmented with a closure rate readout and a fixed, precomputed trajectory prediction algorithm; this algorithm uses a standard flap deflection scheme that is, unlike the other algorithms, not updated during the approach; (2) and (3) the standard TCAS interface with the online trajectory prediction algorithms that optimize for noise only (2) or for noise and separation at runway threshold (3); and (4) and (5) the combination of these two algorithms with a TCAS display that was augmented with a ghost symbol, showing the predicted separation at runway threshold. Second, three different lead aircraft approach trajectories were defined: (a) a nominal approach, on which the precomputed flap schedule was based; (b) a fast lead approach, where, because of tardy pilot action, the preceding aircraft decelerates very slowly relative to the nominal approach and the average ground speed is above nominal; and (c) a slow lead approach, the complement of (b), where, because of aggressive pilot action, the target aircraft decelerates very quickly resulting in averaging a lower ground speed. Note that the baseline interface only provides pilots with a correct flap schedule for the nominal approach. In all other approaches, this interface will not give the right flap schedule as the preceding aircraft does not fly the nominal approach.

Experiment design   The experiment is set up as a 5×3 factorial: five display conditions and three lead traces give 15 conditions for each pilot. During the training runs, each pilot was exposed to all 15 conditions to get acquainted with all the display configurations. During the measurement runs, each condition was flown only once to limit the total time needed for each pilot to one work day. The order in which the conditions were flown was randomized to prevent learning effects.

Procedure   The task was to fly a TDDA approach to a fictitious airport and stay at a safe distance from a preceding aircraft. In all cases the preceding aircraft was a Boeing 737 flying a TDDA as well. The behavior of this aircraft was one of the experiment independent variables. The experiment consisted of 15 approaches, each starting with straight and level flight at 7,000 ft, 250 kt IAS, and established on the localizer. After the pilot had a chance to form a mental picture of the situation, he had to disconnect the autopilot. After glide-slope interception, the procedure

called for maintaining 250 kt until reaching the thrust cutback altitude, where the thrust levers were pulled back to flight idle and the deceleration began.

The pilots were instructed that after the thrust had been set to idle, they were not to advance the throttle levers until reaching the final approach speed. This way it is easier to compare results between pilots and the altitude at which V_{app} is reached can be used as a performance indicator. The pilots were further instructed that under no circumstances were they to let the actual in-trail distance become less than 2.5 nm, but no pilot action was required to close the gap should the separation increase.

After each run, the pilots filled out a NASA Task Load Index (NASA-TLX) form,[9] and after the last run they were requested to complete a questionnaire to give their opinion on the different aspects of the experiment.

Dependent measures   The path-tracking performance was measured by recording vertical and cross-track errors and heading errors relative to the three-degree ILS glide path. Pilot control actions on the side-stick, throttle, and flap selector were also measured. Furthermore the adherence to the flap cues was measured by recording the time between the appearance of the cue and the pilot response to that cue.

As operational performance parameters, the altitude at which V_{app} was reached was recorded as a measure for noise impact; the separation at 1,000 ft was considered as a measure for separation performance. Finally, pilot workload was measured using the NASA-TLX.

Hypotheses   It was hypothesized that pilots would perform better when they are supported by an interface that provides them on-line (i.e., optimized in real time) information on the flap schedule needed to successfully fly the TDDA while maintaining a safe separation from the leading aircraft. The effect of the non-nominal lead traces was expected to degrade pilot performance, but not when the pilot is supported by the interface. Also it was expected that the most complete displays would lower the workload for the TDDA scenario as compared to the baseline display.

3-6   Results and discussion

3-6-1   Pilot controls

Figure 3-8 shows the pilot stick activity. The mean roll activity is more or less constant, but the spread is larger for lead type 3 (slow lead), $F_{2,18} = 3.338, p = 0.058$, most noticeably for the displays unaugmented for traffic; Displays 1 (baseline) and 4 (noise only + ghost). This is caused by the fact that a number of pilots applied

(a) Stick roll activity. [std % deflection from neutral]

(b) Stick pitch activity. [std% deflection from neutral]
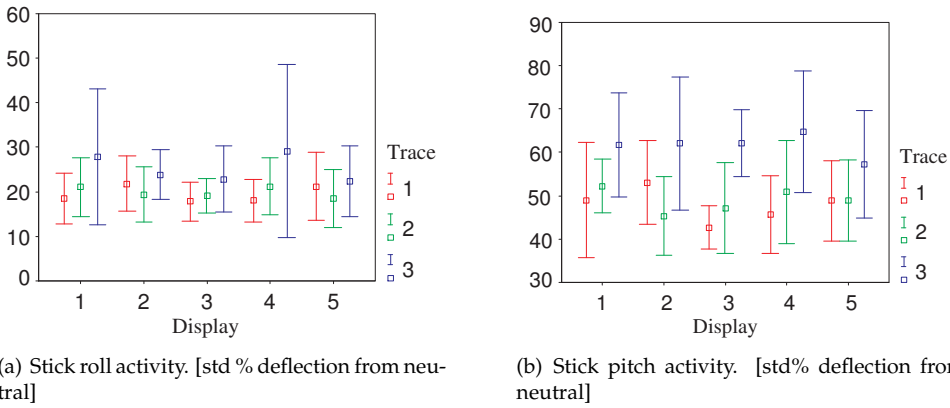
Figure 3-7: The means and the 95% confidence intervals for the pilot control activity measures.

path stretching by performing S-turns to avoid violating the minimum separation. Apparently the addition of spacing information either implicitly (noise + traffic flap cues) or explicitly (ghost symbol) results in better response to the off-nominal lead behavior.

As can be seen in Figure 3.7(b), there is significantly more pitch activity for the slow lead type, $F_{2,18} = 10.358, p = 0.001$. This can be explained by the fact that a number of pilots used the tactic of climbing slightly above the glide slope to bleed off speed faster to increase their separation. This behavior was only observed during slow lead runs. One pilot explained that this is a common tactic to reduce speed faster, where the S-turns are considered a rather drastic measure that he admitted he would not use when carrying passengers because of ride comfort issues.

3-6-2 Throttle

The number of throttle manipulations is much higher for the slow lead type, $F_{2,18} = 21.768, p < 0.001$ (see Figure 3-6-2). Following a slowlead aircraft, the pilots had to start deceleration early, selecting flaps as soon as possible, resulting in a shorter segment at idle thrust. Thus the number of speed adjustments naturally is larger during the final segment of flight where the pilot tries to maintain a constant final approach speed.

3-6-3 Cue response

Figure 3.9(a) shows the number of seconds of delay between the moment the pilot was cued to select the next flaps and the time he actually did this. Positive values mean delay and negative values indicate flap selection before the cue. One thing
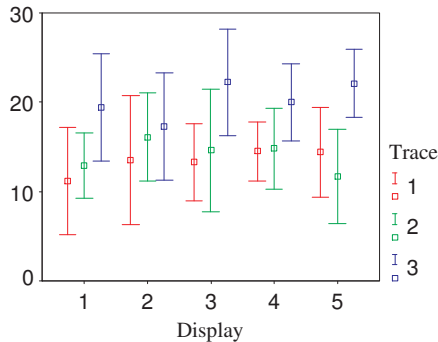
Figure 3-8: The means and the 95% confidence intervals for the number of throttle adjustments. [-].

that stands out is that for lead type 3, pilots typically selected flaps before they were cued to do so, except with Displays 3 and 5. This can be readily explained by the fact that Displays 3 and 5 were the only displays with traffic-optimized cues, so in these cases the pilots could just follow the cues. In all other cases the slow lead type forced pilots to deviate from the flap schedule to maintain separation. The effect of display type is indeed highly significant, $F_{4,36} = 7.723, p < 0.001$. It is also noteworthy that without a ghost display (Display 3), pilots tended to adhere strictly to the cues, but when the ghost was added (Display 5) a spread in the cue response could be observed. Pilots indicated that with the ghost symbol they had a better understanding of the situation and were more relaxed in following the flap cues.

3-6-4 Operational performance

One of the hypotheses was that pilots would perform better when using the more advanced displays, not violating the minimum separation and adhering to the optimum TDDA profile as closely as possible. As the following results indicate, although performance did indeed improve through the use of the displays, the greatest improvement was found in the reduction of pilot workload.

3-6-5 Separation goals

Figure 3.9(b) shows the separation behind the lead aircraft when the aircraft descends through 1,000 ft. Values of less than 2.5 nm indicate a violation of the minimum safe separation. As can be seen in the plot, almost all of the pilots violated the minimum separation when they were trailing a slow lead. A trend toward better performance for the fully optimized cues (Displays 3 and 5) and the ghost display (Displays 4 and 5) is discernible. Also the pilots finished with less excess spacing
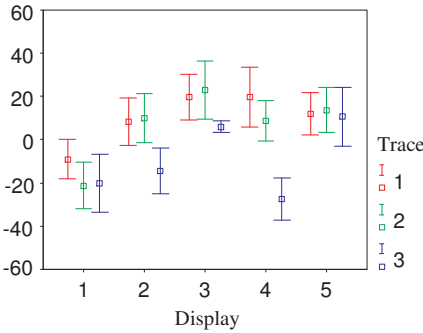
(a) Time between the presentation of the flap cue and the pilot's response to it. [s]
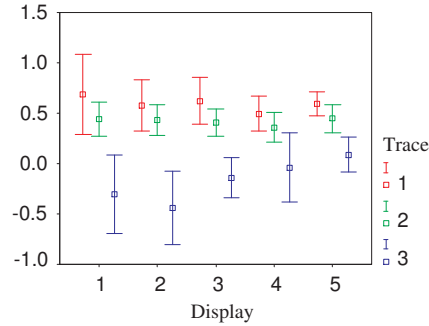
(b) Separation when descending through 1,000 feet. [NM]
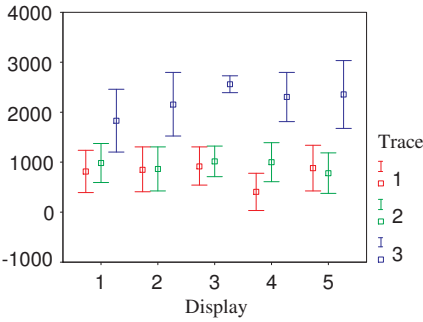
(c) Altitude at which V_{APP} was reached. [ft]
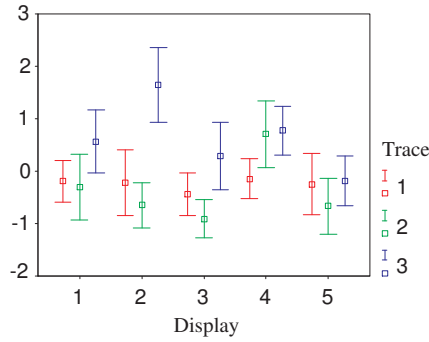
(d) Means and the 95% confidence intervals for the normalized TLX ratings. [-]

Figure 3-9: The means and the 95% confidence intervals for pilot performance measures.

when they have more support from the display; however, the effect of the display is not statistically significant. One point worth noting here is that Display 1 was not a real baseline display, in that the traffic information delivered by ADS-B is more accurate than current TCAS can provide. Also, current cockpits lack the display of closure rate information as used in the experiment. Almost all pilots indicated in the questionnaire that they found this closure rate information to be very useful, with some pilots even claiming that they used the closure rate in lieu of the ghost display.

3-6-6 Noise goals

As can be expected, the altitude at which V_{app} is reached is higher for the slow lead runs, as can be seen in Figure 3.9(c). Again, when pilots are presented with fully

optimized cues, but no ghost symbol to verify it (Display 3), they tend to closely follow the clues. Also it is clear that the pilots typically were capable of reaching V_{app} at 1,000 ft without help from the cuing algorithm, as there is little difference in performance between the displays.

3-6-7   Pilot workload

After each measurement run the pilots were asked to fill out a NASA-TLX sheet to assess the workload they had experienced. The results, averaged and normalized into z scores for all pilots, are shown in Figure 3.9(d).

Clearly, the slow lead caused a substantially higher workload than the other lead types, although this effect seems to be less for Display 3 (noise only + ghost) and also for the displays with traffic-optimized cues (Displays 4 and 5). In fact the effect seems to be absent for Display 5. Indeed, the effect of the lead type is highly significant, $F_{2,18} = 12.875, p < 0.001$, and the type of display is also found to be highly significant on pilot workload, $F_{4,36} = 6.409, p < 0.001$, which indicates that the developed displays do indeed reduce the pilot workload where the unaugmented displays do not.

3-7   Conclusions

An automated tool has been presented for determining the flap position changes during a TDDA procedure, in which the pilot also maintains separation with the preceding aircraft. The cues for flap selection are given as bugs on the speed indicator. A navigation display with traffic information and a presentation of future separation and closure rate enables monitoring and controlling of the separation with the preceding aircraft.

The experiment results indicate a significant reduction in pilot workload with the new pilot support interface. The TDDA task itself was generally performed adequately by all pilots with or without help from the automation, as long as the lead aircraft did not deviate from the nominal profile. The use of on-line separation prediction and flap optimization reduced the effect of off-nominal lead pilot behavior on the performance, although no statistical significance could be shown using only 10 pilots. Larger scale research is required to investigate whether the trend toward better separation performance with the displays can be statistically verified.

The flap optimization algorithm as presented in this article basically functions in one of two modes; that is, it will optimize the schedule to reach a reference altitude shortly before touchdown at the final approach speed until it detects that the minimum separation will be violated, at which time the algorithm neglects any noise impact and just starts reducing the speed to increase separation. Further research should be carried out to investigate whether it is possible to control the flap speeds to reach both goals simultaneously.

References

[1] Minimum Aviation System Performance Standards for Automatic Dependent Surveillance Broadcast (ADS-B). Technical Report RTCA/DO-242, RTCA, Inc., Washington DC, USA, Feb 1998.

[2] J.-P. Clarke. Systems Analysis of Noise Abatement Procedures Enabled by Advanced Flight Guidance Technology. *Journal of Aircraft*, 37, no. 2(AIAA 97-0490), Mar-Apr 2000.

[3] J.-P. Clarke and R. J. Hansman. A Systems Analysis Methodology for Developing Single Event Noise Abatement Procedures. Technical Report ASL-97-1, MIT - Aeronautical Systems Laboratory, Cambridge (MA), USA, Jan 1997.

[4] T. J. Davis, D. R. Isaacson, J. E. Robinson III, W. den Braven, K. K. Lee, and B. Sanford. Operational Test Results of the Passive Approach Spacing Tool. In *IFAC 8th Symposium on Transportation Systems 97*, Chania, Greece, Jun 16-18 1997.

[5] T. J. Davis, K. J. Krzeczowski, and C. Bergh. The Final Approach Spacing Tool. In *13th IFAC Symposium on Automatic Control in Aerospace*, Palo Alto (CA), USA, Sep 1994.

[6] J. L. de Prins, K. F. M. Schippers, M. Mulder, M. M. van Paassen, A. C. in 't Veld, and J.-P. Clarke. Enhanced Self-Spacing Algorithm for Three-Degree Decelerating Approaches. *AIAA Journal of Guidance, Control & Dynamics*, 30(5):576–590, Mar-Apr 2007.

[7] L. J. J. Erkelens. Research on Noise Abatement Procedures. Technical Report NLR TP 98066, National Aerospace Laboratory (NLR), Amsterdam, The Netherlands, Feb 1998.

[8] L. J. J. Erkelens. Development of Noise Abatement Procedures in The Netherlands. Technical Report NLR TP 99386, National Aerospace Laboratory (NLR), Amsterdam, The Netherlands, Nov 1999.

[9] S. G. Hart and L. E. Staveland. Development of a Multi-Dimensional Workload Rating Scale: Results of Empirical and Theoretical Research. *Human Mental Workload*, pages 139–183, 1988.

[10] N. T. Ho and J.-P. Clarke. Mitigating Operational Aircraft Noise Impact by Leveraging on Automation Capability. In *Proceedings of the AIAA Aircraft, Technology, Integration and Operations Forum*, number AIAA 2001-5239, pages 1–8, Los Angeles (CA), USA, Oct 16-18 2001.

[11] A. C. in 't Veld and J.-P. Clarke. Trajectory Prediction or Self-Separation during Decelerating Approaches in a Data-Link Environment. In *AIAA Aircraft Technology, Integration and Operations (ATIO) Forum*, number 2002-5887, Los Angeles (CA), USA, Oct 2002.

[12] A. C. in 't Veld, M. Mulder, M. M. van Paassen, and J.-P. Clarke. Pilot Support for Self-Separation during Decelerating Approaches. In *12th International Symposium on Aviation Psychology (IJAP)*, Dayton (OH), USA, Apr 2003.

[13] A. D. Kershaw, D. P. Rhodes, and N. A. Smith. The Influence of ATC in Approach Noise Abatement. Napoli, Italy, Jun 13-16 2000.

[14] M. F. Koeslag. Advanced Continuous Approaches, an Algorithm Design for the Flight Management System. Technical Report NLR-TR-2001-359, National Aerospace Laboratory (NLR), Amsterdam, The Netherlands, Mar 1999.

[15] K. K. Lee and T. J. Davis. The Development of the Final Approach Spacing Tool (FAST): A Cooperative Controller-Engineer Design Approach. *Journal of Control Engineering Practice*, 4(8):1161–1168, Aug 1996.

[16] R. M. Oseguera-Lohr, G. W. Lohr, and T. S. Abbot. Evaluation of Operational Procedures for Using a Time-Based Airborne Inter-Arrival Spacing Tool. In *AIAA Aircraft Technology, Integration and Operations Forum (ATIO)*, number 2002-5824, Los Angeles (CA), USA, Oct 2002.

[17] C. Quinn and J. E. Robertson III. A Human Factors Evaluation of Active Final Approach Spacing Tool Concepts. In *3rd USA/Europe Air Traffic Management R&D Seminar*, Napoli, Italy, Jun 2000.

[18] L. Ren, J.-P. Clarke, and N. T. Ho. Achieving Low Approach Noise without Sacrifying Capacity. In *22nd Digital Avionics Systems Conference*, number AIAA-2001-5239, pages 1–9, Indianapolis (IN), USA, Oct 12-16 2003.

4

Distance Based Self-Spacing

Enhanced Self-Spacing Algorithm for Three-Degree Decelerating Approaches

J.L. de Prins, K.F.M. Schippers, M. Mulder, M.M. van Paassen, A.C. in 't Veld and
J.-P. Clarke

4-1   Abstract

A current trend in aircraft noise abatement around airports is exploiting the benefits
of procedural means with computational aids, such as on-board and ground-based
trajectory prediction algorithms and displays. The challenge for these upcoming
Advanced Noise Abatement Procedures is to mitigate the noise impact without sac-
rificing runway capacity. The proposed solution, implemented in the Three-Degree
Decelerating Approach (TDDA), is to delegate the task of separating the aircraft to
the cockpit during the approach. To assist the pilots, a flap/gear scheduling algo-
rithm with a complementary interface has been developed that takes noise nuisance
and in-trail separation into account. The design and functionality of this pilot sup-
port system is presented in-depth and evaluated with three experiments. Off-line
Monte-Carlo simulations indicated an adequate and consistent performance and
robustness of the self-spacing algorithm for various wind and traffic scenarios. A
pilot-in-the-loop simulator experiment verified that with the aid of the algorithm,
pilots were able to execute the noise abatement procedure consistently while main-
taining safe separation at all times. The support system showed to reduce pilot
workload up to an effort level comparable to current standard approaches. The
whole concept was demonstrated with an in-flight exploratory investigation which

confirmed the conflict-free performance benefits of the algorithm and the feasibility of self-spacing during continuous decelerating/descent approaches under actual flight conditions.

4-2   Introduction

Several Advanced Noise Abatement Procedures (ANAPs) have been developed, evaluated and continuously improved over the last few years, like the Continuous Descent Approach (CDA)[1,2,5,10,23] whose prototypes are already operational at a few airports during night-time, the Two-Segment Approach (TSA),[4,8,12] the Advanced Continuous Descent Approach[11,16] and the Three-Degree Decelerating Approach (TDDA).[17] These studies have resulted in several piloted simulator experiments emphasizing on noise impact and operational characteristics[8,10,12] and have been recently extended into a flight demonstration test of the CDA procedure at Louisville International Airport.[5,9] Although successful in reducing noise, runway capacity problems have restricted the implementation of the noise abatement procedures to the lower traffic density hours.[23] The main reason is the inability of Air Traffic Control (ATC) to properly separate aircraft that are decelerating at significantly different rates.[14] To compensate for these uncertainties, controllers apply larger separations than necessary resulting in a capacity loss with respect to conventional approaches.[15]

A possible solution to decrease separation distances is to delegate the spacing task to the pilot. In 't Veld et al. (2004) designed an automated tool for determining the flap position changes during a Three-Degree Decelerating Approach procedure, that additionally takes minimum separation constraints with the preceding aircraft into account. A pilot support interface has been developed as well to present the output of the flap scheduling algorithm. Piloted simulator experiments indicated that the algorithm performs adequately in zero-wind conditions and is beneficial especially in off-nominal traffic scenarios.[15] The promising research results created a drive towards enhancing the flap scheduling algorithm to expand its general performance and applicability in multiple wind conditions,[7] this all in consideration of evaluating the feasibility of self-spacing during decelerating approaches under actual flight conditions.

The purpose of this paper is twofold. First and foremost, the design and functionality of the developed flap/gear scheduling algorithm is described in-depth. Second, results of three experiments will be presented. Monte Carlo simulations were designed to evaluate performance of the algorithm in various wind and traffic scenarios, and its sensitivity to relevant prediction errors.[7] The second experiment was a proof of concept to demonstrate the viability of the designed algorithm in real flight.[18] Finally, a pilot-in-the-loop simulator experiment was conducted to explore operational performance and benefits of the support system, including workload assessment, when pilots are confronted with the self-spacing task during a TDDA.[18]
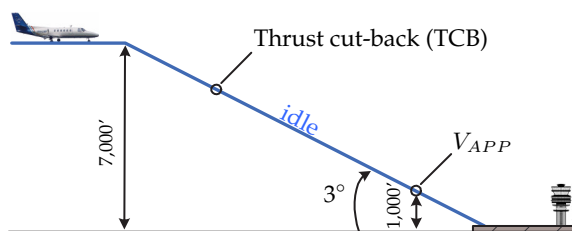
Figure 4-1: The Three-Degree Decelerating Approach.

4-3 The Three-Degree Decelerating Approach and Support System

4-3-1 The Approach Procedure

A Three-Degree Decelerating Approach (TDDA), illustrated in Figure 4-1, requires the aircraft to descend along the fixed 3° ILS flight path to the runway, starting at higher altitude and at higher speeds than the conventional ILS approach. The initial altitude and speed could be for example 7,000 ft and 250 kts, respectively. Speed reductions are achieved by applying idle thrust during the descent and letting the aircraft decelerate along the fixed glide path according to the existing drag forces. This aerodynamic drag is controlled with the selection of flaps and gear. Ultimately, the aircraft should reach the final approach speed V_{APP} (in indicated airspeed (IAS)) at the reference height h_{APP} of 1,000 ft above the runway in complete stabilized landing configuration, and this without applying thrust.[15] At this point thrust can be added to land the aircraft following common procedure. To aid the pilot with managing the aircraft configuration and longitudinal spacing a flap/gear scheduling algorithm has been designed.

4-3-2 The Optimization Algorithm

The moment at which engine thrust must be reduced and the next flap setting or gear must be extended is accurately calculated by a flap/gear optimization algorithm. The flap/gear scheduling routine has two objectives. First of all, minimum safe separation must be assured with the predecessor, i.e., 2.5 NM in case of two light aircraft trailing each other.[14] The second objective is to optimize the flap/gear schedule such that the target speed V_{APP} is reached at the reference altitude h_{APP} without adding thrust. These two objectives will be referred to as, respectively, the *separation goal* and the *noise goal*.

Although reaching V_{APP} below h_{APP} is more beneficial for noise production, the noise goal has been augmented with the constraint that aircraft should be fully

established in landing configuration as close to h_{APP} as possible. Therefore, in the remainder of this paper, re-engaging thrust below h_{APP} will also be referenced as a decline in 'noise' performance.

Since the TDDA is executed with idle thrust along a fixed flight path, the moments of thrust cut-back, flap and gear selection are the only control options to properly achieve the goals. During the descent, the number of control options gradually decreases as thrust is fixed at idle and flaps are selected one by one. Consequently, it is desirable to keep the largest control authority for the latest flap setting, in both tuning directions, such that the algorithm is still able to correct unexpected deviations during the final part of the TDDA. Hereby, the performance of the TDDA objectives can be maximized. The complete flap/gear tuning algorithm is elaborated in detail in section 4-4. For simplicity, the flap/gear optimization algorithm will be referred to as the flap algorithm or flap scheduler from this point on.

4-3-3   The Pilot Support Interface

To support the pilot in his task of flying the TDDA, cues have been added to the Primary Flight Display (PFD) and Navigation Display (ND),[15,18] see Figure 4-2. A green Thrust cue 'T' on the altitude indicator exhibits the thrust cut-back altitude. A green Flap cue 'F' on the airspeed indicator shows the speed of the aircraft at which the next flap has to be selected. A yellow 'G' cue indicates the optimized speed of landing gear selection. The calculated airspeed at which the flap or gear should be extended, is shortened to the term *flap speed* and *gear speed* in the remainder of this paper. When speed brakes or thrust are required, ADD DRAG or ADD THRUST annunciations pop-up.

The Navigation Display (ND) is provided with continuous information on aircraft in the vicinity using standard Traffic Alert and Collision Avoidance System (TCAS) symbology. Additionally, the display has been augmented with information on the future separation trend by adding a *predicted separation arc*.[18] The separation arc indicates the difference between predicted separation at the threshold and minimum safe separation with respect to the current position of the lead aircraft. Thus, when the arc is below the lead aircraft, safe separation is guaranteed. On the other hand, an arc encapsuling the lead indicates future violation of safe separation. In this way, the separation arc serves as an interactive safety corridor, which facilitates pilot's interpretation of the situation.

4-4   The Enhanced TDDA Algorithm

A prediction and optimization algorithm has been developed[15,16] and enhanced[7] to aid the pilot with his self-spacing task and his task to arrive with V_{APP} at the reference height. The routine determines at what altitude thrust should be reduced and at what speed each flap setting and the gear should be selected. This section
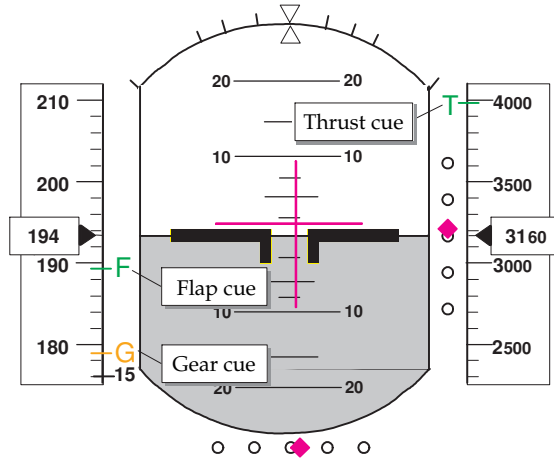
(a) Primary Flight Display.
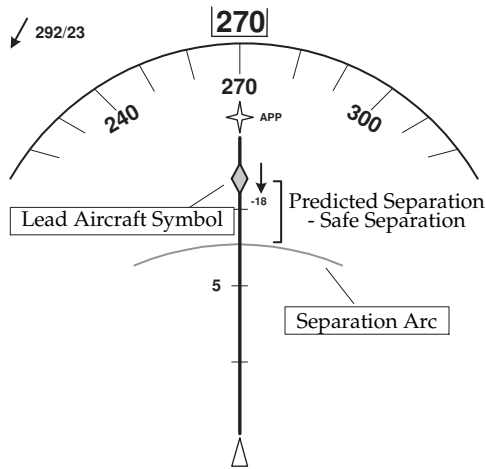
(b) Navigation Display.

Figure 4-2: Primary Flight Display (PFD) and Navigation Display (ND) extended with cues from the pilot support system. The thrust cue 'T' on the PFD altitude tape shows the thrust cut-back altitude calculated by the algorithm; the flap cue 'F' on the PFD speed tape indicates the optimized flap speed at which the next flap should be selected. The filled diamond on the ND shows the current position of the lead, while the separation arc on the ND shows the difference between predicted and minimum safe separation with the predecessor.

presents a detailed description of the algorithm's prediction methods and control laws to satisfy the noise and separation goals simultaneously, under various atmospheric conditions.

4-4-1   Structure of the Flap Optimization Algorithm

The design of the flap optimization algorithm is illustrated in Figure 4-3. First the trajectory of the lead aircraft is predicted. Next, a prediction of the own trajectory is made given the last calculated flap schedule, current aircraft state and estimated wind. Both traces are then compared, yielding the predicted separation trend. If separation is expected to be violated, the flap selection moments are tuned to slow down earlier and hence increase separation. To determine the proper flap speeds, the iteration process first distinguishes between the situations where the aircraft is above or below the thrust cut-back altitude (h_{TCB}). These situations respectively correspond to the *CAPTURE* mode and the *HOLD* mode of the flap scheduler, respectively:

- In *CAPTURE* mode the algorithm calculates the altitude at which the thrust should be set to flight-idle (h_{TCB}). This altitude is determined by the *start altitude optimization* routine such that safe separation is assured while still being able to reach the reference height without applying thrust. As soon as the calculated start altitude is reached the algorithm switches to *HOLD* mode.

- In *HOLD* mode, the flap scheduler runs the *Noise & Traffic (N&T) optimization* routine to adjust the flap/gear speeds. If however, in this part of the approach, separation is predicted to be violated, the noise and separation goals can not be combined anymore. Flaps must be extended at higher speeds to decelerate earlier and increase spacing. Consequently, the aircraft will get to V_{APP} too early and extra thrust is required. The algorithm will now primarily tune the flaps to guarantee safe separation before the target speed is looked after.

The flap schedule tuning process is a binary search algorithm,[15] starting with a coarse flap-tuning routine, followed by a fine-tuning process to determine a satisfying flap schedule. During the rough-tuning, the first coming flap stage is set to its upper/lower bound, followed by the next flap and so on until the relevant constraint (separation or noise) is overcorrected. At each adjustment the trajectory and separation trend are recalculated to check with the constraints. The upper and lower bounds for each flap speed are given by the flap placard speed and the minimum maneuvering speed, respectively. The applicable constraints are further discussed in the description of the Noise & Traffic optimization of section 4-4-6. When the relevant criterion is exceeded, the last adjusted flap setting is fine-tuned to get the constraint within its demanded margins. Fine-tuning is done by setting the last tuned flap speed to midpoint between the nominal speed and the last set
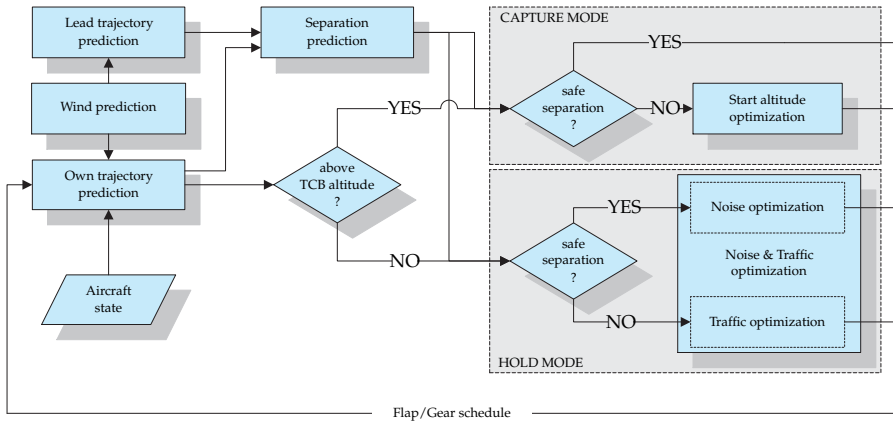
Figure 4-3: Structure of the flap scheduler algorithm.

boundary. This process of setting the flap speed halfway the current midpoint and the previous boundary, is repeated until the applicable constraint is met. It is noted that the term 'optimization' is not entirely correct as the automated tool does not search for the most optimal flap schedule, but rather a satisfactory one, possibly with a small sacrifice in noise abatement. Therefore, '*satisficing*' would be a better expression.[19]

In case flap tuning fails to ensure safe separation or to reach the target speed, the moment of extending the landing gear is an ultimate control variable that can be adjusted by the optimization algorithm. The tuning of the gear speed works identical to the flap tuning. When even the landing gear adjustments are insufficient, speed brakes or thrust must be applied and ADD DRAG or ADD THRUST annunciations are shown on the PFD.

This iteration is repeated every second to compensate for changing wind conditions and deviations from the optimal speed profile. Each element of the algorithm will be treated in more detail in the following sections.

4-4-2 Lead Trajectory Prediction

In order to get the future separation trend between the own aircraft and the predecessor, the flap scheduler needs to accurately estimate the trajectory of the leading aircraft. Its expected trace can be determined by treating the lead as a black box and predicting its future speed and position profile based on Automatic Dependent Surveillance-Broadcast (ADS-B) data.[15]

Prediction Method   The lead state-vector information, broadcast every second via ADS-B, is received on-board and stored. The trajectory prediction algorithm then fits a 4th order polynomial through this data using a least-square error fit and extrapolates this data to get future speed and distance trends, as presented in Figure 4-4. The extrapolated speed profile is cut off at the point where V_{APP} is reached. This process is executed after each ADS-B update.

The possibility of ADS-B to broadcast not only the lead's current state-vector, but also its intent information offers an increase in accuracy for the lead trajectory prediction.[15]   For a TDDA, this information could consist of the lead target speed $V_{APP,l}$ and corresponding reference altitude $h_{APP,l}$. The latter can be easily transformed to the reference position $x_{APP,l}$ given the three degree glide path angle. This extra data point is added to the historical data to get a more accurate fit, as illustrated in Figure 4-4.

The intent information however cannot be used in the time domain since the time at which the lead reaches $V_{APP,l}$ is unknown. To work around this problem, $V_{APP,l}$ (IAS) is converted to $V_{g_{APP,l}}$ (groundspeed). Knowing that the groundspeed V_g is the derivative of the traveled distance (and thus position x), the resulting first order ordinary differential equation can be solved:

$$\left.\begin{array}{rcl} V_g & = & \dot{x} \\ V_g & = & f(x) \end{array}\right\} \quad \dot{x} = f(x), \tag{4-1}$$

where $f(x)$ is the polynomial fit through the known data points in the $x - V_g$-plane of Figure 4-4. Next, the predicted lead trace $u(t)$ is constructed in the time domain using the Runge-Kutta numerical integration routine[21] of Eq. (4-2). The lead's current position is the starting point u_0 of the integration loop. The routine iterates until it reaches the approach speed of the lead, $f(u_{i+1}) = V_{g_{APP,l}}$.

$$\begin{array}{rcl} k_1 & = & hf(u_i) \\ k_2 & = & hf(u_i + 0.5k_1) \\ k_3 & = & hf(u_i + 0.5k_2) \\ k_4 & = & hf(u_i + k_3) \\ u_{i+1} & = & u_i + (k_1 + 2k_2 + 2k_3 + k_4)/6 \end{array} \tag{4-2}$$

The accuracy of the prediction is further improved by passing the ADS-B data through a sliding gain filter.[15]   Older data are filtered out: only the most recent 100 data points are used. The intent information is weighed 10 times as much as a normal measurement.

The lead trajectory prediction described above only generates the decelerating segment of the approach until $V_{APP,l}$ is reached. Then the lead is expected to maintain this speed along the ILS track to the runway, like in Figure 4-4. Therefore, a
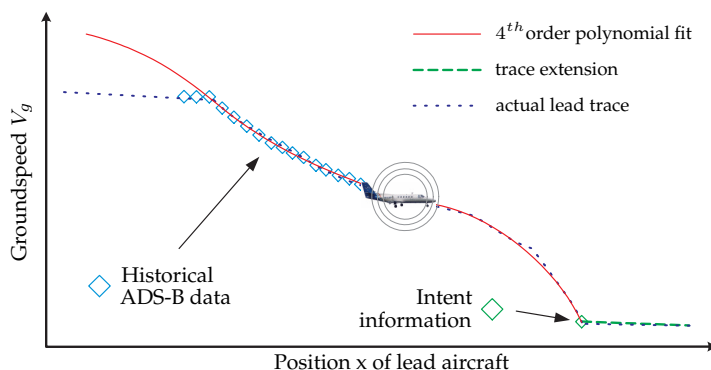
Figure 4-4: Lead trajectory prediction: 4th order polynomial fit through historical ADS-B data (last 100 points) and intent information. At the end, the predicted trajectory is extended with a constant speed trace ($V_{APP,l}$).

path with constant indicated airspeed $V_{APP,l}$ and corresponding traveled distance is added after the above predicted speed and distance profile.

Accuracy of the Prediction   The error in the lead trajectory prediction varies with:

- the governing wind condition.

- the number of data-points received. If not enough data is available, the prediction deviates and is unusable. Hence, the lead trajectory is generated as soon as 80 data points are available, in other words after 80 seconds in the approach. Since aircraft are initially separated approximately 2 minutes apart, enough lead data is available to estimate an accurate trajectory at the beginning of the TDDA. The accuracy increases when more data points become available.

- the length of the time interval over which the extrapolation is carried out. The accuracy of the prediction increases closer to the runway since cumulative errors have less time to grow.

- the deceleration characteristics of the lead type. This effect is elaborated further in the next section.

Correction to Prediction Algorithm   Although the described approach for the lead trajectory prediction proved to be accurate for a Boeing 737 lead aircraft,[15] the performance of the prediction method with a 4th order polynomial decreases with a Cessna C500 Citation I lead type. The predicted separation deviates up to a few nautical miles and decreases well below the minimum safe separation of 2.5 NM.
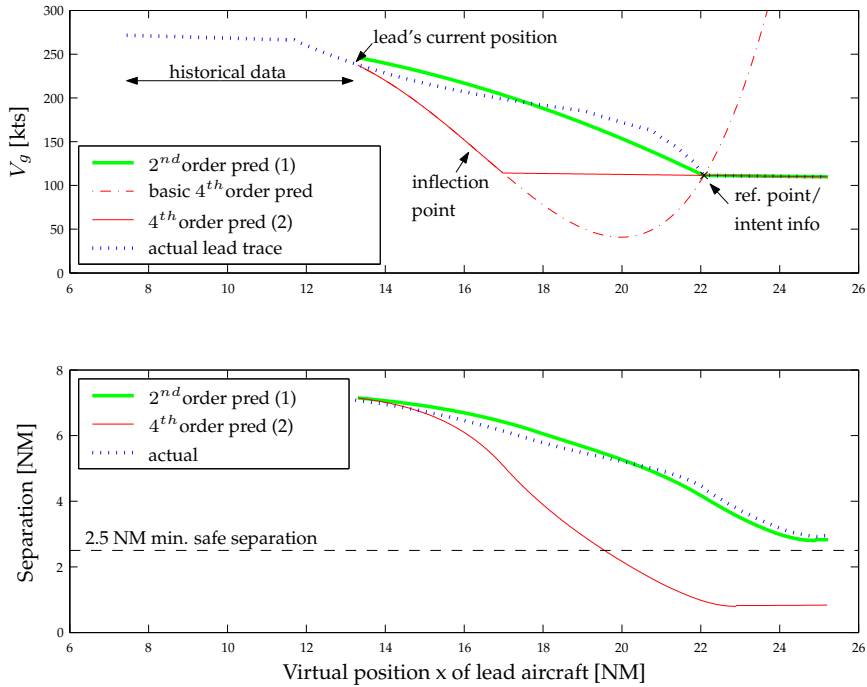
Figure 4-5: Lead trajectory prediction and separation prediction. Underestimation of the lead's ground speed with 4th order polynomial (2) produces a predicted separation trend far below the minimum safe separation. Trajectory prediction with a 2nd order polynomial (1) improves the separation prediction.

Consequently, the algorithm is unable to determine a proper thrust cut-back altitude that satisfies the noise goal in addition to the separation goal. The described diverging prediction is caused by a temporary underestimation of the lead's speed profile.

Figure 4-5 gives an impression of the effect in zero-wind conditions. Due to the convex part in the deceleration profile of the Citation I model (dotted line), the algorithm temporarily creates a convex 4th order extrapolation between the historical data and intent information (dashed line). This convex deceleration characteristic is not present in the 737 speed profile.[15] Although the algorithm corrects the polynomial fit for the lead aircraft known $V_{APP,l}$ (fine solid line (2)), it underrates the lead's ground speed to a large extent and consequently also the separation trend, as clearly indicated in the second plot of Figure 4-5.

A 3rd order polynomial naturally consists of a convex and concave segment, so is not a valid solution. A 2nd order polynomial is forced into the concave curvature due to the initial constant speed segment and therefore reduces the temporary underestimation of the 4th order prediction to a large extent, as shown in Figure 4-5 (bold solid line (1)). However, it results in a less accurate prediction of the separation trend later during the approach. Therefore it has been decided to keep the more accurate 4th order polynomial but switch over to a 2nd order prediction when the underestimation occurs. The trigger for this correction is the position of one of the inflection points of the polynomial: a relatively good polynomial is found as long as the inflection point lies to the right of the reference point or in other words when the second derivative at the lead's reference point is negative. As soon as the 2nd derivative gets positive, the polynomial is reduced to a second order one until the inflection point moves back to the right of the reference point. This correction is sufficient to diminish the divergence in predicted separation and makes the algorithm able to combine adequate noise and separation performance.

4-4-3 Own Trajectory Prediction

Due to the need to calculate the speed profile multiple times per second, the own trajectory is determined using a simple aerodynamic model.[15] The aerodynamic model has been reviewed for application with a Cessna C500 Citation I in order to be used during the in-flight experiment.

Aerodynamic Model The aerodynamic model is a 'point mass' aircraft model with constant mass that only looks at the forces in the symmetric plane of the aircraft (2D). The simulation results will clearly indicate that the influence of lateral force and velocity components can be neglected without significantly reducing the performance of the trajectory prediction. The addition of wind generates a small difference between kinematic flight path angle γ_k and aerodynamic flight path angle γ_a as presented in Figure 4-6. γ_k corresponds to the three degree ILS glide path.
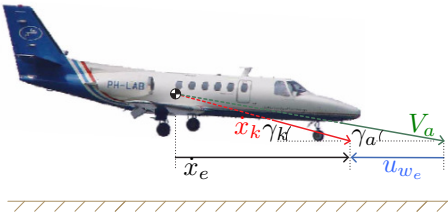
Figure 4-6: The difference between kinematic flight path angle γ_k and aerodynamic flight path angle γ_a
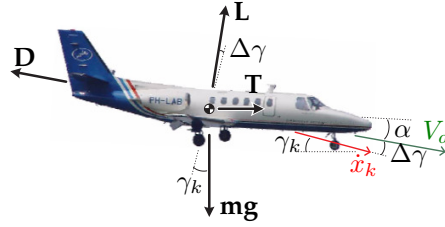
Figure 4-7: Force diagram for 'point mass' aircraft model

γ_a can be determined using two-dimensional trigonometry from the true airspeed (TAS) V_a, defined in the aerodynamic reference frame F_a, and the current ground speed $\dot{x}_e$ and along-track wind speed component u_{w_e}, both defined in the standard Geodetic reference frame F_e (North-East-Down):

$$\gamma_a = \arccos\left(\frac{\dot{x}_e - u_{w_e}}{V_a}\right), \tag{4-3}$$

where V_a can be calculated according to:

$$V_a = \sqrt{(\dot{x}_e - u_{w_e})^2 + (\dot{x}_e \tan \gamma_k)^2}. \tag{4-4}$$

The changing aerodynamic flight path angle causes a small component of the lift force appearing along the three degree glide path. Due to the low speed envelope of the Citation I, $\Delta\gamma$ ($= \gamma_k - \gamma_a$) is relatively large for a Citation (in comparison to for example a B747) and so is the resulting lift component along the flight path which can not be neglected with respect to the thrust and drag force.

Using the force diagram of Figure 4-7 and assuming that the angle of attack α is small ($T\cos\alpha \approx T$, $T\sin\alpha \approx 0$), the following equations of motion can be derived in the kinematic reference frame F_k, along the fixed flight path:

$$
\begin{aligned}
\Sigma F_z: &\quad 0 = & L\cos\Delta\gamma - mg\cos\gamma_k + T\sin\Delta\gamma - D\sin\Delta\gamma \\
\Sigma F_x: &\quad m\ddot{x}_k = & -L\sin\Delta\gamma + mg\sin\gamma_k + T\cos\Delta\gamma - D\cos\Delta\gamma
\end{aligned} \tag{4-5}
$$

Eqs. (4-5) hold if the aircraft is assumed to fly at a constant 3° approach angle (γ_k) and no turns are made. To simplify the calculation of the lift L, the vertical equilibrium of Eqs. (4-5) is further reduced by omitting the relatively small thrust and drag components ($T\sin\Delta\gamma$ and $D\sin\Delta\gamma$).

The lift L easily yields the lift coefficient C_L which is subsequently used to calculate the drag coefficient C_D with an approximation of the drag polar:

$$C_D = c_1 {C_L}^2 + c_2 C_L + c_3 \tag{4-6}$$

where the coefficients c_1, c_2 and c_3 are dependent on flap and gear setting.

During the TDDA the engine setting remains idle. Idle thrust primarily depends on the flap position and the true airspeed. Altitude and temperature effects are neglected. The thrust can be calculated using the following second order polynomial:

$$T = t_1 V_a{}^2 + t_2 V_a + t_3 \tag{4-7}$$

Model evaluation indicated that coefficients t_1 and t_2 are fixed per flap/gear position. The value of t_3, however, depends on the airspeed at which flaps and gear are set. Therefore an initial estimate is taken for t_3 given the nominal flap schedule. To improve the thrust estimation during the approach, the predicted idle thrust curves are constantly corrected using current calculated thrust. This *thrust-prediction-error limiter* substitutes the momentary thrust and true airspeed in Eq. (4-7), yielding an updated t_3 every second.

With Eqs. (4-3) to (4-7) the acceleration along the flight path $\ddot{x}_k$ is determined. This acceleration is then integrated in time with a time step of one second, following the scheme of Figure 4-8, yielding the predicted speed and distance trajectories.

Calculation Direction   The described prediction model of Figure 4-8 can create the trajectory in two directions. It can start at h_{APP} with V_{APP} and calculate backwards until current airspeed is reached (*back-calculation*). Or the model can start at the current height and airspeed and predict the decelerated descent to V_{APP} (*forward-calculation*). The switching between both methods is easily done in real-time by just swapping the initial and end constraints, and adding a minus sign on the left-hand side of the longitudinal equation of motion in case of back-calculation.

Both methods have their particular advantages. When a time-dependent wind profile estimation is utilized,[6] the back-calculation method needs to know the point in time when the aircraft is at the reference height. But in order to determine that time, the aircraft trajectory must be known. Hence, forward-calculation, which starts at the current time, is preferred. However, forward-calculation is not useful to determine the thrust cut-back altitude since this would require multiple iteration loops until the correct altitude is found. Therefore the use of back-calculation is preferred in *CAPTURE* mode which needs only one iteration. Naturally the problem of the unknown time-at-h_{APP} remains. The proposed solution is to take an initial estimate of that time and update it every iteration loop by using the calculated time at h_{APP} from the last iteration.

Trace Extensions   The aerodynamic model only determines the trajectory part of the decelerating descent. To get a complete trajectory prediction, the own trajectory is extended in two ways. Above the thrust cut-back altitude, a constant speed segment is added from the current altitude to h_{TCB}, corresponding to the aircraft's actual indicated airspeed. Below the reference height, when thrust is reapplied: a segment of constant indicated airspeed V_{APP} is added after the trace to the runway.
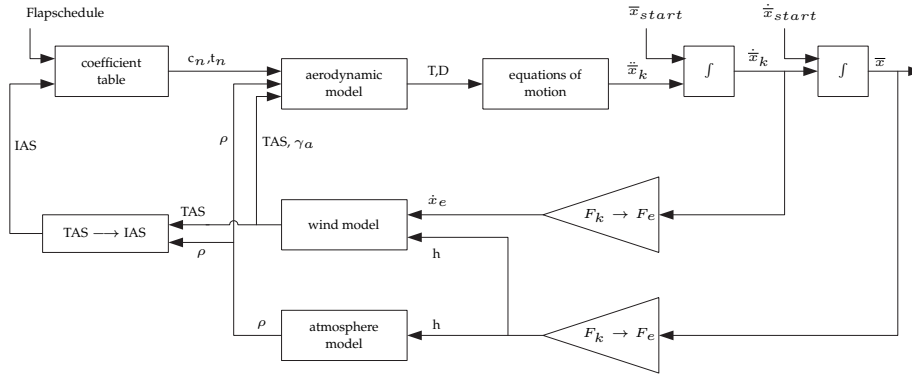
Figure 4-8: Own trajectory prediction model. The start position vector $\overline{x}_{start}$ and start velocity $\dot{\overline{x}}_{start}$ could be either the current aircraft position and speed (*forward-calculation*) or the reference point and approach speed vector (*back-calculation*).

4-4-4   Separation Trend Prediction

With the predicted trajectories for the lead and the own aircraft, the separation trend can be easily calculated. Since the separation trend shows 'closing characteristics', the minimum predicted separation is found at or near the runway threshold. No additional smoothing filter is required.

4-4-5   Start Altitude Optimization

The optimization of the start altitude makes the algorithm able to achieve good noise performance in combination with safe in-trail spacing. The idea is to alter h_{TCB} in such a way that minimum predicted separation increases to a safe level while still being able to reach the target speed without applying thrust. When predicted separation gets problematic after thrust cut-back, it is no longer possible to satisfy both goals. Then, flaps must be extended at higher speeds to decelerate earlier and increase spacing. Consequently, the aircraft will get to V_{APP} too early and extra thrust is required.

The start altitude optimization process only alters h_{TCB} when separation is predicted to get dangerous (Figure 4-3). When safe spacing is guaranteed, no actions are taken. In case of separation excess, the algorithm could also schedule a lower h_{TCB}. However, this requires further investigation into the design of the algorithm's control laws in order to achieve similar performance results as for the conducted Monte Carlo simulations (section 4-5).

Although separation is increased in *HOLD* mode by extending flaps sooner (at higher airspeeds), the mode of thought for the start altitude optimization is
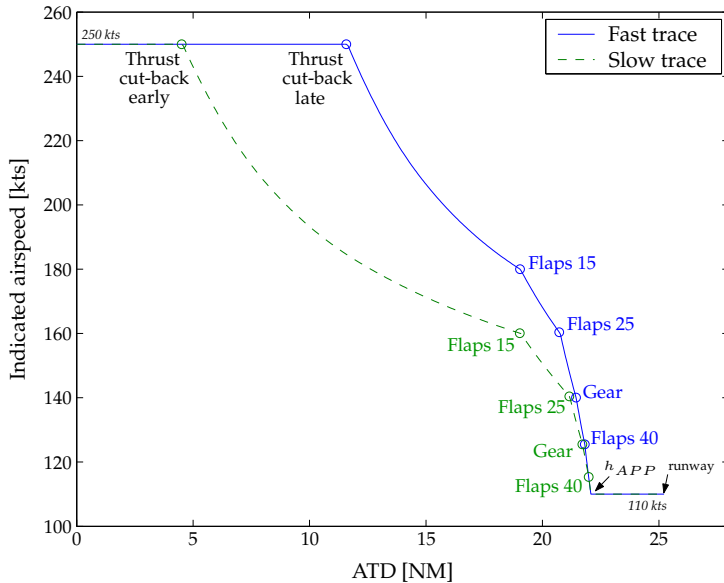
Figure 4-9: Indicated airspeed as function of Along Track Distance (ATD) for a fast and slow approach with the Citation I in zero-wind.

completely opposite. To increase spacing, the time to fly the approach must be longer which corresponds to a lower mean airspeed of the own aircraft throughout the approach. This can only be achieved by decelerating earlier or in other words increasing the thrust cut-back altitude. Since the same amount of kinetic energy must be dissipated and deceleration has been started earlier, the parts of the approach with high deceleration rates (i.e., the segments at the end of the approach, flown with higher flap positions) must be shortened. Consequently, the flap speeds must be *lowered*. Figure 4-9 gives a good indication of the difference between a 'fast' and a 'slow' approach.

The start altitude optimization tunes the flap speeds every second in such a manner that the minimum predicted separation shifts within a distance margin of 0.05 to 0.1 NM above minimum safe separation. This range is chosen to keep a safety margin with respect to the minimum safe spacing on one hand, and to avoid a large overshoot on the other hand. For the latter, it is best to avoid too low flap speeds (i.e., large separation) because this would limit the control range of the flaps/gear when tuning is required later during the approach due to sudden environment changes, uncertainties or prediction errors. As mentioned earlier, it is preferred to save the maximum amount of control authority for the last flap settings.

The coarse and fine-tuning processes are according to the search strategy of section 4-4-1. First, flap speeds are altered roughly to their limits until minimum predicted separation overshoots one of the boundaries of the desired separation margin. Next, if necessary, the previously shifted flap is fine-tuned to get separation within the margin.

4-4-6 Noise and Traffic Optimization

As soon as the aircraft passes the calculated thrust cut-back altitude or idle thrust is set too early, the Noise & Traffic optimization routine is activated. N&T optimization continues until the aircraft passes the altitude of the reference height plus 200 ft in order to avoid late changes of the last flap speed(s).

The Optimization Constraints   The N&T algorithm first determines the own trajectory using the last updated flap schedule and predicts the minimum separation. If all constraints are still met, no changes to the flap schedule are necessary and the algorithm stops the current loop. The constraints for N&T optimization are:

- **Separation goal**: predicted separation must be larger than minimum safe separation. If not, flap/gear speeds must be lowered.

- **Noise goal**: the aircraft must reach V_{APP} at the reference height of 1,000 ft. This constraint is included in the algorithm by checking the difference Δh between h_{APP} and the predicted altitude where the aircraft reaches V_{APP} (see Figure 4-10). When Δh is positive the aircraft is flying too slow and flap/gear speeds must be lowered. A negative Δh indicates that the aircraft is too fast, so flaps have to be extended earlier. A tuning margin for Δh of ± 5 ft is taken, since the altitude corresponding to V_{APP} can only be predicted with an accuracy of maximum 10 ft.

The separation goal has always priority over the noise goal since safety prevails. In case one of the above constraints is violated, the binary search algorithm looks for a satisfying flap schedule.

The Flap Optimization Process   The flap scheduling process has a rough and fine-tuning cycle, as discussed in section 4-4-1. Flap speeds are increased when separation is in danger OR Δh is negative ($< 5ft$). Flap speeds are decreased when Δh is positive ($> 5ft$) AND separation is not a problem. After each flap speed change, the trajectory is recalculated. If tuning for separation, the algorithm increases flap speeds to slowdown faster. Hence thrust will be applied before reaching h_{APP} (Δh is positive). The algorithm is aware of this and will try to reduce the duration of applying thrust to a minimum. This is achieved by scheduling the own aircraft as close as possible behind the lead, so within the +0.05/+0.1 NM separation margin.
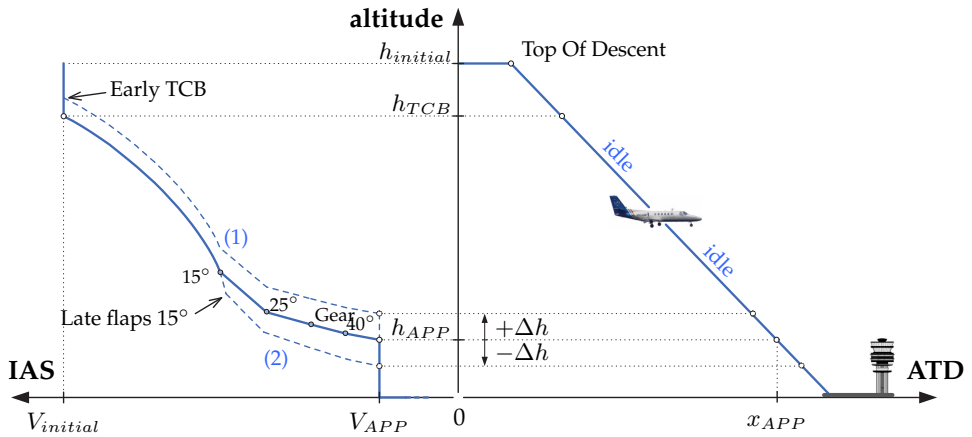
Figure 4-10: Predicted position and speed trajectory with a predicted deviation Δh with respect to h_{APP}. *Noise optimization* (reach V_{APP} at h_{APP}) reduces the constraint Δh to zero. Presented examples show a positive Δh caused by an early thrust cut-back (TCB) (1) and a negative Δh resulting from a late extension of flaps 15° (2).

4-5 Experiment 1: Monte Carlo Simulations

Experiment 1 focused on analyzing the performance of the flap scheduling algorithm for various wind and traffic scenarios and demonstrating the consistency of its achievements with repeated runs. Additionally, the experiment was also an attempt to identify the sensitivity of the algorithm to inaccuracies in the wind prediction and the own approximated aircraft characteristics that are incorporated in the trajectory predictor.

4-5-1 Method

To validate the performance of the TDDA flap scheduling algorithm multiple test scenarios have been evaluated with Monte Carlo simulations. Each of these scenarios are repeated 100 times for random turbulence conditions and varying pilot reaction times to get sufficient statistical data.

Experiment Design The Monte Carlo simulations of the TDDA procedure have been conducted off-line with a 6 degree-of-freedom non-linear model of a Cessna C500 Citation I.[20] It was opted to augment the aircraft model with an extra control variable by adding an additional flap setting, namely flaps 25°. The approach was initiated at 7,000 ft with 250 kts IAS, established on the ILS localizer (runway 360) before the glide slope interception point. The autopilot controls the entire

approach, disengaged the auto-throttle at h_{TCB}, extends flaps and gear at the calculated speeds and re-engages the auto-throttle when reaching V_{APP} to hold this velocity. V_{APP} was set at 110 kts IAS, h_{APP} at 1,000 ft.

Another Cessna Citation I performing a TDDA has been selected as a leading aircraft and was initially separated 7.5 NM in front of the own aircraft. Its trajectory took the governing winds into account. The actual wind profiles were defined according to a time-constant, rotating, logarithmic wind model.[7,22] The model demonstrated a so-called backing and veering effect of the wind vector as illustrated in Figure 4-11. Wind prediction of the flap algorithm is taken identical to the actual wind profile, disregarding turbulence.

The Monte Carlo experiment was divided in two parts. First, general performance has been evaluated following a complete test matrix. Secondly, several errors have been introduced in the algorithm to explore its robustness.

General Performance Analysis: Independent Variables   Three independent variables were varied, listed in Table 4-1, totally resulting in 36 scenarios. First, three *levels of optimization* were investigated: (1) the baseline scenario, which uses a fixed 'standard' flap/gear deflection scheme. Only h_{TCB} is calculated to comply with the governing predicted wind. (2) Noise-Only optimization (NO), where separation is not taken into account. (3) Noise and Traffic optimization (N&T), which includes the separation goal as well.

Secondly, two *lead aircraft approach characteristics*: (1) a 'nominal' approach, determined using the 'standard' flap/gear schedule; (2) a 'fastman' approach where the leading aircraft decelerates early because of early pilot deceleration actions.

Finally, six *wind conditions*: (1) zero-wind scenario; (2) and (3) head wind conditions of 20 and 40 kts; (4) 60 kts crosswind coming from a 45° direction with respect to the approach path; (5) 40 kts pure crosswind; and (6) tailwind of 20 kts.

Robustness Analysis   To evaluate the robustness in flap scheduler performance the following deviations were analyzed: (1) error between the actual and predicted wind profile, (2) error in predicted aircraft mass, and (3) error in approximated drag polar of Eq. (4-6). Only scenarios with a fastman leader are interpreted. Naturally, this traffic scenario is of more interest as it demands more optimization effort.

Random Disturbances   Two random disturbances made each run of the Monte Carlo simulation unique. The first variation is turbulence based on Dryden spectra with additional arbitrary "patchy" characteristics which introduces low-frequency gusts.[3] Secondly, pilot response times to the thrust cut-back, flap and gear cues were varied according to a Poisson probability distribution with a mean time delay of 1.75 seconds. The Poisson distribution has been leveled-off at 5 seconds, hereby defining the maximum delay.

Table 4-1: The Monte Carlo experiment matrix of 36 test scenarios, formed with three independent variables, i.e. *level of optimization*, *lead approach characteristic* and *wind condition*.

Optimization level	Lead trace	Wind condition[*]					
		360/00	360/20	360/40	045/60	090/40	180/20
Baseline	Nominal	1	2	3	4	5	6
	Fastman	7	8	9	10	11	12
Noise-Only	Nominal	13	14	15	16	17	18
	Fastman	19	20	21	22	23	24
Noise	Nominal	25	26	27	28	29	30
& Traffic	Fastman	31	32	33	34	35	36

[*] Wind notation xxx/yy indicates wind coming from a relative angle xxx with a speed yy in kts.

Dependent Measures   The performance of the TDDA procedure was reviewed by means of (1) the altitude at which V_{APP} is reached ($h''@''V_{APP}$) as a *measure for noise impact*[1], and (2) the minimum actual distance with respect to the 2.5 NM safe separation (Δsep_{safe}) as a *measure for separation performance*. A full-factorial model Analysis of Variance (ANOVA) was conducted to evaluate the effect of the independent measures on these performance indicators. Boxplots are created to visualize the center and spread of the results. The boxplots also reveal outliers in the data which are presented in the plots with a circle. These outliers are extreme deviations and mainly caused by the effect of immediate or very late cue response, possibly in combination with high gust peaks.

4-5-2   Results and Discussion: General performance analysis

Separation Goal   Figures 4-13 and 4-14 show the deviation from the minimum safe separation of 2.5 NM encountered throughout the entire approach. As observed, a fastman reduces the relative spacing significantly depending on the governing wind. This yields large violations of safe separation for the baseline and NO optimization level. Noise optimization reduces the variability in minimum separation much as it corrects for deviations, generating more consistent but still unsafe results. Adding traffic optimization clearly gives the algorithm a good consistent performance for all wind conditions, where separation is *never violated*. Statistically, the effect of optimization for a fastman lead type is highly significant ($F_{2,1782}$ = 20319.946, p < 0.001). Also for a nominal lead, the optimization level has a highly significant influence on minimum separation ($F_{2,1782}$ = 836.442, p < 0.001).

The significant performance improvement achieved with N&T scheduling originates from the thrust cut-back altitude optimization. To comply with both noise

---

[1]As defined earlier, a deviation in noise performance could either be an undesirable noise impact or either a too late stabilization in the final approach configuration.
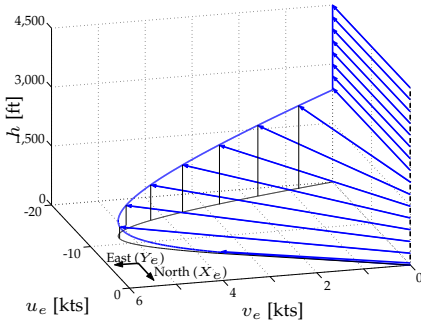
Figure 4-11: Logarithmic wind model for a wind with direction 360 and speed of 20 kts in the upper free atmosphere, showing the backing and veering effect.
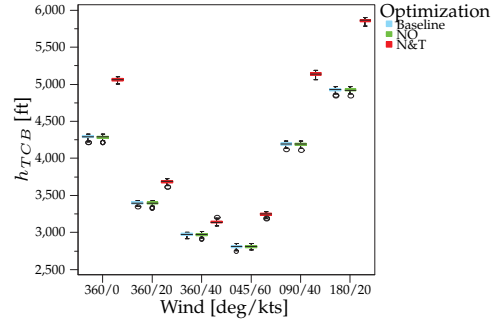
Figure 4-12: Thrust cut-back altitudes in case of a fastman lead trace.

and separation goals as good as possible, TCB heights are raised as presented in Figure 4-12. A positive outcome is the lower noise production, which is penalized however with a reduced downward control authority of the flaps and gear since the margin with respect to its lower speed boundary decreases.

A small excess in final separation can be observed caused by the limited accuracy of the lead trajectory prediction during the initial part of the approach (2nd order fit, Figure 4-5). The form of the lead aircraft deceleration characteristic primarily effects the performance of the separation prediction. The exact deceleration rate of the lead depends on both the governing wind and the lead's behavior type. These two independent variables even significantly interact with each other to get the resulting actual minimum separation ($F_{5,1188}$ = 17349.046, $p < 0.001$ for NO optimization). Notice that also the aircraft type of the lead has an influence. So the actual separation trend is highly variable and therefore hard to predict accurately most of the time. Increasing the accuracy of the separation prediction algorithm is expected to be a challenging quest.

Noise Goal   As expected and shown in Figures 4-15 and 4-16, $h@V_{APP}$ lies consistently closer to the targeted 1,000 ft when the algorithm schedules the flaps and gear accordingly ($F_{2,1782}$ = 1944.213, $p < 0.001$ and $F_{2,1782}$ = 334.689, $p < 0.001$, for, respectively, the nominal and fastman lead). A post-hoc analysis on the optimization level (Student-Newman-Keuls (SNK), $p = 0.05$) reveals that the difference between baseline and optimization is indeed significant. On the other hand, the mutual difference between the two algorithm levels (NO and N&T) is not significant. The algorithm can reach similar performance with respect to noise for all headwind type conditions, independent from the fact that separation was predicted to be in danger or not. Lead type has no significant influence on $h@V_{APP}$ ($F = 0.273$, $p = 0.601$). Hence, noise and separation goals can be combined excellently.
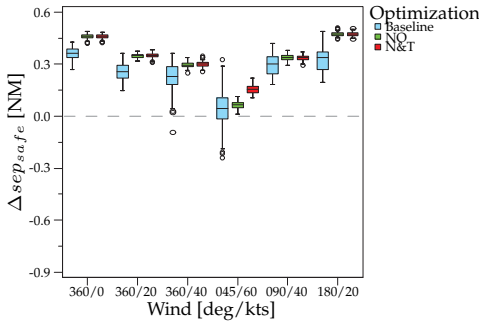
Figure 4-13: Deviation from 2.5 NM safe separation for a *nominal* lead type under all wind conditions.
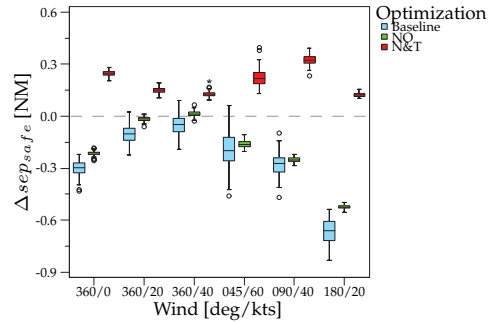
Figure 4-14: Deviation from 2.5 NM safe separation for a *fastman* lead type under all wind conditions.
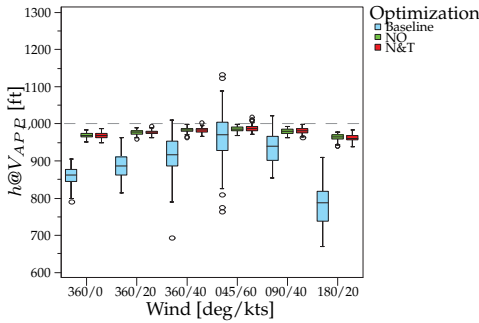
Figure 4-15: Altitude at which V_{APP} is reached for a *nominal* lead type under all wind conditions.
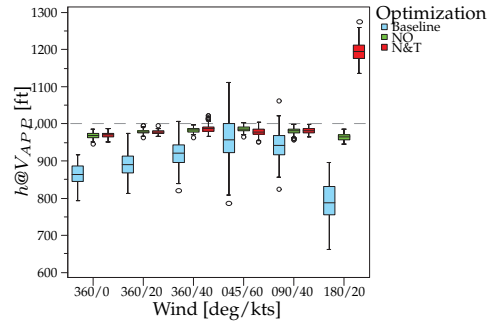
Figure 4-16: Altitude at which V_{APP} is reached for a *fastman* lead type under all wind conditions.

For the tailwind scenario 180/20, some noise abatement has to be sacrificed to keep a safe distance behind the fastman lead. The algorithm had to come up with a h_{TCB} of almost 6,000 ft to solve the separation conflict (Figure 4-12). Consequently the separation prediction algorithm has less lead data points to accurately generate the separation trend before TCB. The lack of data points in combination with the effect of tailwind on the form of the lead's trajectory, results in an overestimation of separation.

Finally, the two-dimensional own trajectory prediction with the point mass model proves to have good performance for every three-dimensional wind profile. Although ANOVA indicates that the wind has a highly-significant effect on the target altitude when both optimization levels are applied ($F_{5,1188} = 316.706$, $p < 0.001$), the absolute mutual differences are only very small.

Conclusions on General Performance   It can be concluded that the TDDA algorithm is able to adequately combine the noise and separation goals in most scenarios. With respect to traffic, the support system *always* assures a consistent, safe approach in any wind condition for a nominal and fastman lead. A satisfying accuracy for h_{APP} was found in the order of 0 to 40 ft, independent of the lead type.

An important note is that an exact wind prediction has been used for the above analysis. Wind prediction offsets are investigated in the following robustness analysis. A further analysis on wind errors and a comparison of the logarithmic wind profile prediction and a statistical based wind estimator for the TDDA algorithm has been described by de Gaay Fortman et al. (2005).[6]

4-5-3   Results and Discussion: Robustness analysis

Sensitivity on Wind Prediction Errors   The predicted wind velocity in the free atmosphere was offset with +/-10 kts and +/-20 kts for the 360/40 headwind, +/-10 kts for the 045/60 side wind. Figure 4.17(a) presents the separation achievements. Overestimation of the wind naturally has a negative effect on separation due to the later TCB. Still, N&T optimization has no problem to ensure safe spacing, even for an error of 20 kts. The algorithm also attains a relatively good precision in target altitude (Figure 4.17(b)). When underrating wind, $h@V_{APP}$ increases since the aircraft decelerates faster than expected. Notice that even better results are achieved than without the wind error (Figure 4-16) due to some compensation by the last tardy flap selection. Predicting more head wind reduces the accuracy slightly by 20 ft per 10 kts error (NO scheduling). Adapting the approach for slow traffic is handled nicely by the N&T algorithm without the need to add thrust too early.

Sensitivity on Mass Prediction Errors   A 10% mass error has been evaluated with respect to the standard 5,000 kg weight of the Citation I, so a predicted mass of 4,500 kg and 5500 kg. Predicting 10% lower mass decreases h_{TCB} significantly (the along track gravity force component is smaller) and consequently has a detrimental impact on minimum separation (Figure 4.18(a)). Nevertheless, N&T optimization is still able to correct the lack of separation to 2.6 NM. As indicated in Figure 4.18(b), this is however achieved at the cost of noise nuisance since thrust is reapplied earlier. Still the algorithm can bring the target altitude relatively close to 1,000 ft. The 5,500 kg prediction eases the traffic situation and realizes a better target altitude than with the exact mass since it compensates the cue delays.

Sensitivity on Drag Polar Errors   Finally, errors are applied to the predicted drag polar by off-setting the C_L-C_D curve sideways: Eq. (4-6) has been augmented with gains of +/-5% and +/-10%. A higher predicted drag naturally lowers h_{TCB} and accordingly decreases minimum separation (Figure 4.19(a)). The algorithm is once more capable of resolving the traffic conflict. Figure 4.19(b) shows that safe separation in the C_D+10% scenario can only be guaranteed by arriving at V_{APP} up to

(a) Deviation from 2.5 NM safe separation

(b) Altitude at which V_{APP} is reached
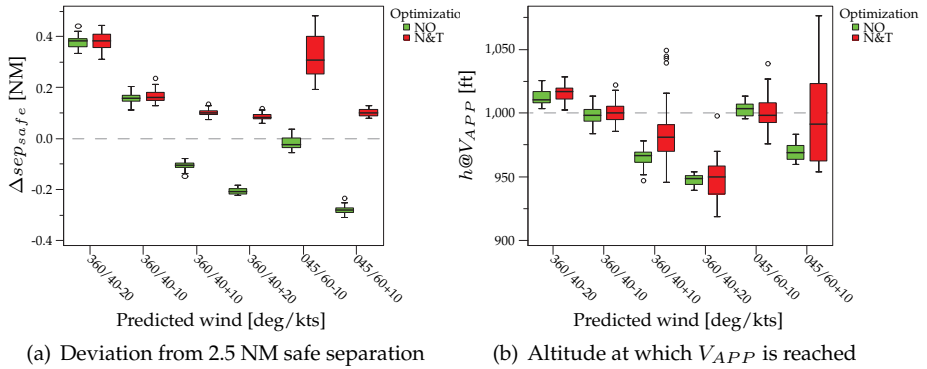
Figure 4-17: Robustness performance for a fastman lead and wind prediction error of $+/$-10 kts and $+/$-20 kts.

(a) Deviation from 2.5 NM safe separation

(b) Altitude at which V_{APP} is reached
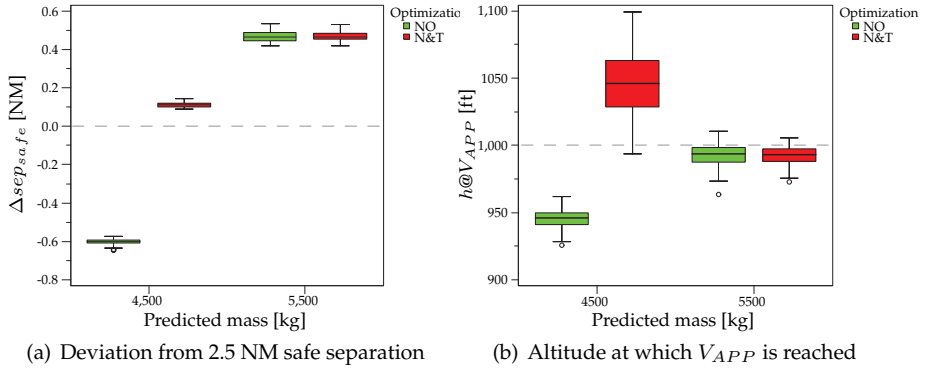
Figure 4-18: Robustness performance for a fastman lead in zero-wind and aircraft mass error of $+/$-500 kg.

(a) Deviation from 2.5 NM safe separation

(b) Altitude at which V_{APP} is reached
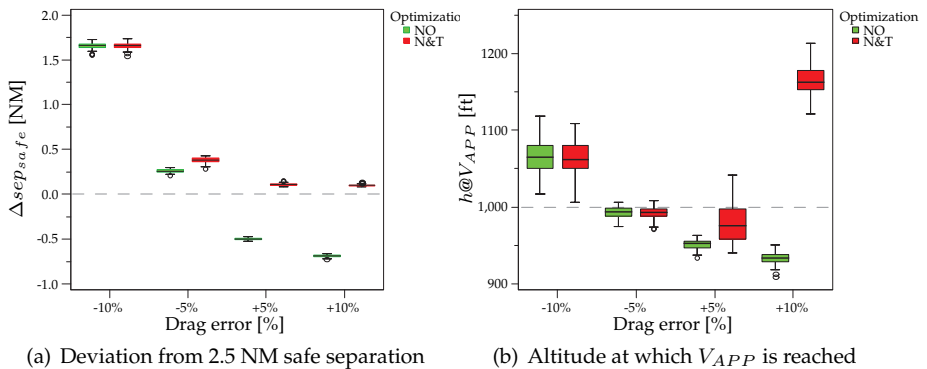
Figure 4-19: Robustness results for a fastman lead in zero-wind and drag coefficient error of $+/$-5% and $+/$-10%.

200 ft above the desired h_{APP}. Considering the amount of drag error and slower lead, this is still a limited drop in noise performance. For the other scenarios one can observe an obviously later stabilization in case drag is overvalued and a small noise penalty when underrating drag. An absolute target altitude deviation of 50 ft to 100 ft for respectively the 5% and 10% mismatch of C_D, is still acceptable.

Conclusions on Algorithm Robustness   The sensitivity analysis reveals that the flap/gear scheduling algorithm can cope with errors in wind, mass and drag prediction relatively good. The separation goal is *always* achieved, while the noise performance is only little declined. A comparison of all the results indicates that the optimization algorithm is most sensitive to mismatches in the drag polar. However drag and lift information can be determined rather accurately with sufficient flight test data.[18] Aircraft mass at take-off and fuel consumption should be able to be calculated with a precision of less than 10% of the total weight. Therefore, the highest expected error during TDDA operations is probably a mismatch between predicted and actual wind.

4-6   Experiment 2: In-flight Investigation

Experiment 2 was the first attempt to evaluate the feasibility of self-spacing during continuous decelerating approaches in real flight. The experiment should also complement the previous Monte Carlo studies, especially in support of the robustness characteristics of the scheduling algorithm. The flight tests, conducted in February 2005 at Soesterberg military airport (EHSB), included one test flight and one actual exploratory flight with multiple approaches.[18] Only the results of the experiment addressing the algorithm performance will be described.

4-6-1   Method

Apparatus: Aircraft and TDDA Display   The Cessna C550 Citation II laboratory aircraft of Delft Aerospace, a light twin-engined corporate jet, was used in the test flight. The aircraft has standard three flap settings (flaps UP, 15° and 40°). Like for the Monte Carlo simulations, a new flap setting was indicated in the cockpit, namely flaps 25°, to increase the control range of the approach procedure. The TDDA interface of Figure 4-2 was presented on a 15 inch LCD screen that was mounted in front of the co-pilot's seat. The aircraft was equipped with a Flight Test Instrumentation System (FTIS), developed in-house, that gathers the aircraft data from the on-board Flight Management System (FMS) and ARINC Data Bus and publishes this information to a distributed double laptop set-up which ran the TDDA software.

Table 4-2: Review of experiment flight results. The table presents the different scenarios along with the calculated thrust cut-back (TCB) altitude, time differences between cue presentation and actual flap/gear selection, as well as the altitude at V_{APP} (120kts) and the minimum separation with the predecessor during the approach.

#	Lead Type	TCB	Δt F15	Δt F25	Δt F40	Δt LG	h@V_{APP}	min. sep.
		[ft]	[s]	[s]	[s]	[s]	[ft]	[NM]
1	nominal	3550	2.9	-1.9	0.6	0.8	760[*]	4.0
2	nominal	3520	-1.9	7.3	5.9	0.8	917	4.4
3	fastman 7.5NM	3410	-[**]	-[**]	1.0	0.5	953	3.58
4	fastman 7.5NM	3200	-0.7	2.1	1.3	1.8	1012	3.45
5	fastman 6.0NM	3280	1.6	1.0	3.4	3.1	955	2.7
6	fastman 5.5NM	3850	2.0	2.1	-0.5	-7.3	914	2.7

[*] Thrust was added already at 1060 ft while V_{APP} was not yet reached. Extrapolation of the deceleration rate suggests an adequate target performance.

[**] Unreliable data in this part of the logged data file.

F15: Flaps 15°, F25: Flaps 25°, F40: Flaps 40°, LG: Landing Gear.
Δt > 0 indicates too late flap/gear selection.

Procedure and Instructions to Subjects All approaches were performed by one pilot crew who was extensively briefed before the flights. During the TDDA, the right pilot was the pilot flying (PF), while the left pilot (captain) acted as a safety pilot. Prior to the start of the TDDA procedure, the captain brought the aircraft with the aid of the autopilot to level flight at 5,000 ft, with 230 kIAS, and fully established for the localizer interception of Soesterberg's active runway 27. Meanwhile the experiment controller sitting in the back, initiated and started the new experiment run on the laptops. The initialization also includes the generation of a 'virtual' lead aircraft, based on a simple aerodynamic model of a Cessna Citation I and the current meteorological conditions. The PF then disconnected the automation aids and flew the TDDA procedure with the aid of the flight director. The pilot was instructed to strictly adhere to the flap/gear and thrust-cut back cues. This way the performance of the algorithm in real-flight could be fully assessed. The safety pilot was asked to deploy flaps and gear on the PF's command and to communicate with Air Traffic Control (ATC). Each successful approach was aborted at an altitude of approximately 800 ft, after which the captain returned the aircraft to the experiment start position. Every approach the governing wind profile was recorded and used during the next approach as a persistence wind prediction for the flap algorithm and lead's trajectory generation.

Data Acquisition and Processing Most aircraft parameters are retrieved directly from the aircraft. Two important variables, flap position and landing gear position, could not be acquired and had to be manually incorporated by the in-flight experiment controller, triggered by the pilot's flap/gear call-out. Wind direction and

speed were calculated by comparing the available ground and airspeed vectors. ILS localizer/glide slope together with flight director signals were computer generated using GPS positioning data. After all, glide slope signals can not be intercepted during the initial part of a straight-in approach from 5,000 ft.

4-6-2   Results and Discussion

In Table 4-2, all data of interest for the second experiment flight are summarized. A total of six consecutive approaches were performed in which the initial separation with the lead aircraft was gradually decreased to call in traffic scheduling. As a result of the slower lead aircraft, the algorithm selected a higher h_{TCB} to ensure conflict resolution. The pilot showed a strict adherence to the flap/gear cues. The average delay between cue presentation and actual flap/gear selection was measured to be 1.17 seconds. A few anomalies in cue follow-up occurred (runs 2 and 6) caused by misinterpretation between pilot and experiment controller, pilot anticipation to the cues and ATC communication interferences.

For all approaches, minimum separation was never violated, even with a very slow lead aircraft in front (run 6). The target speed V_{APP} was always reached below the target altitude of 1066 ft[2] and averaged 950 ft. The lower target altitudes are mainly caused by delays in flap/gear selection and deviations from the 3° ILS glide path once the algorithm stops scheduling the lasts flaps within 200 ft of the target altitude.[7]

The current results show that, with the current algorithm and using persistence wind data, it is possible to perform a TDDA with a small jet aircraft while achieving the noise *and* separation goal. Figure 4-20 illustrates the flap and gear behavior, wind information and the in-trail distance with the predecessor for run 4. The course of the flap and gear cues indicates a gentle tuning process that oscillates near the nominal speeds. Upper and lower speed boundaries are avoided.

4-6-3   Conclusions

The flight tests were the first to investigate the viability of self-spacing during decelerating approaches in real flight. The results are well in line with the previously conducted Monte Carlo experiments[7] and prove that it is possible to perform a TDDA in real-life with the current algorithm and persistence wind data. All approaches showed a consistent target performance in terms of reaching V_{APP} at the pre-specified altitude, while simultaneously the algorithm managed to take care of separation with traffic in front when necessary.

---

[2]1,000 ft plus field elevation (66 ft).
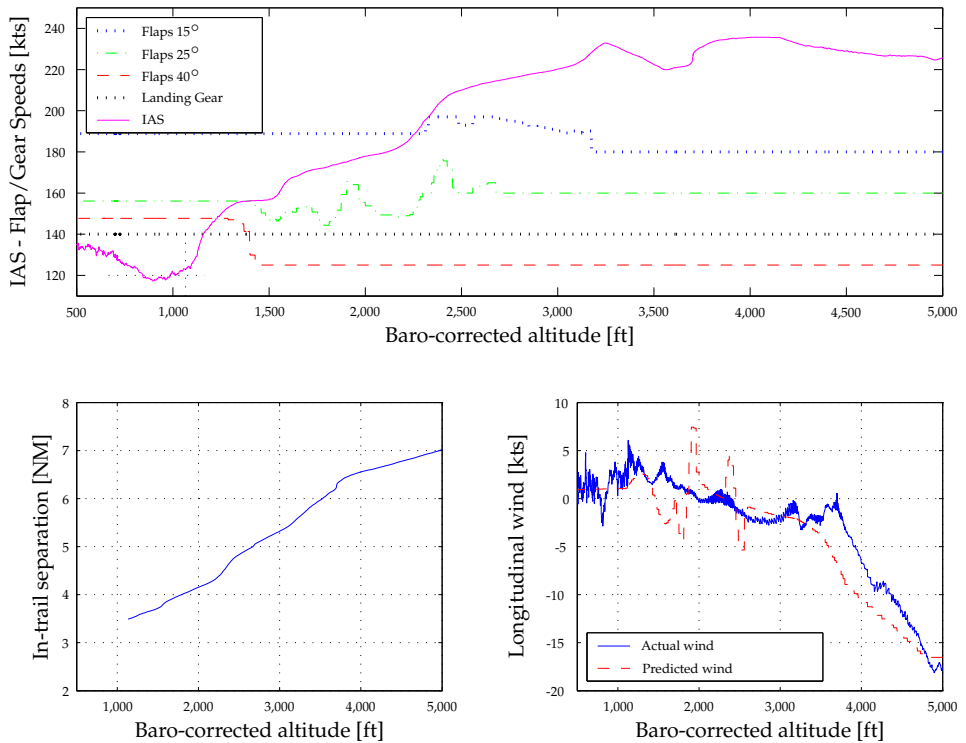
Figure 4-20: Flap/gear behavior, separation trend, and longitudinal wind component of one representative run during the second experiment flight. All data is sampled at 10 Hz. (Note: a positive wind component is a tailwind.)
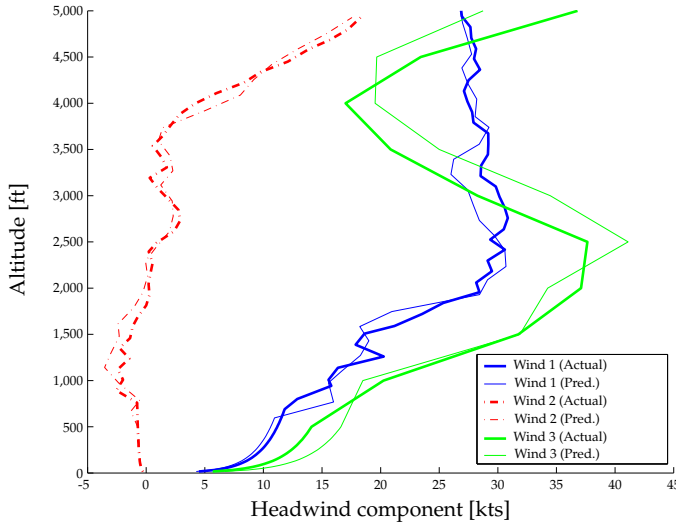
Figure 4-21: Predicted and actual wind speed profiles during the simulation experiments. A positive value indicates headwind.

4-7 Experiment 3: Piloted Simulator Tests

Experiment 3 primarily aimed at complementing the previous studies by evaluating operational performance when pilots manually fly a TDDA aided by the automated tool. Its additional focus was to determine whether pilots would do equally well without assistance of the algorithm and to quantify pilot workload.

4-7-1 Method

Apparatus The SIMONA Research Simulator, a high-fidelity 6 degree-of-freedom flight simulator, was used for the experiment. All approaches were performed at runway 27 of Schiphol (EHAM) airport. Aircraft control was provided via a wheel/column combination (with trim button) and rudder pedals. Flap selector, gear handle and throttle levers were positioned on the right-hand side of the captain's seat. Real jet aircraft sound, coupled on throttle setting, was played during the experiment runs.

Aircraft Model and Atmospheric Disturbances The aircraft flown was a nonlinear 6 degree-of-freedom Cessna C500 Citation I mathematical model,[20] as before augmented with the extra flap setting of 25°. Wind was simulated by replaying a data file containing pre-recorded wind observations partitioned into altitude intervals of 500 ft (Figure 4-21). Similar to the in-flight investigation, persistence wind

Table 4-3: Experiment wind information (METAR).

	0 ft	5,000 ft
Wind condition 1 (W1)	220/10	240/30
Wind condition 2 (W2)	160/1	290/20
Wind condition 3 (W3)	300/8	310/50

data (10 minutes old) was used to predict the own trajectory. Atmospheric turbulence was considered to be a stationary stochastic process based on Dryden spectra with 'patchy' behavior.[3]

Independent Variables   Three independent variables were varied throughout the experiment: (1) level of optimization, (2) deceleration characteristics of the lead aircraft, and (3) wind type.

Level of Optimization and Display Type - Two levels of optimization were applied in the experiment. First, the TDDA procedure was performed with *no optimization* (baseline). The pilot was required to schedule thrust cut-back, flaps and gear at his own discretion to achieve the noise goal and/or separation goal. The pilot was only supported by an approach plate, with indications on thrust cut-back altitude and flap/gear timing for a zero wind condition. On the ND, only the actual position of the lead aircraft was presented. In this way, the pilot was left with only the information available in the cockpit nowadays. Second, *N&T scheduling* was enabled. In this case, the pilot was supported by a full display (Figure 4-2), with flap/gear cues, TCB cue, thrust/drag annunciators, and separation arc information. The baseline approach serves as a threshold for data and workload analysis to compare with the optimization algorithm.

Lead Characteristics - Two different lead trajectories have been evaluated: (1) a nominal lead, which follows the same (fixed) common-procedure flap schedule is used, and (2) a fast lead, which decelerates earlier resulting in a separation violation if no action is taken. In all cases, the preceding aircraft was a Cessna Citation I that executed the standard TDDA procedure, initially separated 7.5 NM with the own aircraft. Both aircraft had an identical V_{APP} and h_{APP}, i.e., 110 kts and 1,000 ft, respectively.

Wind - A total of three wind conditions were defined (Table 4-3): two conditions which were recorded during the flights with the Cessna Citation II laboratory aircraft (W1, W2), and one cross wind condition of 50 kts with a direction of approximately 45 ° with respect to the approach path (W3). Each condition was accompanied with random patchy atmospheric turbulence.

Table 4-4: Experiment matrix for the piloted simulator tests.

	Wind condition 1 (W1)		Wind condition 2 (W2)		Wind condition 3 (W3)	
	Nominal	Fastman	Nominal	Fastman	Nominal	Fastman
Baseline	1	2	3	4	5	6
N&T	7	8	9	10	11	12

Experimental Design and Procedure   A full-factorial within-subjects design was applied, yielding the 12 conditions ($2 \times 2 \times 3$) of the experiment matrix of Table 4-4. The different scenarios were randomized for every pilot. Each subject first conducted a couple of training sessions in which each lead type and optimization level was at least encountered once. When familiarized with the procedure, each pilot completed every experimental condition once (12 runs).

Each approach scenario started at level flight at 5,000 ft, 230 kts IAS, with the aircraft fully established on the localizer of runway 27 prior to the ILS glide slope interception. Before the start of each run, the pilots were informed about the wind speed and direction yielding at the ground and start altitude. Flight path control occurred manually, assisted by the flight director signals. The approach speed V_{APP}, set at 110 kts IAS, had to be achieved at a reference altitude of 1,000 ft. Minimum safe separation was fixed at 2.5 NM. A single approach lasted approximately 6 minutes.

A single pilot was used for data collection, with one of the authors in the right seat. The 'co-pilot' solely selected the appropriate flaps and gear position on the pilot's call-out. The two-person arrangement provided the opportunity to collect data and investigate pilot workload, while still preserving the realism of multi-crew tasks.

After each subsequent run, pilots were asked to fill in a NASA Task Load Index (TLX)[13] which is used to assess pilot workload. In addition, a post-experiment questionnaire was administered after the completion of all runs. The questionnaire invited pilots to give their opinion on several topics, such as: display/algorithm properties, lead aircraft behavior, workload, situational awareness, simulation properties, etc.

Subjects and Instructions to Subjects   In total, ten qualified captains and first officers, all males, participated in the experiment (Table 4-5). Most of them had previous experience with noise abatement procedures (NAPs). The mean age and flight time of the pilots were 43.4 years and 10830 hours, respectively. Prior to the experiment, pilots were briefed about the TDDA procedure, the objective of the experiment and characteristics which may influence the outcome. All pilots were instructed to perform the TDDA procedure manually as accurately as possible, with the engines running completely at idle. They were commanded to maintain 230 kts IAS until thrust cut-back. Then, the throttle levers had to be placed to their idle detent position. During the approach, the pilots had to minimize deviations from

Table 4-5: Pilot subjects overview.

pilot	sex	age	hours	aircraft type	previous NAPs
A	M	36	4,500	Jetstream 31, F50	-
B	M	44	12,000	B737-200/300/400, B747-400, B767	CDA
C	M	33	3,100	Lynx helicopter, B737, C550	Steep approach
D	M	38	6,100	B747-400, B767, B777	CDA
E	M	54	21,000	B737-700/800, B757	CDA
F	M	39	6,600	DC10, B767, B737	CDA
G	M	26	1,300	C550	-
H	M	66	13,200	DC3/CV640, F27/F28, DC8, B747, C550	CDA
I	M	42	10,500	B737-200/300/400/700/800	CDA
J	M	56	30,000	B707, B737-200/300, DC10, A310, A330, A340	CDA/Red. flaps

the $3°$ glide path and flap/gear cue advisories. At all times, the aircraft had to be delivered fully configured (full flaps and landing gear down) at ultimately 1,000 ft. Furthermore, the pilots were instructed that, at no time, the in-trail distance should be less than the 2.5 NM. In addition, the power levers should not be moved from their idle position apart from when thrust is required to maintain V_{APP}.

Dependent measures Operational performance was reviewed by means of the altitude at which the approach speed V_{APP} was reached ($h@V_{APP}$), and deviations from the minimum safe separation (Δsep_{safe}). Pilot performance was evaluated by recording flap/gear activities, as well as the time delay between flap/gear cue presentation and pilot response. At last, pilot workload was judged using the NASA TLX ratings.[13]

Experiment hypotheses It was hypothesized that pilots would achieve better operational performance when they are assisted by the algorithm. Especially in the cases of a fastman lead aircraft, the algorithm should outperform the pilot's interpretation. With the aid of the scheduler, it was expected that V_{APP} would be reached at h_{APP} more consistently, while safe separation would never be violated, and in full landing configuration. In addition, it was hypothesized that stronger winds would deteriorate the pilot's ability to achieve V_{APP} at h_{APP}, while this effect would be less expressed when cues are presented. Another hypothesis was that algorithm and accompanying interface would decrease workload as compared to the baseline.

4-7-2 Results

Operational performance Noise Goal - For the fastman baseline approaches (Figure 4-22), pilots were typically not capable of reaching V_{APP} at h_{APP}, except for the 'easier' wind condition 2, but this was in spite of violating safe separation (Figure 4.23(b)). A nominal lead behavior yielded a significant better target altitude accuracy ($F_{1,9} = 9.366$, p = 0.014). Stronger winds significantly deteriorated the baseline

performance for a fastman lead($F_{2,18}$ = 7.072, p < 0.001), however no statistically significance could be found for the nominal lead ($F_{2,18}$ = 2.533, p = 0.107).

When presented with the pilot support interface, pilots were clearly capable of reaching the target altitude more consistent which is expressed in the lower variability and means closer to the target altitude (nominal lead: $F_{1,9}$ = 10.512, p = 0.010; fastman: $F_{1,9}$ = 8.668, p = 0.016). Because the algorithm will always prioritize on safe separation, a slower lead aircraft evidently decreases the noise reduction performance of the algorithm ($F_{1,9}$ = 26.059, p = 0.001). Wind however showed to have no significant influence ($F_{2,18}$ = 2.504, p = 0.110).

(a) Nominal lead aircraft.   (b) Fastman lead aircraft.
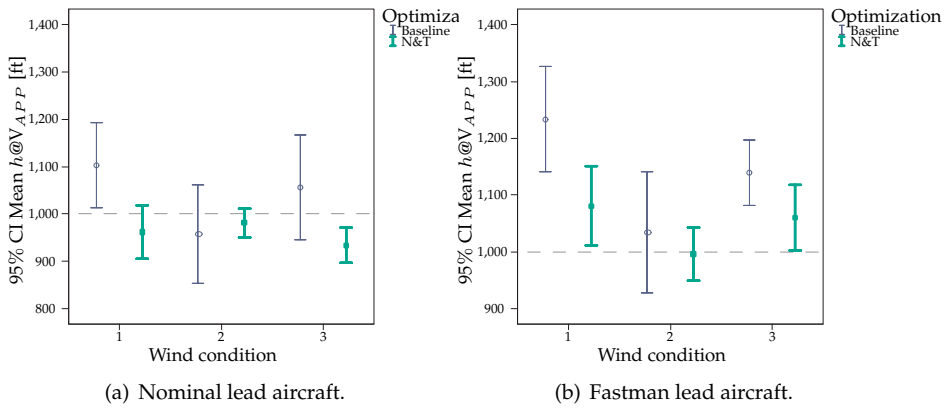
Figure 4-22: The means and 95% confidence intervals of the altitude at which V_{APP} was reached.

(a) Nominal lead aircraft.   (b) Fastman lead aircraft.
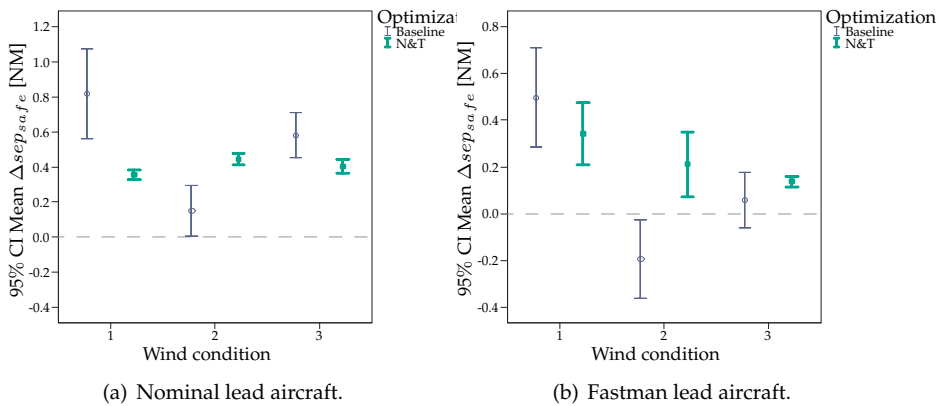
Figure 4-23: The means and 95% confidence intervals of the deviations from the minimum safe separation throughout the whole approach. A negative value indicates safe separation violation.

Separation Goal - Figures 4-23 illustrates the deviations from the minimum safe separation of 2.5 NM throughout the whole approach. As foreseen, safe separation distinctly decreased with slower lead aircraft (fastman) when pilots are not assisted ($F_{1,9}$ = 84.125, p < 0.001). They only managed to cope with a fastman in the first wind scenario, however this was accompanied by a detrimental effect on h@V$_{APP}$ (Figure 4.22(b)). Actually, the more the pilots were trying to achieve V_{APP} at the target altitude, the more they exceeded or tended to exceed the safe separation threshold. The wind characteristics also significantly influenced the separation performance ($F_{2,18}$ = 23.600, p < 0.001).

When the algorithm comes into play the scatter in data reduced expressively for a normal decelerating predecessor (W1: $F_{1,9}$ = 16.552, p = 0.003; W2: $F_{1,9}$ = 21.288, p = 0.001; W3: $F_{1,9}$ = 11.684, p = 0.008) and fastman lead. Accordingly as in the baseline, Δsep_{safe} becomes much smaller for a fastman lead with respect to a normal predecessor ($F_{1,9}$ = 32.790, p < 0.001).

The most important contribution of the algorithm is that safe separation is never violated. In fact, the algorithm is able to "close the gap" in comparison with the baseline. An ANOVA analysis revealed that optimization had a borderline significant effect on deviating from 2.5 NM separation with a fastman lead ($F_{1,9}$ = 4.345, p = 0.067), where the effect is highly significant for wind 2 ($F_{1,9}$ = 12.602, p = 0.006).

Pilot controls   To be fully configured, a total of three flap and one gear activities have to be performed. When assisted by the cues, the pilot was able to be fully configured at the end of the TDDA, while this was certainly not always the case for a baseline approach in the more 'severe' wind conditions. Wind and optimization proved to have a (borderline) significant effect on achieving full configuration (respectively $F_{2,18}$ = 3.273, p = 0.061 and $F_{1,9}$ = 3.578, p = 0.091). Choosing a too early thrust-cut back, forced the pilots to delay flap and gear extension to extend the glide. So in some cases, this resulted in not selecting the last flap or gear before V_{APP} was reached. No significant differences due to lead behavior were discovered ($F_{1,9}$ = 2.250, p = 0.168).

The pilot response time on the flap and gear cues demonstrated a trend towards anticipation on the cues when confronted with a sluggish predecessor (Figure 4-24). Indeed, the effect of lead was analyzed as significant ($F_{1,9}$ = 9.270, p = 0.014). Pilots were not anticipating on the thrust-cut back cue, but were awaiting the cue (Figure 4-25).

Workload and Post-Test Questionnaire   The workload ratings in Figure 4-26 show a highly significant decrease in workload with the aid of the current algorithm and pilot support interface as expected ($F_{1,9}$ = 107.622, p < 0.001). No significant differences were found for wind condition ($F_{2,18}$ = 2.131, p = 0.148).

Pilot comments and subjective ratings given in the post-test questionnaire indicated that the pilot support interface was indeed a helpful tool to execute a TDDA, and
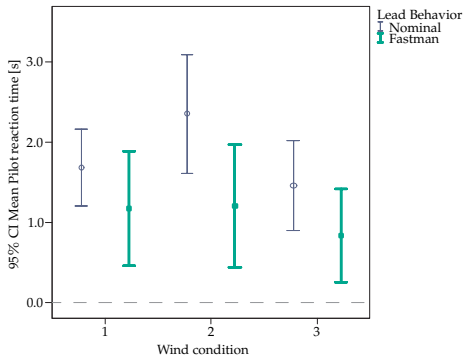
Figure 4-24: The mean and 95% confidence intervals of the pilot response time on flap and gear cues.
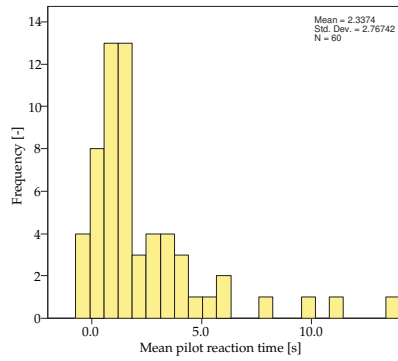
Figure 4-25: Histogram of the pilot response time on the thrust cut-back cue.
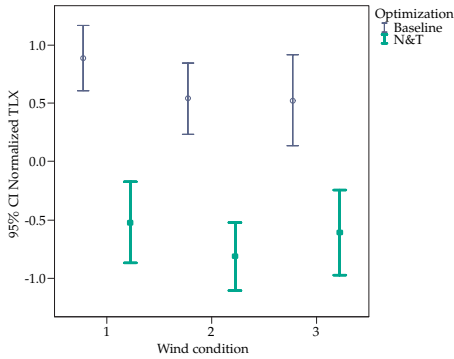
Figure 4-26: The means and 95% confidence intervals for the normalized TLX scores.

which in return brought instrument scan, workload and situational awareness to a comparable level as in current ILS approaches.

4-7-3   Discussion and Conclusions

For the tested wind conditions, it can be concluded that when pilots have to time thrust-cut back, flap and gear selection on their own, they are able to reach V_{APP} at the projected altitude when a nominal lead is in front. However, pilot performance deteriorates significantly with more sluggish lead aircraft, either by re-applying thrust too early to maintain V_{APP} or by violating minimum safe separation. A distinctly better and more consistent noise performance is found when optimized cues are presented, while safe separation with the predecessor is guaranteed at all time. Additionally, the assistance of the algorithm and display clearly decreases pilot workload up to an effort level comparable to current standard approaches. All in all, the pilot support interface and accompanying scheduling algorithm provides an essential tool to perform Three-Degree Decelerating Approaches.

4-8   Conclusions

The developed prediction and scheduling routine demonstrated to be a valuable tool to achieve adequate and consistent performance in executing a self-separated noise abatement procedure, like the TDDA.

Off-line Monte Carlo results showed that the optimization algorithm is able to adequately combine safe separation with target altitude accuracy in various scenarios. An evaluation of the sensitivity of the algorithm pointed out that the TDDA algorithm is able to limit the effect of relatively large prediction errors for wind, aircraft mass and drag of the aircraft to only 200 ft.

The human-in-the-loop simulator experiment showed that, for the tested wind and traffic conditions, pilots can achieve the target speed at a pre-specified altitude quite accurately when tailing a nominal lead without any assistance. However, if faced with a more sluggish predecessor, larger deviations from the projected target altitude were distinguished, while in some cases separation became hazardous. When aided by the support tool, a significantly better performance and decreased workload was reached. The projected target speed was achieved more consistently at the target altitude, while safe separation was guaranteed at all times. The subject pilots generally rated the workload level with the TDDA procedure similar to that with standard ILS procedures.

The exploratory demonstration flight proved that the current algorithm, using persistence wind data, is able to guide the pilot to the projected target altitude relatively accurately under actual flight conditions. This all, while guaranteeing again safe separation with the predecessor throughout the whole approach.

4-9   Acknowledgments

References

[1] Sourdine D3: Establishment of Noise Abatement Solutions. Technical report, Amsterdam, The Netherlands, 2000.

[2] Sourdine D5: Final Report. Technical report, Amsterdam, The Netherlands, 2001.

[3] M. Baarspul. *Flight Simulation Techniques*. Faculty of Aerospace Engineering, Delft University of Technology, Delft, The Netherlands, 1982.

[4] J.-P. Clarke. *A Systems Analysis Methodology for Developing Single Event Noise Abatement Procedures*. Sc.D. Dissertation, Massachusetts Institute of Technology, Cambridge (MA), USA, 1997.

[5] J.-P. Clarke, N. T. Ho, L. Ren, J. A. Brown, K. R. Elmer, K. Tong, and J. K. Wat. Continuous Descent Approach: Design and Flight Test for Louisville International Airport. *AIAA Journal of Aircraft*, 41(5):1054–1066, 2004.

[6] W. F. de Gaay Fortman, M. Mulder, M. M. van Paassen, A. C. in 't Veld, and J.-P. Clarke. Wind Profile Prediction to Support Three-Degree Decelerating Approaches. In *Proceedings of the AIAA Guidance, Navigation and Control Conference & Exhibit*, number AIAA 2005-6141, pages 1–23, San Francisco (CA), USA, Aug 15-18 2005.

[7] J. L. de Prins, K. F. M. Schippers, M. Mulder, M. M. van Paassen, A. C. in 't Veld, and J.-P. Clarke. Enhanced Self-Spacing Algorithm for Three-Degree Decelerating Approaches. In *Proceedings of the AIAA Guidance, Navigation and Control Conference & Exhibit*, number AIAA 2005-6140, pages 1–22, San Francisco (CA), USA, Aug 15-18 2005.

[8] K. Elmer, J. Wat, G. Gershzohn, B. Shivashankara, J.-P. Clarke, N. T. Ho, L. Tobias, and D. Lambert. A Study of Noise Abatement Procedures Using Ames B747-400 Flight Simulator. In *8th AIAA/CEAS Aeroacoustics Conference & Exhibit*, number AIAA 2002-2540, pages 1–10, Breckenridge (CO), USA, Jun 17-19 2002.

[9] K. Elmer, J. Wat, B. Shivashankara, J.-P. Clarke, K. Tong, J. Brown, and A. Warren. Community Noise Reduction using Continuous Descent Approach: A Demonstration Flight Test at Louisville. In 9th *AIAA/CEAS Aeroacoustics Conference & Exhibit*, number AIAA 2003-3277, pages 1–9, Hilton Head (SC), USA, May 12-14 2003.

[10] K. Elmer, J. Wat, B. Shivashankara, D. McGregor, and D. Lambert. A Continuous Descent Approach Study using Ames B747-400 Flight Simulator. In *AIAA's Aircraft Technology, Integration, and Operations (ATIO) Technical*, number AIAA 2002-5869, pages 1–9, Los Angeles (CA), USA, Oct 1-3 2002.

[11] L. J. J. Erkelens. Research into New Noise Abatement Procedures for the 21st Century. In *AIAA Guidance, Navigation, and Control Conference & Exhibit*, number AIAA 2000-4474, pages 1–10, Denver (CO), USA, Aug 14-17 2000.

[12] G. Gershzohn, J. Wat, J. P. Dwyer, K. Elmer, J.-P. Clarke, and N. T. Ho. Advanced Noise Abatement Procedures: An Experimental Study of Flight Operational Acceptability. In *AIAA's Aircraft Technology, Integration, and Operations (ATIO) Technical*, number AIAA 2002-5867, pages 1–9, Los Angeles (CA), USA, Oct 1-3 2002.

[13] S. G. Hart and L. E. Staveland. Development of NASA-TLX (Task Load Index): Results of Empirical and Theoretical Research. In P. A. Hancock and N. Meshkati, editors, *Human Mental Workload*, pages 139–183. Elsevier Science Publishers, Amsterdam, The Netherlands, 1988.

[14] N. T. Ho and J.-P. Clarke. Mitigating Operational Aircraft Noise Impact by Leveraging on Automation Capability. In *Proceedings of the AIAA Aircraft, Technology, Integration and Operations Forum*, number AIAA 2001-5239, pages 1–8, Los Angeles (CA), USA, Oct 16-18 2001.

[15] A. C. in 't Veld, M. M. van Paassen, M. Mulder, and J.-P. Clarke. Pilot Support for Separation Assurance during Decelerated Approaches. In *Proceedings of the AIAA Guidance, Navigation and Control Conference & Exhibit*, number AIAA 2004-5102, pages 1–13, Providence (RI), USA, Aug 16-19 2004.

[16] M. F. Koeslag. Advanced Continuous Descent Approaches, an Algorithm Design for the FMS. MSc. Thesis, Faculty of Aerospace Engineering, Delft University of Technology, 2001.

[17] L. Ren, J.-P. Clarke, and N. T. Ho. Achieving Low Approach Noise without Sacrificing Capacity. In 22nd *Digital Avionics Systems Conference*, number AIAA-2001-5239, pages 1–9, Indianapolis (IN), USA, Oct 12-16 2003.

[18] K. F. M. Schippers, J. L. de Prins, M. Mulder, M. M. van Paassen, A. C. in't Veld, and J.-P. Clarke. Investigation of a Three-Degree Decelerating Approach of a Twin Engined Jet Aircraft. In *Proceedings of the AIAA Guidance, Navigation and Control Conference & Exhibit*, number AIAA 2005-6139, pages 1–28, San Francisco (CA), USA, Aug 15-18 2005.

[19] H. A. Simon. *Models of Man*. Wiley, New York (NY), USA, 1957.

[20] C. A. A. M. van der Linden. DASMAT - Delft University Aircraft Simulation Model and Analysis Tool. Technical Report LR-781, Delft University of Technology, Delft, The Netherlands, Aug 1996.

[21] J. van Kan. *Numerieke Wiskunde voor Technici (in Dutch)*. Delft University Press, Delft, The Netherlands, 2000.

[22] J. Wieringa and P. J. Rijkoort. *Windklimaat van Nederland (in Dutch)*. Staatsuitgeverij, The Hague, The Netherlands, 1983.

[23] F. J. M. Wubben and J. J. Businik. Environmental Benefits of Continuous Descent Approaches at Schiphol Airport Compared with Conventional Approach Procedures. Technical Report NLR-TP-2000-275, National Aerospace Laboratory (NLR), Amsterdam, The Netherlands, May 2000.

5

Stochastic Wind Profile Estimation

5-1   Abstract

Wind is one of the major contributors to uncertainty in continuous descent approach operations. Especially when aircraft that are flying low or idle thrust approaches are issued a required time of arrival over the runway threshold, as is foreseen in some of the future ATC scenarios, the on-board availability of both dependable and accurate wind estimates becomes a necessity. This paper presents a method for real-time estimating the wind profile in the terminal maneuvering area, based on data transmissions of nearby aircraft that produces real-time wind profile estimates in a form that is usable for accurate trajectory prediction. The AMDAR wind prediction algorithm (AWPA) is designed to process data that is of the form currently used in the Aircraft Meteorological Data Relay (AMDAR)-program. The algorithm combines a stochastic estimation based on this data and a traditional logarithmic estimator in order to be able to produce a valid estimation even when there are no data available from other aircraft.

5-2   Introduction

Various research into advanced Continuous Descent Approaches procedures such as the Tailored Arrivals, the LAX descent procedures and the time based Three-Degree Descent Approach have shown that accurate trajectory prediction is only possible with a sufficiently accurate wind model[4,6] . Such a wind model needs to have a fine resolution and high update frequency to be able to cater for the fast changing wind profile as experienced by aircraft flying an appraoch. Different programmes have turned to different solutions, ranging from a simple profile based on the wind measured on-board the aircraft and the wind report at the runway,[6] to up-linking entire high resolution wind grids from the National Oceanic and Atmospheric Administration (NOAA).[4]

This research proposes a relatively easy to implement wind profile estimator that produces real-time wind profiles with sufficiently high resolution that they are usable for accurate trajectory prediction on-board an aircraft flying an advanced approach procedure. The idea is to leverage on the fact that in th near future aircraft will be equipped with data-link capability such as ADS-B which allows aircraft to gather state information from nearby aircraft. In fact the aircraft in the Terminal Maneuvering Area (TMA) can be seen as a set of airborne weather sensors providing among other data current wind speed and direction at their location.

The idea of using aircraft data to improve meteorological data is not new. The Aircraft Meteorological Data Relay program (AMDAR) was first proposed by the World Meteorology Organization in the 1970s and has been using aircraft data to improve their weather models since the late 1990s.

Because of the high degree of variability and hence unpredictability of wind profiles near the ground, a wind prediction algorithm has been developed that uses AMDAR, providing a.o. wind speed measurement data. In this research, the algorithm has been made applicable to the three-dimensional situation of the TMA, and more robust to situations with lower information density (when not enough measurement reports are available).

5-2-1   AMDAR Characteristics

Modern commercial aircraft are equipped with meteorological sensors and associated sophisticated data acquisition and processing systems. These provide input in real time to the aircraft flight management, control and navigation systems and other on-board systems.[8] Aircraft participating in the AMDAR project automatically relay (a selection of) these data to the ground receivers. This is usually done through the Aircraft Communication Addressing and Reporting System (ACARS) system, or a satellite based equivalent. According to ICAO ADS-B specifications, the elements to be reported in a single observation are position and altitude, time, temperature, wind direction and speed, turbulence, humidity and icing, phase of
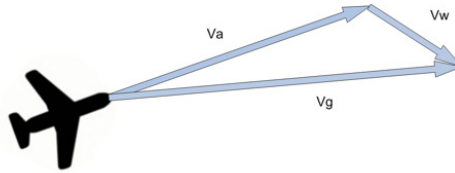
Figure 5-1: Calculation of the Wind Speed Vector

flight, some aircraft state variables such as roll and pitch angles, and an aircraft identifier.

The wind speed is calculated by resolving the two speed vectors V_a, the measured airspeed, and the groundspeed V_g, which is calculated within the FMS (typically based on IRU and GPS data), see Figure 5-1. The combined accuracy of both speed vectors (in magnitude and direction) is about 2-3 m/s.[8]

As of yet, no broadcasting standard has been defined. Data may be transmitted through VHF, SSR or satellite communication. The source of the available data is not of particular concern to this research.

Obviously, the meteorological reports are spatially concentrated around the busiest routes at cruise altitudes and in the TMAs around the major airport hubs. This will lead to a loss of accuracy in the wind prediction at less crowded airports or during slow traffic hours. This is not expected to cause any problems since in these situations the demanded runway capacity is usually substantially less than the maximum available capacity and less accuracy is acceptable.

5-2-2   The Wind Prediction Algorithm

The obtained wind observations are first grouped together into altitude intervals of for instance 500 ft. Next, the noise in the data is filtered out. The smoothed data is then used to get a wind prediction for every altitude interval over a short-term time interval. These predicted wind speeds and directions are then combined to form the predicted wind profile. The complete process is repeated when new observation data has been collected. Every step of this iteration process will be explained in more detail in the following paragraphs.

A Kalman filter has been selected for the data smoothing task. The purpose of the filter is to extract the noise components of the measured wind data and to assign smaller weights to measurements that were taken further away in time or are taken at a greater distance from the reference trajectory.

For the short-term wind prediction an Auto-Regressive Moving-Average (ARMA) model is used.[3] This is a sophisticated statistical model based on the Kalman filter and calculates a forecast value as a linear combination of the last N measured values. Here these values are wind speed and wind direction, expressed in North and East velocity components V_N, V_E. The coefficients of the ARMA prediction model are first determined using a recursive Kalman filter. Then the predicted wind can be calculated by filling in the previously observed wind parameters into the ARMA model.

Finally, the predicted wind profile is created by fitting a cubic spline through the predicted wind speeds. A cubic spline consists of piecewise polynomials that follow the altitude dependent wind predictions smoothly. This way every possible wind profile can be fitted and predefined models can be avoided.

The strength of this wind prediction algorithm is its flexibility. It provides an accurate profile based on a statistical model when sufficient data is present, but reverts to a logarithmic estimation when data are sparse. This has the added benefit that the accuracy increases when the traffic density increase, i.e. when the accurate trajectory prediction is most important.

5-3   Physical Wind Model

Wind is one of the primary atmospheric factors affecting airplane performance. It is the movement of air relative to the Earth. Wind can be quantitatively described with its velocity and its direction. The wind direction is defined as the direction from which the wind originates. Wind direction is defined in the Earth reference frame F_E. The movement of air is mainly the result of three major mechanisms being air pressure gradients, the influence of the rotation of the Earth and the surface friction forces.[11]

1. The air pressure gradients are caused by the uneven distribution of solar heat over the Earth on a large scale (Equator to Polar region) and on a minor scale (local natural and artificial heat sources and sinks like lakes, cities, etc.).

2. The rotation of the Earth induces a force that acts on moving air. This force is called the Coriolis force.

3. The surface friction force arises from the relative motion of the air with respect to the ground. The influence of the friction force is naturally larger closer to the Earth's surface. Its magnitude is mainly dependent on the degree of roughness of the terrain.

Hence, three mechanisms are able to influence the movement of air. Two of them, the rotation and the solar heating of Earth, define the always present gradient force G and Coriolis force C. The friction force W on the other hand depends on the

(a) Geostrophic wind, no friction.

(b) Change of wind due to friction.
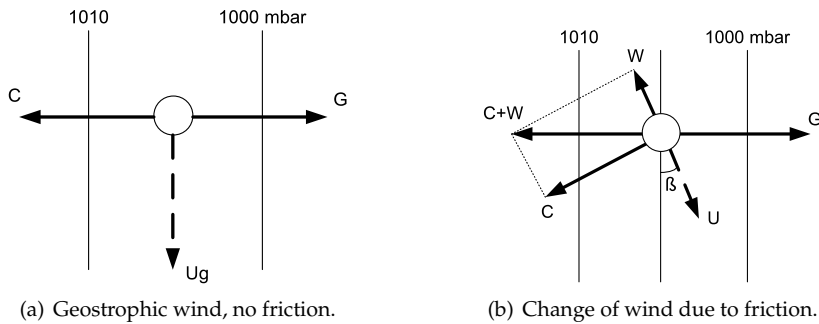
Figure 5-2: Influence of pressure gradient force (G), Coriolis force (C) and friction force (W) on movement of air in Northern hemisphere

distance to the surface and can be neglected at high altitudes. So two alternative situations arise, presented in Figure 5-2.[9,11] Figure 5.2(a) shows a non-friction situation which is valid at large distance from the Earth surface. The Coriolis force C has to balance the gradient force G to ensure the equilibrium. As a result the wind vector U is parallel to the isobars since the Coriolis force is always perpendicular to the wind vector. The wind velocity in this "frictionless" part of the atmosphere ("free" atmosphere) is usually called the *geostrophic wind U_g*.

Figure 5.2(b) describes the lower part of the atmosphere where surface friction is no longer negligible. A surface friction force W arises along the wind vector U in opposite direction. The gradient force G remains fixed. As a result, the gradient force needs to be balanced by the resultant of the Coriolis force and the friction force. Therefore the wind direction changes over an angle and the magnitude of the wind decreases. The wind velocity decreases gradually from its geostrophic value to zero at the ground. The deviation of the wind direction with respect to the geostrophic wind (β) becomes larger when the friction force increases, so closer to the ground. In the Northern hemisphere the wind vector rotates counter clockwise with decreasing altitude. This layer of the atmosphere where surface friction occurs is called the Planetary Boundary Layer (PBL). Its top is typically between 200 m and 2000 m above the surface.[10]

The above describes the general mechanism of wind generation on a large scale. But wind is also influenced locally by specific surface obstacles such as trees, buildings, etc. and by local differences in temperature. These distortions can be of great influence on the local wind profile. For this analysis the effect of local obstacles is less important, since they influence the wind profile only very close to the ground (< 1000 ft). For the accurate execution of continuous descent approaches it is acceptable to use the general surface roughness classification. The local temperature differences define the local stability of the atmosphere. The atmospheric stability is of more interest since it influences the wind profile over the whole PBL. This will be elaborated further in the next section.

5-3-1   The Atmospheric Stability

The atmospheric stability is one of the mechanisms that influences the local wind profile of the planetary boundary layer (PBL). The gradient of the wind velocity with the altitude depends on the amount of horizontal motion that is exchanged vertically.[5] The momentary temperature profile determines this stability, one of the major factors is the rate of change of air temperature with altitude.[2] Due to time evolution in terms of changing vertical thermal build-up, the boundary layer is a rather complicated object. The PBL has three broad types of structure with typical characterizing conditions:[5]

1. Unstable/convective boundary layers: light winds and a high surface heat flux

2. Neutral boundary layers: high winds and/or small surface heat flux

3. Stable boundary layers: light winds and a negative surface heat flux (most during night time)

The strong vertical heat exchange in an unstable atmosphere causes the horizontal wind speed to be maximally exchanged downwards.[11] As a result, the mean wind has a sharp increase near the surface. But throughout most of the boundary layer the mean flow is fairly uniform.[5] The stable boundary layer is the most variable of the three kinds of layers and is usually in a continuous state of evolution. This usually occurs between the hours of sunset and sunrise when the surface is cooling or when warm air moves over a cool surface. In these conditions there is very little vertical exchange of wind. This can lead to light winds near the surface and strong winds up in the atmosphere. Typical wind profiles for a stable atmosphere are illustrated by the solid line in Figure 5-3. The stable boundary layer is more responsive to Coriolis accelerations. This leads to the direction of the wind changing over the depth of the layer by 25-40°.[5]

In neutral boundary layers the wind profile does not depend on the vertical heat exchange but only on the surface roughness. The atmosphere has a neutral stability when clouds are present or in case strong winds occur. Extended cloud cover reduces the warming or cooling of the Earth's surface leading to little vertical heat exchange. With strong winds the vertical exchange of winds can be considered purely mechanical, the thermal effects are negligible.[9,11] The wind profile of a neutral boundary layer lies between the two extremes of a stable and unstable atmospheric condition.

Several wind measurements presented in[10] indicate that the difference in wind velocity of stable/unstable versus neutral atmospheric conditions remains relatively small. For instance, the daily change of mean wind velocity over 18 days of clear sky at an altitude of 124 m varied between 9 m/s (night) and 5 m/s (day).[10] Other
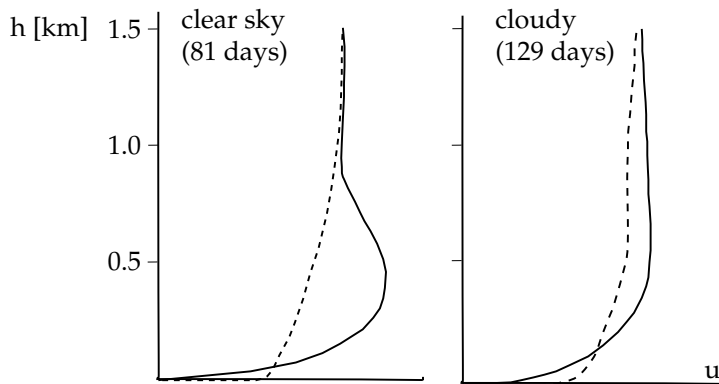
Figure 5-3: Mean wind profile for clear and clouded skies at Warszawa 1960: solid line = 0h00, dashed line = 12h00. [Source: Wieringa[10]]

wind data, presented in Figure 5-3, show a maximum difference of 4 m/s between the stable (solid line) and unstable wind profile (dashed line) at 350 m above the ground for 81 days of clear skies. During 129 clouded days the mean maximum difference was only 1 m/s. The wind profile of a neutral boundary layer lies between the two extremes of a stable and unstable atmospheric condition. So in the examples above, the maximum deviation of the wind velocity with respect to a neutral wind profile will be smaller than 4 m/s. The measured differences will probably increase a little for geostrophic winds that are somewhat stronger than 8 m/s. Nevertheless the deviations are expected to remain of the same order as the atmospheric boundary layer tends to get more neutrally stable with increasing wind.

For an efficient execution of a continuous descent approach a good estimation of the wind profile is necessary. The accuracy of the estimation becomes more critical when stronger winds occur. For these conditions a wind profile for a neutral boundary layer is applicable. In case of light winds and clear skies, the wind profile changes continuously due to the daily evolution of the stability in the PBL. The daily wind pattern changes from an unstable atmosphere during the day to a stable boundary layer during the night. The amplitude of the daily evolution varies on his turn with the seasons and depends on the climate. It can be concluded that these atmospheric evolutions are very complex and have much variety, so the modeling of the wind could be simplified a lot by assuming neutral stability at all times.

These observations indicate that the neutrally stable wind profile could be taken as an approximation to cover all situations of the planetary boundary layer.

Given the above considerations, it can be concluded that it is justified to assume a neutral atmospheric boundary layer.

5-3-2 The Mathematical Wind Model in Neutrally Stable Atmosphere

Different models have been used in literature to describe the wind profile in a neutrally stable planetary boundary layer. This section discusses these methods and defines which mathematical model will be used in this research. Before continuing it is important to know that the planetary boundary layer can be subdivided in two layers:[10]

- The lowest 20% of the PBL is the *surface layer*, usually with the top between 60-100 m. Here some simplifications may be applied that are not allowed for the whole PBL, for instance neglecting the Coriolis force.

- The other 80% of the PBL is the so-called "Ekman layer" where the profile is influenced by both friction and Coriolis force.

Since aircraft flying an approach generally need to be configured for landing and maintaining a stabilized airspeed by the time they reach 1000 ft above the ground, only the wind profile in the "Ekman layer" is of interest.

Hewitt and Jackson give the following mathematical description of the wind profile in the neutral boundary layer.[5] Over the lowest 100 m the profile is logarithmic and depends on roughness length z_0. In the upper part of the boundary layer, the profile depends on (z/h) and the power-law profile is a useful approximation. There is a systematic turning of the wind with height due to the Coriolis acceleration, ranging from about $5°$ to $20°$. The direction and magnitude of this turning is quite sensitive to changes in surface roughness and upper-layer conditions. Furthermore the strength of the Coriolis-force is dependent on the latitude.
Wind profiles are traditionally estimated with the *power-law*:[10]

$$V = V_0 \left(\frac{h}{h_0} \right)^p \tag{5-1}$$

where the wind speed V at altitude h is dependent on the windspeed V_0 at a reference height h_0. The exponent p is emperically derived constant, which for neutraly stable atmospher is approximataly $\frac{1}{7}$.[12]

Even if the reference point (h_0, V_0) is chosen to fit the actual situation best, this equation only yields a very general approximation of the wind profile in the PBL. Especially since the PBL is characterized by the interaction between the free stream wind at higher altitudes and the disturbing forces of friction caused by the earth's roughness, this approximation can differ significantly from the true wind profile. In order to derive a generally useful model that is not dependent on local surface roughness or the local latitude, the power-law is used as a baseline for the first approximation of the wind profile and to fill in the gaps when measeurment data is sparse. Subsequent estimates of the wind-profile are updated using available data from other aircraft as will be explained in the next section.

5-4   AMDAR wind prediction algorithm (AWPA)

The spatial and temporal variations of the wind affect the performance of the aircraft along the approach trajectory in the Earth-fixed reference frame. Accurate knowledge of the wind profile in the TMA is therefore required for an accurate own trajectory prediction and time-to-fly estimates. The wind profile is modeled using a statistical model. The advantage of such a model is that it does not rely on the physical processes that govern wind behavior but instead uses observations to estimate any profile shape. On the other hand, a logarithmic profile estimate based on the power-lawEq. (5-1) is able to provide at least an initial estimate when data are insufficiently available. This way the algorithm combines the best of both world, showing purely stochastic estimator behavior when data are abundant, but still producing a working estimate when such is data is not available.

In the near future various data-link scenarios are envisaged for instance in the SESAR and NextGen programs.[1] As the details of the proposed data-link systems such as ADS-B are not yet fully developed, this algorithm is based on the format of the AMDAR data. With the transmission of AMDAR-like data to nearby aircraft a wealth of meteorological information will become available for processing either board the aircraft or in ground-based system. ACARS is the communication system most widely used by aircraft participating in the AMDAR program. The AMDAR reports consist of meteorological measurements made on-board the aircraft such of the pressure altitude, airspeed, the air temperature and the wind vector, but also the aircraft position and altitude.

The structure of the algorithm that drives the wind prediction model is shown in Figure 5.4(a). The wind prediction model is driven by historical Automated Meteorological Data Relay (AMDAR) data. AMDAR data consist of meteorological observations such as wind speed and direction as well as position coordinates. They are broadcast through the Aircraft Communications Addressing and Reporting System (ACARS) to in-trail aircraft which then store the historical data in a Flight Management System (FMS) database. The data are processed to make estimates of the current and future wind profile by making predictions based on the historical data. The algorithm is designed with a high-traffic scenario in mind but when the number of historical AMDAR observations available is scarce (e.g., between arrival and departure peaks), a wind profile can still be constructed using the available data, without making predictions, however.

The algorithm consists of three steps, as illustrated by Figure 5-5. First, AMDAR data of preceding aircraft, each tagged with a corresponding time and altitude interval, is collected and stored in the FMS. Second, per altitude interval, the historical AMDAR data are filtered using a Kalman filter to remove measurement noise from the observations. The series of historical AMDAR data are then used to determine an auto-regressive model of the time series. Third, the wind profile is constructed by connecting the predictions per altitude interval by linear interpolation.

The prediction algorithm uses incoming ACARS data from other aircraft within a

(a) Structure of the wind prediction algorithm.

(b) Time-dependent wind profile at Chicago O'Hare on 7th of January 2005.
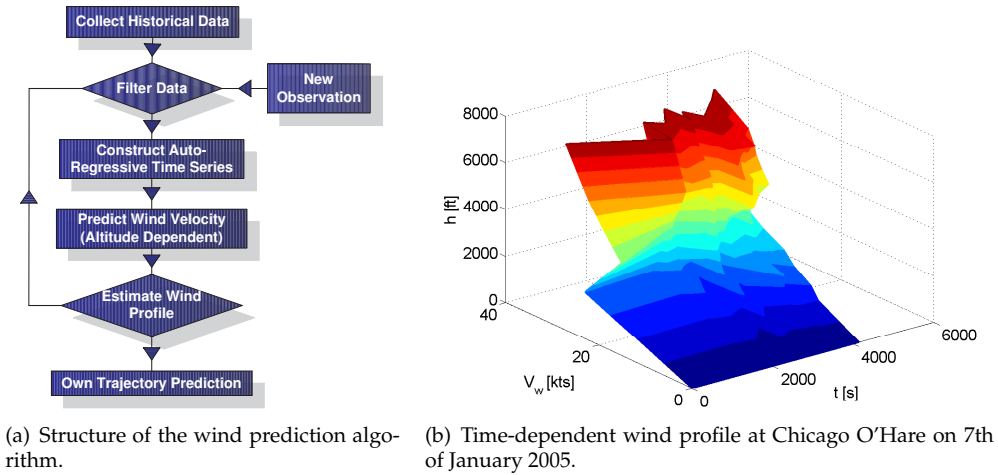
Figure 5-4: The wind prediction algorithm allows predictions to be made of the wind profile in the TMA.

certain range (for instance the TMA). The algorithm can be run either in the air, where data are processed on-board in the FMC, or on the ground; in this case the wind profile prediction could be up-linked to the aircraft.

The spatial coverage of AMDAR data makes it suitable for the wind prediction algorithm as the observations are made near and often on the same approach track. Temporal coverage of AMDAR data is highly variable due to peaks and lows in air traffic density. The wind estimation improves in high density traffic environments where aircraft spacing is critical to maintain high runway capacity.

The accuracy of AMDAR data depends on instrument measurement errors. Sources of error include calibration error, short-term random instrument error, calibration drift and static source error. These errors are corrected as much as possible by the ADC. Typical uncertainty of AMDAR data is in the range between 2 and 3 m/s.[7] System cross checks, gross error limits and outlier rejection are various methods used by the onboard quality monitoring system to eliminate bad data. Note that these measurement and quality monitoring systems may differ per aircraft type, which subsequently may affect the accuracy of the AMDAR data. Wind profile prediction in three dimensions is possible. Using all available measurements throughout the TMA and tagging them with position information, the algorithm can calculate the profile estimate based not only on height, but also on horizontal position. This yields a 2-dimensional prediction (North and East components of the wind speed) along any 3-dimensional path through the TMA.
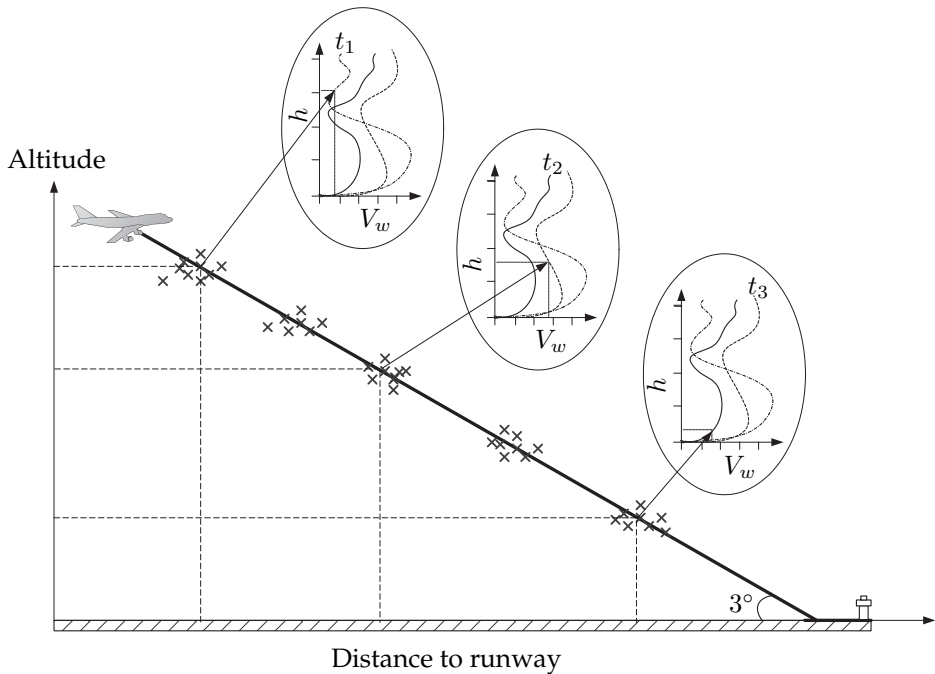
Figure 5-5: Time-dependent wind profile prediction. Spatially distributed AMDAR observations are represented by crosses. Each set of AMDAR observations is associated with an altitude, a longitude and a latitude.

5-4-1 Kalman Filtering and Algorithm Design

The following steps are taken in the construction of the wind profile prediction algorithm.

- Determine the nominal flight track. This track is the intended approach route under normal circumstances. Along this track, the wind profile will be estimated. The altitude resolution of the state vector is arbitrary, but in this case set to 500 feet. It is noted that the accuracy of the estimation depends on the accuracy, the amount and the spatial and temporal spread of the incoming data, and not on the resolution of the state vector.

- Generate an initial estimate when the first wind measurements come in. These might be either a nominal wind speed at certain altitude provided by ATS, or the first incoming data from ADS-B soundings from other aircraft. Based on these first measurements, a standard logarithmic wind profile is constructed according to Eq. (5-1))This logarithmic profile thus becomes the

initial state estimate, which will be updated whenever new data comes available.

- After this the filter is updated every 15 seconds, .

The general Kalman state equation and measurement equation are given by respectively:

$$
\begin{aligned}
v_{t+1} &= \phi_t x_t + w_t \\
z_t &= H_t v_t + u_t
\end{aligned}
\tag{5-2}
$$

In Eq. (5-2) v_{t+1} is the state estimate of the wind speed at time $t + 1$, ϕ_t is the transition matrix and w_t is the process noise. In the measurement equation z_t is the measured wind speed at time t, H_t is the measurement matrix and u_t the measurement noise. Since no system dynamics are incorporated in the model, the transition matrix $\phi_t = I(n \times n)$, where n is the number of states to be estimated (depending on the altitude resolution), and the measurement matrix $H_t = 1$.

The elements of the Kalman filter are constructed through steps 1 - 6 as follows at time instant k:

1. The state vector $\hat{x}$ is an $2n \times 1$ vector, where n is the number of altitudes, depending on the chosen resolution (in this case 500 ft, depicted as Flight Levels). The odd and even elements represent the North and East wind components, respectively:

$$
\hat{x}(k|k-1) = \begin{pmatrix} x_N^{10} & x_E^{10} & x_N^{15} & x_E^{15} & x_N^{20} & x_E^{20} & \ldots & x_N^{200} & x_E^{200} \end{pmatrix}^T
$$

2. When an observation comes in, the wind speed and direction are transformed into a North and East velocity component, which are stored along with the altitude at which the observation was broadcast (for example 1700 feet, FL 17):

$$
y(k) = \begin{pmatrix} v_N^{17} & v_E^{17} \end{pmatrix}^T
$$

3. In the next step, an $(2 \times 2n)$ C-matrix is set up to determine which elements of the state vector can be updated when a measurement comes in. In this case, it's the two points that are closest to the altitude of the measurement. The weights in the matrix are determined based on the altitude difference between the states of interest and the measurement.

$$
C(k) = \begin{pmatrix} c_N^{10} & 0 & c_N^{15} & 0 & c_N^{20} & 0 & \ldots & c_N^{200} & 0 \\ 0 & c_E^{10} & 0 & c_E^{15} & 0 & c_E^{20} & \ldots & 0 & c_E^{200} \end{pmatrix}
$$
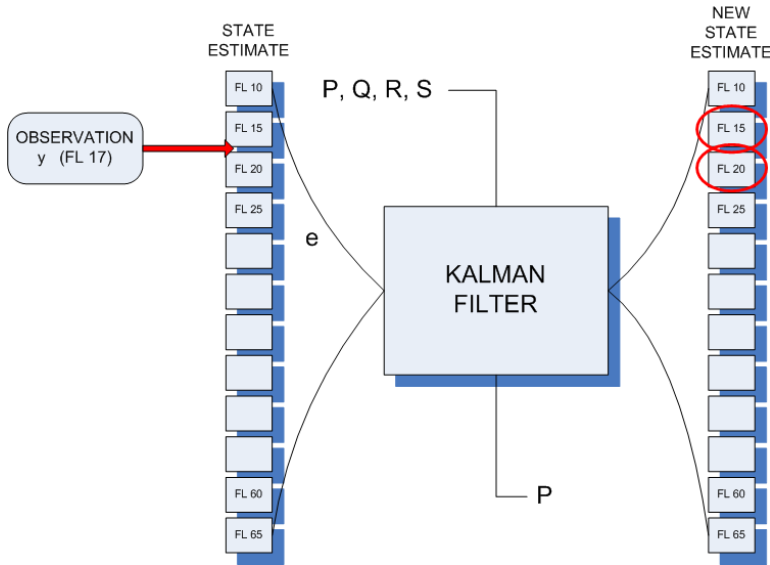
Figure 5-6: State estimate update schematic. The encircled elements of the state vector around the observation altitude are updated.

In this example, with the observation taken at FL 17 (so between FL 15 and FL 20), the C-matrix would be filled like this:

$$C(k) = \begin{pmatrix} 0 & 0 & 0.60 & 0 & 0.40 & 0 & \dots & 0 & 0 \\ 0 & 0 & 0 & 0.60 & 0 & 0.40 & \dots & 0 & 0 \end{pmatrix}$$

4. With this C-matrix, the current estimate for the altitude of the observation can be calculated, and its value can be compared to the measured value to determine the innovation e (2×1):

$$\hat{y}(k|k-1) = C(k)\hat{x}(k|k-1)$$

$$e(k) = y(k) - \hat{y}(k|k-1)$$

This way, an incoming measurement only influences the states in its (altitude) vicinity. This is also shown in Figure 5-6, where the encircled elements of the state vector are the updated values.

5. This innovation is to be multiplied with the Kalman gain to obtain a new state estimate. The Kalman gain is based on the relative magnitudes of the uncertainties in the current estimate and the new measurement. The measurement noise covariance matrix ($R(n \times 2)$) has been made dependent of the distance between the point of the measurement and the own track d, so

$$R(k) = \begin{pmatrix} R_0 + \alpha d(k) & 0 \\ 0 & R_0 + \alpha d(k) \end{pmatrix}$$

where α is assigned a value of 0.5 (if d is in nautical miles), which is not investigated or tested. In the first step, the covariance of the estimate is projected ahead:

$$P(k|k-1) = AP(k-1|k-1)A^T + Q$$

With this projection, the covariance of the innovation step can be represented by the scalar S:

$$S(k) = C(k)P(k|k-1)C(k)^T + R(k)$$

where P is the prediction error covariance matrix ($2n \times 2n$). These matrices together determine the Kalman gain K ($2n \times 2$):

$$K(k) = AP(k|k-1)C(k)^T S(k)^{-1}$$

A high [low] uncertainty in the current estimate (high [low] P) and much [little] confidence in the accuracy of the measurement (low [high] S) yield a high [low] value of the Kalman gain, which in turn assigns a large [small] weight to the incoming measurement in updating the state estimate through the innovation:

$$\hat{x}(k|k) = A\hat{x}(k|k-1) + K(k)e(k)$$

6. In the last step, the prediction error covariance matrix P is updated, according to:

$$P(k|k) = AP(k|k-1)A^T + Q - K(k)C(k)P(k|k-1)A^T$$

where Q is the process noise covariance matrix. This iteration is repeated with a constant time step of 15 seconds.

It can be seen that when no new observation data is available, there will be no innovation, and the loop is reduced to updating the prediction error covariance P. In this way, the uncertainty about an estimate increases when time goes by without new incoming measurements. A schematic of this loop is given in Figure 6-3.

Figure 5-8 shows that the initial estimate (dashed line), based on the single first incoming measurement, equals the logarithmic profile. For this estimate, the initial covariance matrix P is set high, which will yield a high Kalman gain, giving a high weight to the first set of ACARS data, in this case a sounding by one aircraft,
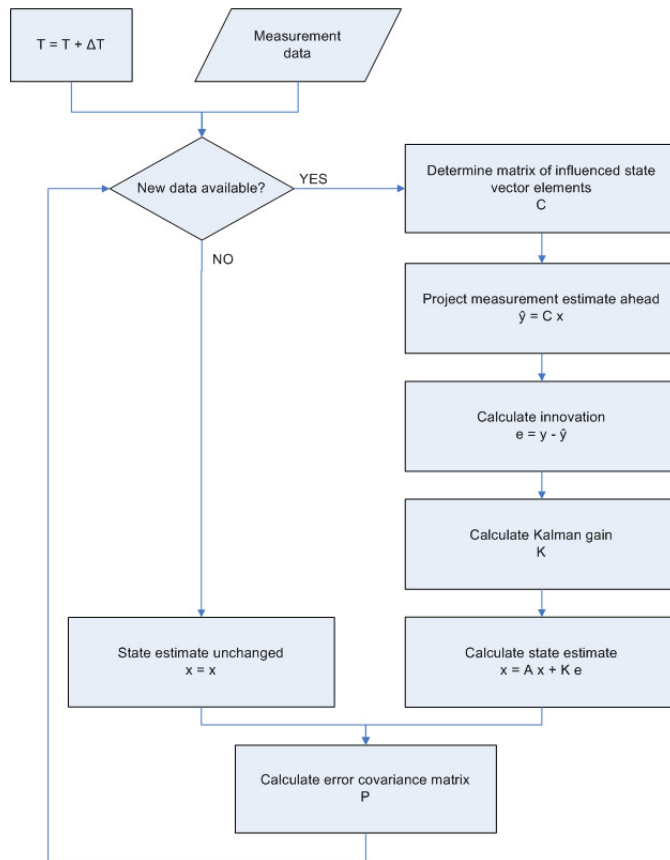
Figure 5-7: Kalman filter schematic.
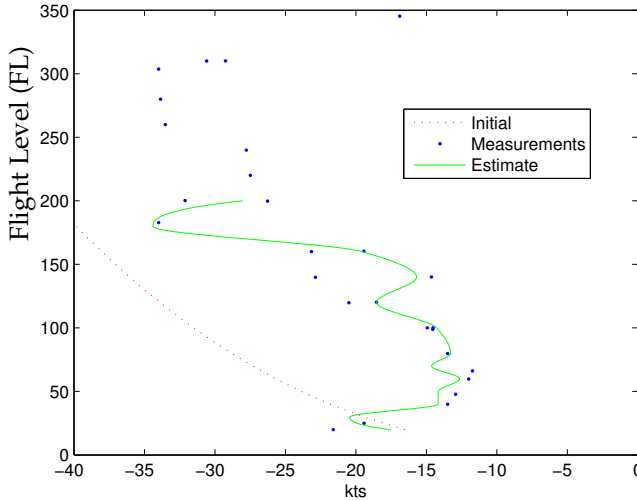
Figure 5-8: Wind profile update process, T = 0 minutes

descending from FL300 to FL20. The blue dots represent the actual incoming measurements, and the green solid line is the new wind profile estimate. Seven minutes later, a total of 29 new data broadcasts have come in, thirteen of which are in the altitude range of interest (FL10-200). Based on these thirteen measurements, the previous estimate (red dotted line in Figure 5-9) is updated to become the solid line in Figure 5-9, and so forth.

The influence of the measurement error covariance (R) is shown in Figure 5-10. This plot is based on the same data as Figure 5-9, only for a higher value of R. Since this higher value indicates noisier measurements, their influence on the update of the windprofile decreases.

5-4-2   Wind profile construction

The output of the algorithm is a set of predictions per 500 ft altitude interval along the planned arrival trajectory, which represent the evolution of the wind speed along the time axis, starting from the present time of the aircraft until the time t minutes ahead at the end of the continuous descent aapproach procedure. For each prediction step, the wind profile is constructed by connecting the predictions per altitude interval by linear interpolation. Also, the wind profile between prediction steps is determined by linear interpolation.
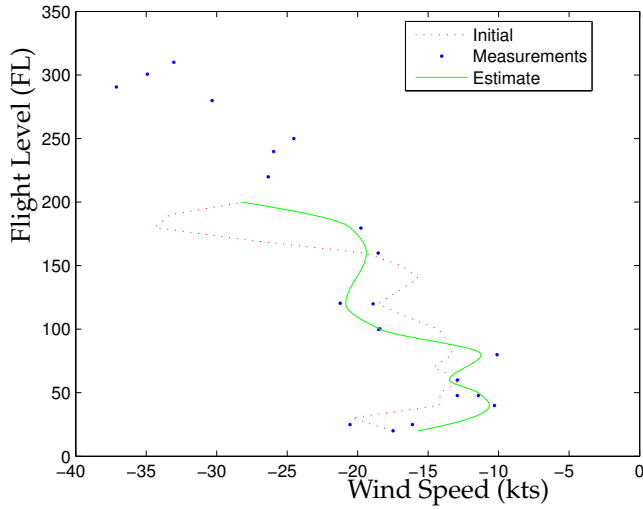
Figure 5-9: Wind Profile estimate (North component), T = 7 minutes
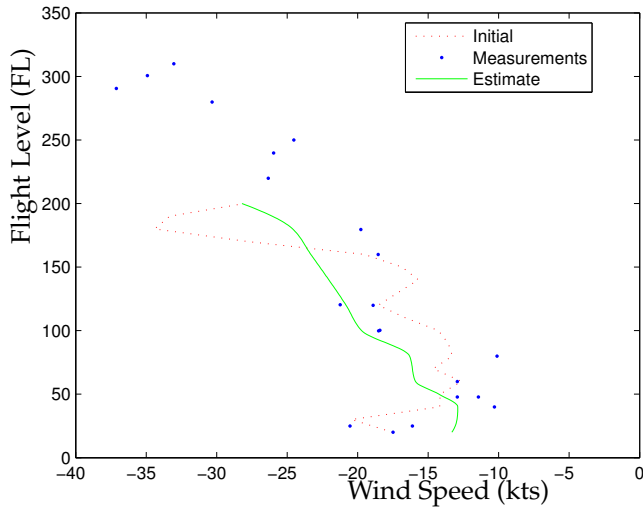
Figure 5-10: Wind profile estimate (North component), T = 7 minutes, high measurement error covariance

5-5   Wind Prediction Performance Evaluation

The functioning of the wind predictor in an off-line simulation is visualized in Figure 5-11. For this specific simulation, measurement data from ADS-B soundings at Chicago O'Hare (2 January 2005, 14.10pm - 15.05pm) from nine consecutive incoming or outgoing aircraft (in multiple bearings) have been used. As these aircraft fly through the TMA, measuring and broadcasting (a.o.) wind speeds, the filter is updated every time step (15 seconds) where new data has come in. So every time an aircraft passes along its data, a new estimate is made. Figure 5-11 shows the development of the wind profile with every passing aircraft. For clarity, it is assumed in this simulation that one aircraft finishes its entire approach or departure, before the next enters the area of interest.In reality the algorithm handles every incoming measurement at any time, regardless of the number of aircraft in the TMA.

Since the filter uses the relative distance between the location of the measurement and the own aircraft to adjust the measurement error covariance matrix R, an arbitrary 3-dimensional approach path has been set up for the own aircraft. An example of this path is shown in Figure 5-12. In fact, the wind profiles as given in Figure 5-11 are along this approach track, so in effect they are 3-dimensional.

5-5-1   Check on relevant parameters

The most important parameters calculated in the Kalman filter (as described in Section 5-4-1) are the innovation step (the difference between the 'projection ahead' at a certain point of interest and the value measured at that point) and the Kalman gain. For a single aircraft passing along the altitudes of interest the response of these quantities is shown in Figure 5-13. In this case, the altitude range for which a wind profile is to be constructed is FL10-FL200. As long as the aircraft is above this altitude, the broadcast data are not used. It can be seen in Figure 5-13 that after approximately 23 minutes the aircraft descends into this altitude range, and its broadcasts are used to update the wind profile estimate. From this moment on, every innovation step is assigned a weight (the Kalman gain, depicted with the green dotted line), to determine the new estimate for this altitude. The area of influence of an incoming measurement is indicated by the drop-back of the Kalman gain. After a measurement has come in, the gain drops back to zero (first very steeply, later more gradually), decreasing the influence of this measurement on other elements of the estimated state vector.

According to Kalman filter theory, the accuracy of an estimate depends on the quality of the system model, the accuracy of the available measurements and the number of them. In this case, the system dynamics are zero, so the accuracy of the wind prediction depends on the measurements alone. It is therefore hypothesized that the prediction error will decrease as more data becomes available. This is shown in Figure 5-14. Here the mean value of the prediction error covariance matrix P is plotted against time. This (scalar) value $\bar{p}$ is calculated according to:
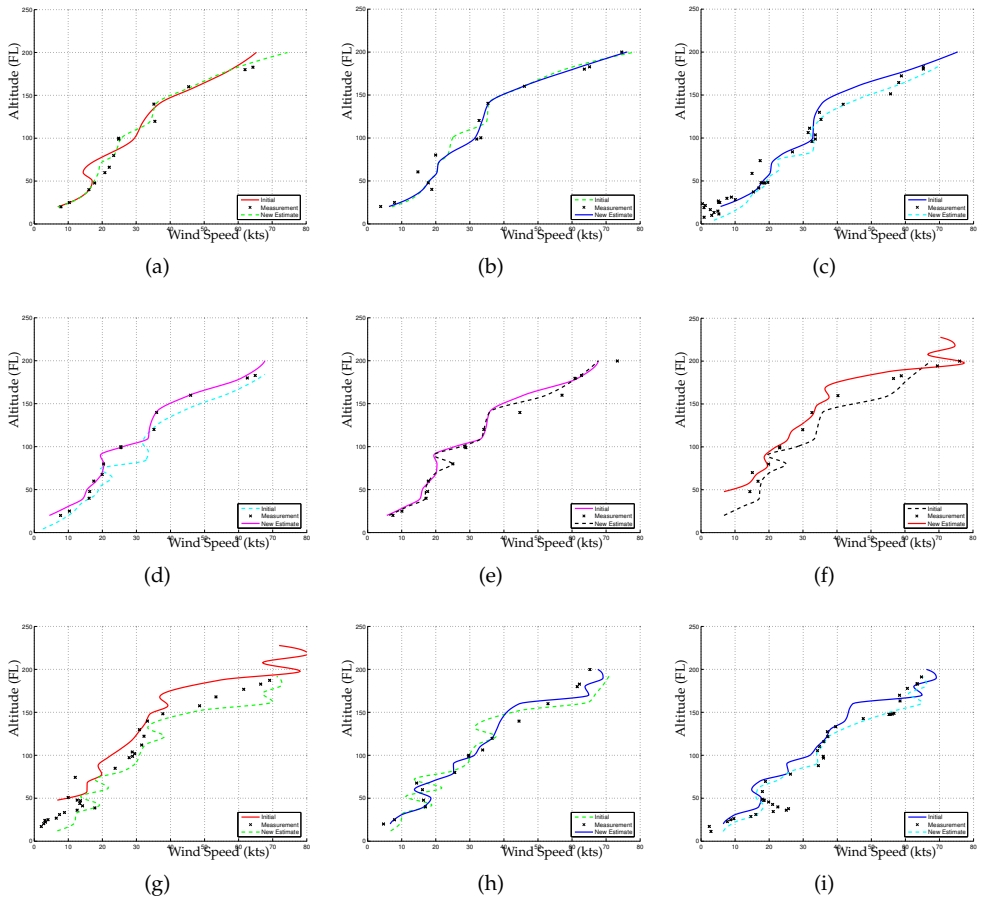
Figure 5-11: Influence of new data from subsequent incoming aircraft on the wind profile prediction. Each new estimate becomes the 'initial estimate' in the next subfigure.
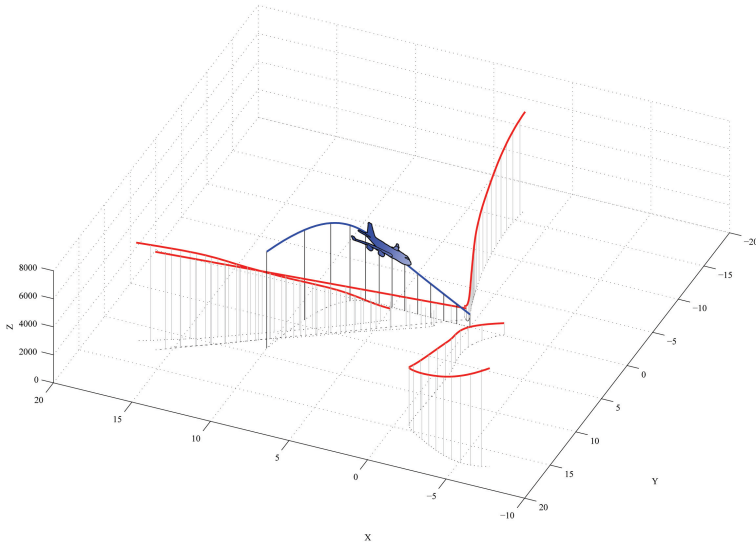
Figure 5-12: Own track of an aircraft (with symbol). The tracks of previous aircraft are also shown.
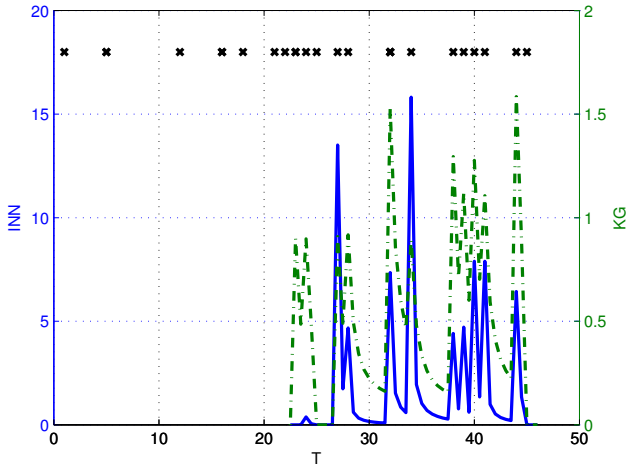
Figure 5-13: Innovation step (solid line) and Kalman gain (dash dot) of a single aircraft data set. The black crosses indicate that a new measurement has come in at that time. Note that the observations up to 23 minutes are disregarded because they are taken above the altitude of interest.
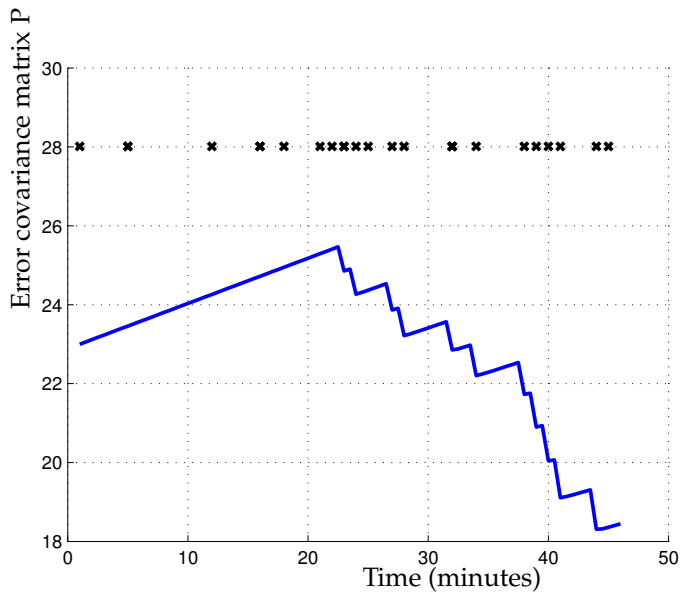
Figure 5-14: Development of the Error covariance matrix P in time. The black crosses indicate that a new measurement has come in at that time. Note that the observations up to 23 minutes are disregarded because they are taken above the altitude of interest.

$$\overline{p} = \sqrt{\sum_{i=1}^{n}\sum_{j=1}^{n}\frac{P(i,j)^2}{n^2}} \tag{5-3}$$

for the $n \times n$-matrix P. The figure shows that while time goes by without (significant) measurements coming in (so up to 23 minutes), the value of $\overline{p}$ increases. This higher covariance means the uncertainty about the quality of the current estimate increases. As a consequence,

- when a new single measurement comes in, it will be assigned a relatively high weight: the confidence in the current estimated value has dropped with respect to the confidence in the new measured value, and

- when new data becomes available the uncertainty in the estimate is reduced. This can be seen in the decrease of $\overline{p}$ whenever a measurement comes in, starting at T = 23 minutes.
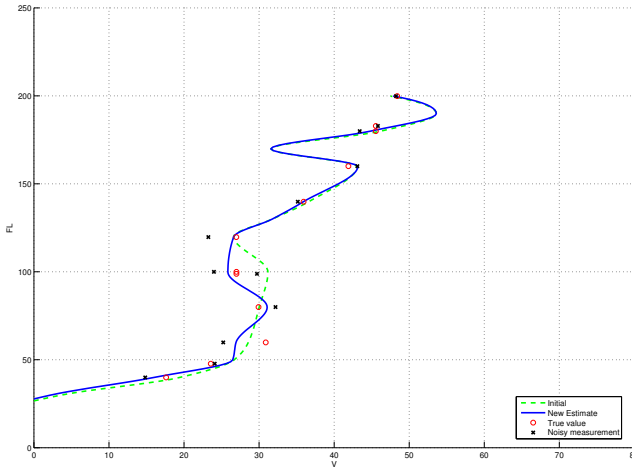
Figure 5-15: Wind profile estimate with simulated observations.

5-5-2 Performance accuracy

In order to see how well the noise is filtered from the observation data, an extra noise has been added to the data set. So for this case, an available observation set is considered to be the true wind speed, which is to be estimated. A normally distributed noise (mean: 0, std: 3 kts, representing average FMS accuracy) is added to this data set, to represent the incoming measurements. These simulated measurements are the input for the AWPA algorithm. The estimate it produces can then be compared to the real values. This process is shown in Figure 5-15. The 'true' values (taken from the observation data) are represented by the circles, while their noisy counterparts are depicted as crosses. The estimate is shown in the solid line.

To check the robustness of the simulation, a bootstrap sample has been used to calculate the mean and 95% confidence intervals of Root Mean Squared of the prediction error. For this case, the RMS of the prediction error is around 3.2 kts, see Figure 5-16. For comparison, the RMS of the (simulated) measurement deviation is depicted on the right in this figure.

5-6 Conclusions

The proposed AMDAR wind prediction algorithm (AWPA) estimates and predicts wind profiles based on the meteorological data broadcast by nearby aircraft, ef-
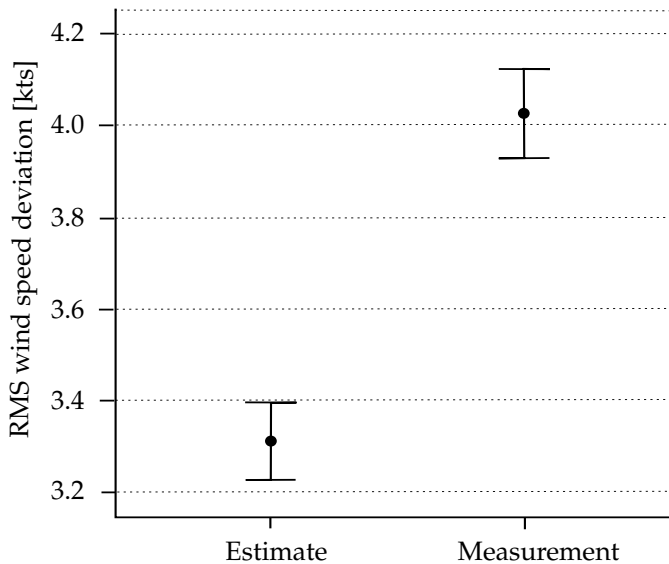
Figure 5-16: RMS of the wind speed prediction error.

fectively using them as real-time wind sensors in the TMA. The algorithm has the advantage of producing high-fidelity, high-resolution wind profiles that can immediately be used. Advanced approach procedures that require constant trajectory prediction and optimization can directly utilize the produced profiles. Validating the algorithm against a set of AMDAR data from Chicago O'Hare showed that the RMS of the prediction error is in the order of 3.2 kts which is of the same order as the accuracy of the measurements.

References

[1] SESAR Master Plan-Deliverable 5. Technical report, SESAR Consortium, 2006.

[2] M. Baarspul. *Flight Simulation Techniques*. Faculty of Aerospace Engineering, Delft University of Technology, Delft, The Netherlands, 1982.

[3] E. A. Bossanyi. Short-Term Wind Prediction Using Kalman Filters. *Journal of Wind Engineering*, (9(1)):1–8, 1985.

[4] R. A. Coppenbarger, R. W. Mead, and D. N. Sweet. Field Evaluation of the Tailored Arrivals Concept for Datalink-Enabled Continuous Descent Approaches. In 7th *AIAA Aviation Technology, Integration and Operations Conference (ATIO)*, number AIAA-2007-7778, Belfast, Northern Ireland, Sep 18-20 2007.

[5] C. N. Hewitt and A. V. Jackson. *Handbook of Atmospheric Science, Principles and Applications*. Blackwell, Oxford, UK, 2003.

[6] J. K. Klooster and K. D. Wichman. 4D Trajectory and Time-of-Arrival Control to Enable Continuous Descent Arrivals. Honolulu (HI), USA, Aug 18-21 2008.

[7] W. R. Moninger, R. D. Mamrosh, and P. M. Pauley. Automated Meteorological Reports from Commercial Aircraft. Technical Report ARP 5430, World Meteorological Society, 2003.

[8] D. Painting. AMDAR Reference Manual. Technical report, World Meteorological Organization-AMDAR Panel, 2001.

[9] A. P. W. Steentjes. Design and Development of a Generic Terrain-Based Wind Atmosphere Module for Future Flight Simulators. MSc. Thesis, Faculty of Aerospace Engineering, Delft University of Technology, 2001.

[10] J. Wieringa. *De Atmosferische Grenslaag (in Dutch)*. Lecture notes, Faculty of Applied Sciences, Delft University of Technology, 1987.

[11] J. Wieringa and P. J. Rijkoort. *Windklimaat van Nederland (in Dutch)*. Staatsuitgeverij, The Hague, The Netherlands, 1983.

[12] N. M. Zoumakis and A. G. Kelessis. Methodology for Bulk Approximation of the Wind Profile Power-Law Exponent under Stable Stratification. *Boundary-Layer Meteorology*, 55(1-2):199–203, 1990.

6

Time Based Spacing

Implementing Time Based Spacing for Continuous Descent Approaches in Realistic Wind Conditions

A.C. in 't Veld, R.D. Groenouwe, M. Mulder and M.M. van Paassen

Submitted to the AIAA Journal of Aircraft, December 2009

6-1 Abstract

Although very effective at mitigating noise impact on the populated areas that surround airports, continuous descent approaches generally reduce runway capacity with respect to standard ILS approaches. Large uncertainties in descent trajectories force air traffic controllers to apply large separations in order to ensure safe operation. In this paper, a solution is presented that addresses the problems of variability in deceleration profiles and wind uncertainty. Spacing is done by providing pilots with a required time of arrival. A support system then helps the pilot in meeting this time goal. A wind prediction algorithm has been developed that creates a wind profile estimate along the intended three dimensional approach track, using filtered wind data observations broadcast by nearby aircraft. By combining these wind estimates with a flap scheduling algorithm, accurate on-board track and speed guidance becomes available. An interface has been designed that aids the pilot both in flying a controlled continuous descent approach and in meeting the time target set by air traffic control. To test the combined support system, a piloted simulator experiment was set up. Performance in terms of time goals was found to be consistent under all tested conditions and significantly better in comparison with the non-supported condition. Also, workload is acceptable and significantly lower

with the display optimization present. Providing the pilot with continuously up-dated time performance information based on actual meteorological circumstances was shown to be an important requirement for the implementation of CDAs in a time based spacing environment.

6-2   Introduction

All over the western world, and especially in Europe, aircraft noise is a major limit-ing factor of airport capacity growth.[2] Much attention is paid to mitigating airport nuisance affecting the surrounding communities. Many different approaches are taken, for instance, in the fields of aircraft engine technology and airport infras-tructure planning.[1] The approach under study here will focus on noise abatement approach procedures, and how these can attribute to lowering aircraft noise impact on the ground. In this field there is still significant room for improvement, since the procedures currently in place hardly make use of advances in guidance, navigation and surveillance technology.

Over the years, several noise abatement approach procedures have been devel-oped.[4,5,7,8] Variants include general procedures like different versions of the Con-tinuous Descent Approach, and airport-specific measures.[7–9,16,25] One character-istic aspect of many of these proposed procedures is that part of the approach is carried out with more or less idle thrust settings. Also, aircraft avoid flying level segments at low altitude, which are typical for the current standard procedures, in-cluding ILS approaches. These new procedures have been shown to reduce aircraft noise, but at a cost: differences in deceleration between different aircraft perform-ing the descent procedures force air traffic controllers to apply larger initial separa-tions to ensure safe operation. As a result, runway capacity is reduced.[6,9,14,18,22,23]

In this paper a solution to this problem is proposed by introducing a pilot support system that enables time based separation during the approach. In other words, pilots are given a Required Time of Arrival (), rather than radar vectors. It then be-comes the pilot's task to comply, within bounds, with this time goal, whereas final responsibility for safe separation remains with . The resulting system enables con-tinuous descents, while still guaranteeing safe separation. This research focuses in particular on curved approach procedures under realistic wind conditions. Wind has a major influence on the accuracy of time based separation, and prediction of the wind profile encountered during the approach could be of great importance. A tool capable of accurately predicting wind conditions along a three-dimensional approach track was developed. Together with an algorithm that calculates the op-timum settings for parameters such as the altitude where thrust is reduced to flight idle, this forms a support system that helps the pilot in flying idle thrust, continu-ous descent approaches while meeting arrival times instructed by ATC. This should allow ATC to sequence and space aircraft in the more tightly, eliminating the capac-ity reduction currently associated with many noise abatement procedures.
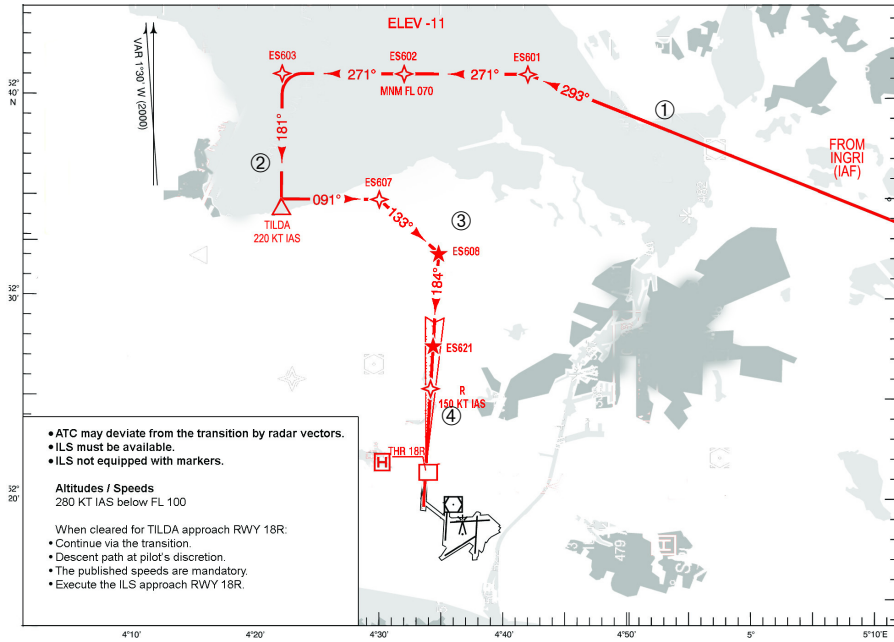
Figure 6-1: The approach route, top view. The starting points of the phases of the CDA procedure are indicated. ① Level flight at 7,000 ft, ② Constant IAS descent along $3°$ glide path, ③ Idle thrust descent, ④ Constant final approach speed along ILS.

This paper discusses (i) the characteristics of the particular Continuous Descent Approach procedure investigated in this paper, (ii) the algorithms that form the pilot support system and (iii) the results of a piloted simulator experiment that was set up to test the behavior of the system under realistic circumstances.

6-3 Continuous Descent Approaches

6-3-1 Description of the procedure

Based on practical experience with Noise Abatement Procedures at Amsterdam Airport Schiphol in the Netherlands and previous research,[9,23] a procedure resembling a standard nighttime transition[3] was chosen as the scenario for this research. These transitions typically involve a number of turns to avoid flying directly over the most densely populated areas. Obviously, these turns will cause considerable variation of the headwind and crosswind components when flying these transitions.

As can be seen from Fig. 6-1, the procedure consists of four parts. In phase ①, the aircraft is flying level at a relatively high altitude, but within TMA boundaries, for instance 7,000 ft. Nominal airspeed in this part is 220 kts IAS. At about 22 NM out, the aircraft intercepts a 3° glide path, but maintains its nominal indicated airspeed (phase ②). At a predetermined altitude, thrust is reduced to flight idle, marking the beginning of phase ③. This is the most crucial phase of the procedure, because the aircraft is now decelerating at idle thrust, and manipulation of the flap schedule is the only control for the flight crew to control both the time of arrival and the decelaration to reach the final approach speed precisely at the reference point. When the aircraft reaches its final approach speed, thrust is reapplied and this speed is maintained (phase ④) until touchdown on the runway. For safety reasons, the aircraft should reach this approach speed no later than when it reaches 1,000 ft altitude, approximately 3 NM from the runway threshold. This point will be later in this paper referred to as the reference window and is located at RNAV waypoint R ('*Romeo*'). At this point, the aircraft should be fully configured for landing, with full flaps extended and landing gear down. From here, the remainder of the approach is identical to a standard ILS approach procedure.

This type of approach procedure requires certain technologies to be available in aircraft throughout the arrival stream. For example, following a 3° glide path, while not yet aligned with the runway centerline, would require VNAV-path or Microwave Landing System (MLS) capabilities on board of the aircraft. Although not yet widely implemented, these technologies are already available today.

6-3-2   Time based separation

Variations in the characteristics of this approach trajectory would make it difficult for an air traffic controller to space incoming traffic. Three factors are identified as having an important influence on the CDA's characteristics:[10]

- Different aircraft types with their own characteristic idle-thrust deceleration profiles,

- Varying wind conditions, and

- Uncertainties in pilot behavior.

As all of these factors need to be accounted for in spacing, uncertainty adds up and controllers apply large initial separations as a safety buffer. Transferring all or part of the spacing task to the cockpit could greatly reduce the problem of the different deceleration profiles, since in general the flight crew will have access to more aircraft-specific and situation-specific information on own aircraft characteristics than an air traffic controller on the ground.[17,18] One way to go about this is the concept of time based separation, providing each pilot in the chain with a Required Time of Arrival (RTA) at touchdown and other waypoints along the approach trajectory. These RTAs allow the controllers to increase runway landing
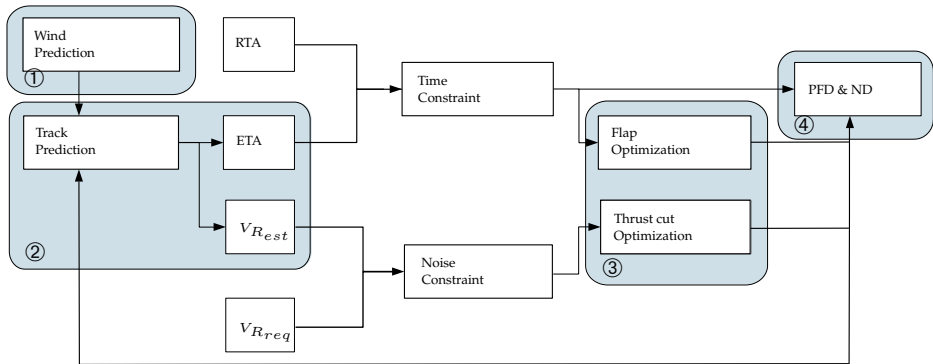
Figure 6-2: Schematic of the support system algorithm. The four modules are indicated ① - ④.

capacity, by providing the aircraft under their control with optimized arrival times. It then becomes the pilot's task to navigate his aircraft to the runway, respecting the time constraints as demanded by ATC. The focus of this research is to investigate whether implementation of a system of time based separation is feasible under actual operating conditions (curved trajectories, varying winds), without putting too much workload on the flight crew.

6-4   Support System Design

To help the flight crew in meeting the goals stated above, a support system has been developed. Its main aim is to provide the pilot with continuous information on the aircraft status with respect to the time goal and the execution of the continuous descent approach. The support system consists of four modules, shown as encircled blocks in Figure 6-2. In this section the first three modules (wind prediction (①), track prediction (②) and an optimization module (③)) are explained. The last module (module ④) translates some of the parameters in the system into information for the pilot, information which is then presented on the cockpit displays, along with a time performance indication. This is described in Section 6-6.

6-4-1   Wind profile prediction

As indicated in the previous Section, the wind encountered during the approach has a large influence on the accuracy with which the entire procedure is flown. It is, therefore, very important to have a tool that accurately predicts the wind profile ahead of the own aircraft. An algorithm was developed, capable of predicting horizontal wind speed and direction along any path in a three dimensional space. This wind profile prediction algorithm is based on previous research,[10] which
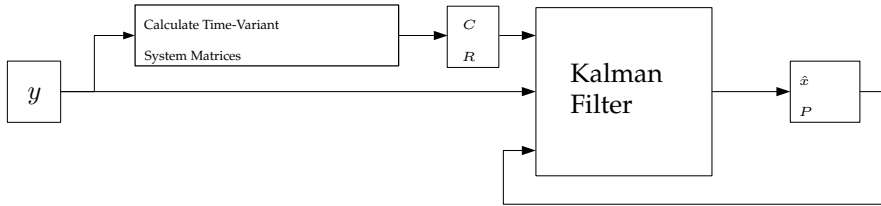
Figure 6-3: Schematic of the filtering process in the wind prediction algorithm.

assumes measurements of wind data are available, for instance through ADS-B soundings from other aircraft in the vicinity. These measurements are then filtered using a Kalman filtering technique to produce an estimate of the wind profile the aircraft will encounter. The Kalman filter is well-suited to deal with integrating noisy measurements in the prediction.[19] In addition, it is easily implemented in a recursive algorithm, thereby reducing the need to store large quantities of wind data on board.

This model was modified to be usable in three dimensions, making wind profile prediction along any curved approach trajectory, from any position and altitude, possible. In addition, functionality to use every incoming observation was incorporated, where in earlier work only data around certain fixed altitude intervals was used. This allows optimal use of the information at hand, and is expected to make the prediction more reliable, especially in situations where data density is low. A description of the way the wind prediction algorithm works is given below.

First, an initial wind speed estimate vector $\hat{x}$ is set up. This vector contains wind speeds for a number of altitudes. In this study, the altitude interval is set to 500 ft. This interval is arbitrary, since the accuracy of the prediction only depends on the amount and accuracy of the available wind measurements. The set up of this initial wind profile guess is arbitrary. It may consist of unfiltered measurements of ADS-B soundings, or a standard profile uploaded from an Air Traffic Services unit. In this case a standard logarithmic wind profile is constructed as follows:

$$\hat{x} = V_0 (\frac{h}{h_0})^{\kappa}, \tag{6-1}$$

with κ the Von Karman constant, equal to 0.4.[11] This equation bases the wind speed $\hat{x}$ on the free stream wind velocity V_0 at a corresponding altitude h_0, whereas h is the altitude at which we want to determine the wind speed.

Whenever new data come in, this profile is updated. An incoming observation y_k is split into North and East components, to be able to estimate these separately. Next, a weight matrix C is set up that determines the influence this observation will have on the state estimation of the wind speed. The weights in the matrix are determined

based on the altitude difference between the states of interest and the measurement. With this C-matrix, the current estimate for the altitude of the observation can be calculated, and its value can be compared to the measured value to determine the innovation e. This way, an incoming measurement only influences the states in its altitude vicinity:

$$\hat{y}(k|k-1) = C(k)\hat{x}(k|k-1) \qquad\qquad (6\text{-}2)$$
$$e(k) = y(k) - \hat{y}(k|k-1) \qquad\qquad (6\text{-}3)$$

This innovation is multiplied with the Kalman gain to obtain a new state estimate. The Kalman gain is based on the relative magnitudes of the uncertainties in the current estimate and the new measurement, represented by the prediction error covariance matrix P and the measurement noise covariance matrix R, respectively. Since data from aircraft on the same approach track rather than elsewhere in the TMA are of more use for this prediction, the measurement noise covariance matrix R has been made dependent of the distance between the point of the measurement and the own track d:

$$R(k) = f(R_0, d(k)) \qquad\qquad (6\text{-}4)$$

Here, R_0 represents the uncertainty in an incoming observation, mainly caused by measurement error. The accuracy of wind measurements in ADS-B soundings is approximately 2 kts.[20] The prediction error covariance matrix P is given by:

$$P(k|k-1) = AP(k-1|k-1)A^T + Q \qquad\qquad (6\text{-}5)$$

In this equation, the matrix A represents the system dynamics. However, since the filter is used only as a noise filtering mechanism, no system dynamics are present and A reduces to the Identity matrix. Q is the (constant) process noise covariance matrix, which is determined empirically. At the same time as when the initial wind profile is set up, the P matrix is assigned a large value. This represents the large uncertainty in the accuracy of the profile at this point, and ensures that in the beginning, incoming observations have a large influence on the wind profile estimate. With this projection, the covariance of the innovation step $e(k)$ can be represented by the matrix S:

$$S(k) = C(k)P(k|k-1)C(k)^T + R(k) \qquad\qquad (6\text{-}6)$$

The covariance matrices together determine the Kalman gain K:

$$K(k) = AP(k|k-1)C(k)^T S(k)^{-1} \qquad\qquad (6\text{-}7)$$

A high uncertainty in the current estimate (high P) and much confidence in the accuracy of the measurement (low S) yield a high value of the Kalman gain, which

in turn assigns a large weight to the incoming measurement in updating the state estimate through the innovation. By the same rationale, much confidence in the current estimate and little in the accuracy of an incoming measurement yields a small value of the Kalman gain and consequently little influence of the observation on the wind speed estimate:

$$\hat{x}(k|k) = A\hat{x}(k|k-1) + K(k)e(k) \qquad (6\text{-}8)$$

In the last step, the prediction error covariance matrix P is updated, according to:

$$P(k|k) = AP(k|k-1)A^T + Q - K(k)C(k)P(k|k-1)A^T \qquad (6\text{-}9)$$

This iteration is repeated with a constant frequency of 1 Hz. It can be seen that when no new observation data are available, there will be no innovation, and the loop will be reduced to updating the prediction error covariance P. In this way, the uncertainty about an estimate increases when time goes by without new incoming measurements. A schematic of this loop is shown in Fig. 6-3.

Interpolation between the updated elements of the state vector yields the wind profile the aircraft is expected to encounter during its approach flight. The results of one such wind profile prediction are shown in Fig. 6-4. Here, a random wind profile (crosses) is shown, together with its best estimation (circles) based on the available observations. A best fit logarithmic profile (diamonds) is shown for reference. It is clear that the Kalman filtering method is much more capable of capturing the random variations in realistic wind profiles than a logarithmic profile can. For the wind speed profiles used in the piloted simulator experiment (see Section 6-6), the average root mean squared (RMS) of the wind speed prediction error for the Kalman filter based predictor is 2 kts, corresponding to the accuracy of the wind speed measurements available through ADS-B soundings. Prediction accuracy is much lower for a logarithmic predictor, with RMS values averaging 6 kts, occasionally running as high as 9 kts.

6-4-2   Track and time prediction

In the proposed scenario, the track to fly is fixed and determined by RNAV waypoints, as shown in Fig. 6-1. During the flight, an algorithm estimates the speed and time profiles along this track, taking into account the actual condition parameters such as predicted wind speed profile along this track, aircraft weight, flap setting, etc. The track prediction, consisting of speeds and times calculated for every point on the track, is repeated every second.

Between the constant speed segments of initial airspeed and final approach speed, deceleration takes place by selecting a flight idle thrust setting. The deceleration profile is influenced by varying wind conditions. Flap extension towards landing
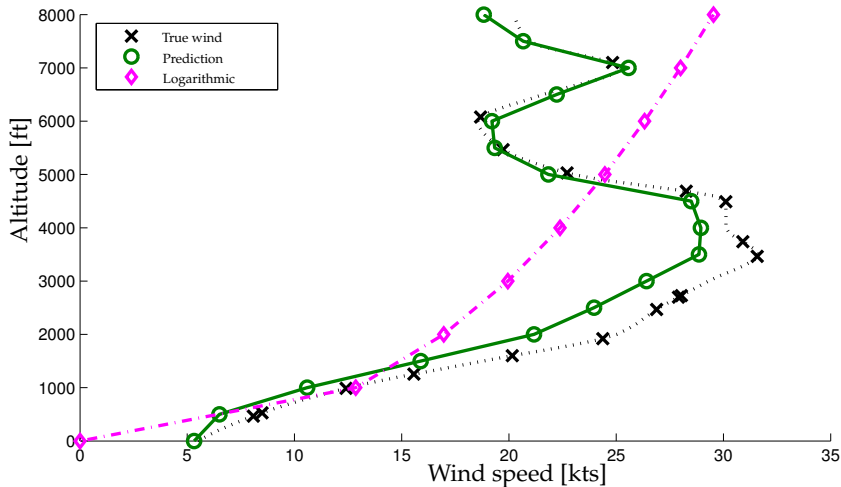
Figure 6-4: Wind profile prediction performance. A typical wind profile and its estimate (in 500 ft intervals). For reference, a best-fit logarithmic profile is also shown.

configuration also takes place in this phase, resulting in very non-linear aircraft behavior. To predict the aircraft motion in this phase, a simple three degrees-of-freedom aerodynamic model of the B747-200 was used. The model is a point mass model that only looks at the forces along the flight-path and perpendicular to it. The resulting accelerations along the flight trajectory are integrated over time to yield speed, distance and time profiles. Since the model is two dimensional, it is fed with only the along-track component of the predicted wind speed.

6-4-3 Optimization of support system performance

To introduce greater flexibility and robustness in the aforementioned prediction modules, an algorithm was added to optimize two CDA parameters, flap speeds and thrust cut altitude. This third module is based on a flap scheduling algorithm, used in previous research in various forms.[10,21,24] It uses the same aircraft model mentioned in the previous Section, to calculate the effects of changed flap settings on the speed and time profiles in the trajectory ahead.

The flap schedule algorithm works in two modes: in HOLD mode and CAPTURE mode. In CAPTURE mode the algorithm calculates the thrust cut altitude, the altitude at which the thrust should be set to idle so that V_{APP} can be reached at h_R using the nominal flap schedule. This information is communicated to the pilot through a cue on the PFD, see Section 6-6.

Once the thrust has been set to idle the module switches to HOLD mode. In HOLD mode the algorithm determines a flap schedule such that the aircraft reaches V_{APP}

at h_R. This deviation from the nominal schedule can be used to cope with errors caused by for instance an inaccurate wind prediction, unexpected behavior from preceding aircraft, etc. In this mode, the algorithm predicts the aircrafts trajectory based on the current flap schedule. This yields an ETA, which is then compared to the RTA commanded by ATC:

$$\Delta T = ETA - RTA \qquad\qquad (6\text{-}10)$$

Based on this difference, the flap scheduler does a rough tuning of the flap speeds to either their upper or their lower bounds, depending on the sign of this ΔT. In case the aircraft is predicted to arrive early, deceleration needs to be faster than the current (nominal) flap schedule will provide. The flap speeds will thus be set to their upper bounds, and the resulting new trajectory is calculated. This process is repeated for the consecutive flap speeds, until the target is overshot (ΔT changes sign). From here, the flap scheduler fine tunes the previous flap speed so that the aircraft arrives exactly at its RTA.

The combination of thrust cut altitude and flap selection speeds ultimately determines the CDA performance. Changes in the one parameter necessarily cause changes in the other, if the final configuration and airspeed are to be adhered to. For example, if thrust reduction is delayed (executed at a lower altitude), the aircraft will reach h_R with a speed higher than the approach speed. This can be prevented by selecting flaps at speeds higher than according to the nominal schedule, in order to increase the deceleration rate. The upper and lower bounds of the flap speeds hence define the boundaries of the control space the pilot has during the approach. Within this control space, the pilot can maneuver the aircraft to anticipate or delay his arrival time. The *time goal* requires that the aircraft touches down within a small time window around the RTA. With the aircraft on final approach, the majority of the work needed to reach this goal is already done. The flap scheduler algorithm helps the pilot to fine-tune his exact arrival time. Off-line simulations have shown that for a straight-in continuous descent approach from 7,000 ft, 250 kts IAS, this control space is limited to 8-30 seconds, depending on wind conditions.[10] For this reason, it is important that the flight crew is able to steer their aircraft to within these bounds, before they start the descent.

6-5   Pilot Interface

6-5-1   Conventional Display

In the base-line condition, the pilot interface consists of a conventional Primary Flight Display (PFD), Navigation Display (ND) and a display showing the Mode Control Panel (MCP). The required information for the time based CDA procedure is printed on two cue cards, see Figure 6-5. This cueing system is loosely based

on a system developed at the Massachusetts Institute of Technology.[13, 15] This system places "gates" at strategic locations on the track. These gates correspond to information on thrust setting, aircraft configuration and time.

The first cue card is designed to focus primarily on the *safety goal*, by providing the pilot with continuous descent parameter information in the final phase of the approach. The card shows a profile view of the track to fly, similar to conventional approach charts. For four wind speeds (0, 15, 30 and 50 kts) and three wind directions (headwind and crosswind from either side on Final), the thrust cut altitude and speeds for Flaps 5, Flaps 10 and Flaps 20 are given in a table. The pilot has to interpolate between these parameters to match them with the actual situation. The printed wind speeds assume a logarithmic wind profile with the reference wind speed measured at 7,000 ft altitude.

The second cue card focuses on the *time goal*, by providing the pilot with time gates at certain waypoints. The card shows a top view of the track to fly, comparable to Figure 6-1. The time slots at these gates are based on the aircraft following the nominal speed (IAS) profile. Taking the wind conditions mentioned above (4 wind speeds, two directions) into account yields a series of time-over-waypoint datasets. These datasets are displayed in a table.

6-5-2 Augmented Display

The information produced by the prediction and optimization algorithms described in Section 6-4 must be presented to the pilot in a logical and intuitive way. Display modifications and augmentations must also be designed to minimize clutter on the current lay-out of displays. The modifications explained below are shown in Figure 6-6.

One cue was added to help meet the *safety goal*. To indicate the altitude where thrust should be reduced to flight idle in order to meet the approach speed V_{APP} at h_R, a letter 'T' is added on the altitude tape of the Primary Flight Display. This is shown as item ② in Figure 6.6(a).

To help meeting the *time goal*, a series of display augmentations was introduced. To minimize ΔT in the final phase of the arrival, a letter 'F' is presented on the speed tape of the PFD at the optimal speed for the next flap selection. This is shown as item ① in Figure 6.6(a). On the Navigation Display, several augmentations are present. The elapsed time since the start of the approach and the Required Time of Arrival are shown as item ③ in Figure 6.6(b). At ④ an indication of the current situation with respect to the RTA is given as ΔT in seconds, combined with an amber EARLY/LATE indication in case this deviation is greater than 10 seconds. This time indication is also reflected in a ghost symbol, through item ⑤. This ghost is an image of the own aircraft flying the intended approach track, keeping a position where the aircraft should be if ΔT were zero. The ghost symbol is a dashed variant of the white (solid line) own aircraft symbol.

RWY 18R TILDA TRANSITION		ILS GS 3°	GW 564 klbs			CONTINUOUS DESCENT APPROACH					
	WIND SPEED AT FL 70	0 KTS			15 KTS			30 KTS			50 KTS
CDA WPT	WIND DIRECTION		90	180	270	90	180	270	90	180	270
TCB	Altitude (ft)	3410	3310	3130	3870	3270	2910	4260	3210	2650	2650
	IAS (kts)	220	220	220	221	219	220	220	220	220	220
WP1, Flaps 5	Altitude	3210	3000	3090	3790	3200	2840	4200	3000	2430	2450
	IAS	216	210	219	220	218	220	219	215	215	216
WP2, Flaps 10	Altitude	2620	2450	2370	2980	2490	2090	3100	2320	2010	2030
	IAS	200	200	200	201	200	200	200	200	200	200
WP3, Flaps 20	Altitude	1910	1830	2000	2080	1920	1790	2420	2120	1780	1800
	IAS	190	191	190	190	190	191	190	190	190	191

(a) Cue card focussing on safety goal

RWY 18R TILDA TRANSITION		ILS GS 3°	GW 564 klbs			CONTINUOUS DESCENT APPROACH					
INTERMEDIATE	WIND SPEED AT FL 70	0 KTS			15 KTS			30 KTS			50 KTS
TIME GATE	WIND DIRECTION		90	180	270	90	180	270	90	180	270
ES601	TIME (mm:ss)	9:50	9:53	10:11	10:09	9:49	10:28	10:25	9:21	10:58	10:21
(7000 ft)	IAS (kts)	220	220	220	220	220	220	220	220	220	220
ES602	TIME	8:19	8:27	8:40	8:32	8:28	8:57	8:41	8:08	9:26	8:37
(7000 ft)	IAS	220	220	220	220	220	220	220	220	220	220
TOD	TIME	6:11	6:24	6:29	6:18	6:28	6:42	6:20	6:18	7:05	6:01
(7000 ft)	IAS	220	220	220	220	220	220	220	220	220	220
ES608	TIME	3:27	3:33	3:40	3:40	3:29	3:48	3:46	3:36	4:02	3:32
(3490 ft)	IAS	220	220	220	220	218	220	214	217	220	209
R	TIME	1:07	1:13	1:14	1:15	1:11	1:18	1:15	1:10	1:17	1:13
(1000 ft)	IAS	150	150	150	150	150	150	150	150	150	150
RWY	TIME	0:00	0:00	0:00	0:00	0:00	0:00	0:00	0:00	0:00	0:00

(b) Cue card focussing on time goal

Figure 6-5: Different types of cue cards used for the base-line display configuration.
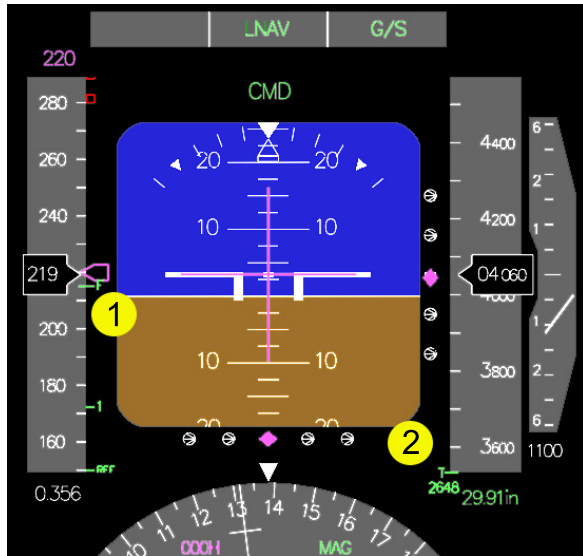
(a) Primary Flight Display
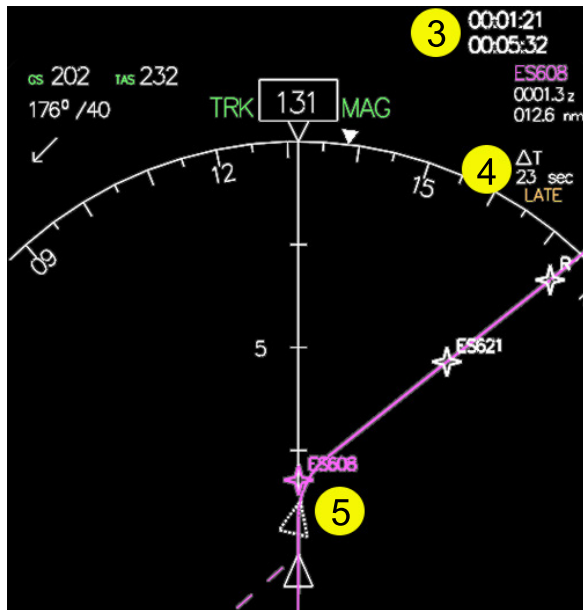
(b) Navigation Display

Figure 6-6: Display Modifications. (a) PFD, with ① the Flap Cue and ② the Thrust cue. (b) ND, with ③ Elapsed time and RTA, ④ Time performance and EARLY/LATE indicator and ⑤ Ghost symbol.

6-6   Experiment

To test the effectiveness of time based spacing and identify the operational constraints of implementation, a piloted experiment was conducted. Seven professional airline pilots tested the system under various operating conditions in a fixed base flight simulator.

6-6-1   Independent variables

The first independent variable is the display configuration. The baseline condition is a conventional display layout consisting of a Navigation Display (ND) and Primary Flight Display (PFD). The second display configuration, for the augmented condition, consists of an ND and a PFD extended with information derived from the flap scheduler and optimization algorithms, as described in Section 6-5.

Second, four different wind conditions are defined that together represent a realistic set of wind conditions that could be encountered during any approach. A typical wind profile is shown in Figure 6-4. These profiles are all taken from data sets of actual wind measurements, but scaled and rotated to correspond to the wind speeds of interest. These wind conditions, listed in Table 6-2, comprise two headwind conditions on Final, and two crosswind conditions. For each wind direction, two wind speeds at the starting altitude of 7,000 ft are defined. The choice for wind speed values is such that the lower value could be encountered under normal, regularly occurring circumstances. The higher wind speed occurs in more rare situations. The wind speeds for crosswind approaches are lower, in correspondence to crosswind and headwind limits for landing.

6-6-2   Experiment design

The experiment design matrix is factorial, combining the four wind conditions with both displays, each condition flown once by each pilot. This yields eight experiment runs per pilot. Seven professional airline pilots (over 4,500 flying hours on average, see Table 6-1) flew a set of these eight runs, yielding 56 experiment runs in total. Each set was preceded by four to six practice runs, to familiarize the pilots with the procedure and wind conditions.

6-6-3   Apparatus

The experiment was conducted in a fixed base research simulator at the Control & Simulation Division. The pilots were seated on the copilot side, controlling the aircraft with a side stick. The Primary Flight Display, Navigation Display and the Mode Control Panel were shown on two 18" screens. An outside visual was shown of a landscape with a fictitious airport with two parallel runways.

Table 6-1: Pilot experience.

	Age	Aircraft types	Flying hours
Pilot A	68	DC3, CV640, DC8, B747-3/400, C550	13,200
Pilot B	31	F100	1,200
Pilot C	31	B747-400	300
Pilot D	23	PA28, DA42	190
Pilot E	50	military, B737, BA146, DC10, A320	12,500
Pilot F	33	B757, B767	6,000
Pilot G	26	B747-400	1,650

6-6-4 Aircraft

The aircraft model used is a non-linear six-degrees-of-freedom model of the Boeing 747-200. The flight is executed with the autopilot in LNAV mode, leaving only manual pitch control and throttle control to the pilot. The reason for maintaining partial manual control throughout the flight was to introduce a basic level of workload during the approach. With autopilot engaged and no radio traffic or ATC present, an experiment run would comprise a lot of idle time between autopilot inputs. For guidance along a three-dimensional glide path, a Microwave Landing System (MLS)-type vertical guidance was available. This allows the pilot to fly a continuously descending path, irrespective of his position with respect to the runway. To improve lateral stability, a yaw damper was used.

6-6-5 Scenario

Initial conditions, such as position along the track and airspeed, are varied per wind condition, to limit the influence of learning effects on the way the track is flown. The required arrival times are tuned to each initial condition, based on a relative deviation from the nominal RTA for that condition, so that only the effects of the wind conditions influence the pilot's performance. The initial conditions are listed in Table 6-2. In the level flight segment following each initial condition, the pilot can position the aircraft as good as possible for meeting the RTA. This is done by choosing a higher airspeed (in case a pilot is late), or a lower airspeed (in case a pilot is early) than the 220 kts chosen for the nominal speed profile. The pilot then has to maintain this airspeed until his ΔT is reduced to zero, after which he can return to the nominal 220 kts until the point of thrust cut.

6-6-6 Procedure

The pilot's task is to fly a Continuous Descent Approach, while meeting both *safety* and *time goals*. The aircraft starts in one of the initial conditions listed in Table 6-2 at an altitude of 7,000 ft, with Flaps 1° extended and with autopilot and autothrottle

Table 6-2: Initial conditions

	Wind speed [kts]	Wind dir. [°]	Airspeed [KIAS]	Distance to go [nm]	RTA [min:sec]
A	26	90	270	47.7	11:23
B	26	180	270	46.3	11:46
C	44	180	250	31.6	09:39
D	12	90	250	30.8	07:59

Table 6-3: Dependent measures

	Measure	Description
	ΔV_{APP}	Deviation from V_{APP} at R
Safety goal	ΔV_{final}	RMS of the deviation from V_{APP} at R
	Flap setting	Aircraft should be fully configured at R
Time goal	ΔT	Deviation from the RTA at R
Workload		Number of throttle setting changes
		NASA Task Load Index (TLX) score

engaged. The pilot is given an RTA, which is entered through an interface window in the Mode Control Panel. After this, the autopilot is switched to LNAV mode, and the autothrottle is disengaged.

6-6-7 Dependent measures

The dependent variables consist of both objective and subjective measures. Objective measures include operational performance and pilot control activity. Operational performance was judged by measuring the accuracy with which the targets were reached. For the *safety goal*, the deviations from the final approach speed V_{APP} at the reference window and in the remainder of the approach were measured. For the *time goal*, the deviation from the RTA was measured. Pilot control activity was measured by counting the number of thrust changes during a run. The subjective measures were taken from a questionnaire, aimed at giving an insight into pilot acceptance of the system, and a NASA Task Load Index (TLX)[12] sheet to assess pilot workload for each run. The dependent measures are listed in Table 6-3.

6-6-8 Hypotheses

The first hypothesis is that for the augmented display time performance will improve with respect to the baseline condition. The reasoning for this is that with the help of the support system, the pilot has continuous information about his *time goal* performance at hand, which will allow for smoother and more accurate transitions

between the different phases in the flight. When time information is only provided at discrete points (the gates), own performance estimation is clearly more difficult.

Secondly, CDA performance (reaching the approach speed of 150 kts at 'R', preferably no sooner but definitely not later) is expected to increase. The idea is that this performance mainly depends on the moment of thrust cut. The altitude where this is done depends heavily on the wind speed and direction on Final, so a more accurate prediction of this wind profile will increase the *safety goal* performance.

Finally, it is hypothesized that workload will be higher for the baseline condition, since in this case the pilot will have to interpolate continuously between the data on his cue cards to retrieve the appropriate parameters. Moreover, the wind used to set up the cue card data resembles standard logarithmic profiles. The discrepancy between this profile and the actual wind will require extra corrective pilot action, hence increasing the workload.

6-7   Results and Discussion

6-7-1   Operational Performance

Two types of performance measures are selected, each related to either the deviation from V_{APP} (mandatory performance targets) or the deviation from the RTA (optimization). It appeared throughout the experiment that the variation in wind *speed* does not have a significant influence on performance ($F_{2,6} = 0.244$, $p = 0.784$ for the deviation from V_{APP}, $F_{2,6} = 1.930$, $p = 0.156$ for the deviation from the RTA). For that reason, the four wind conditions are reduced to two clusters, defined by the wind direction.

Deviation from V_{APP}   To investigate how well the aircraft is established for landing at the reference window, three performance parameters are defined. The first one is the deviation from the target approach speed of 150 kts IAS, when passing the reference window (waypoint 'R', 3.14 nm from touchdown, 1,000 ft altitude). The means and 95% confidence intervals for this score per wind condition (headwind or crosswind) are plotted in Figure 6.7(a). In this figure the deviation for the optimized configuration is lower in both headwind and crosswind, but this effect is obscured by the large spread in the data. An analysis of variance (ANOVA) shows that this spread is indeed too large to see any differences; the effect of the display configuration on the speed deviation is not significant ($F_{1,6} = 0.023$, $p = 0.883$).

What can be seen from the error bar plots, is that crosswind has a negative effect the accuracy of achieving V_{APP}. This effect is only significant for the deviation from V_{APP} at 'R', when the optimized display configuration is used ($F_{1,6} = 9.160$, $p = 0.023$). This can be explained from the fact that the display optimization only uses the headwind component of the estimated wind speed to predict its time and speed profile. In a headwind condition, this works out well, but in a crosswind an
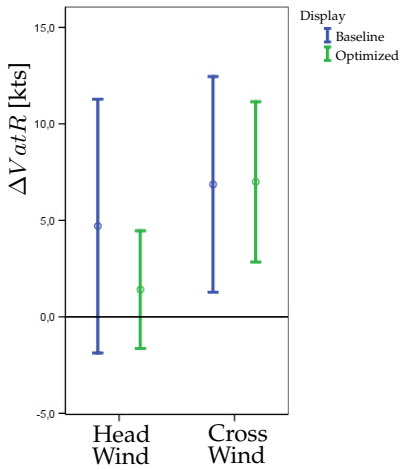
(a) The means and 95% confidence intervals for the deviation from V_{APP} at h_R.
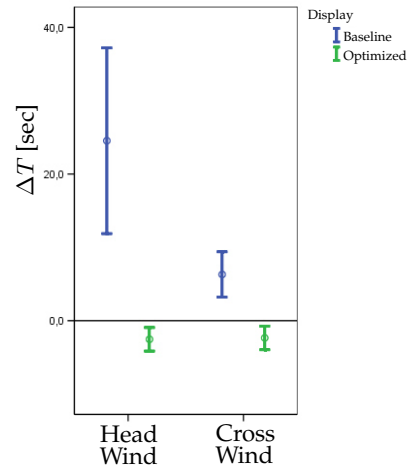
(b) The means and 95% confidence intervals for the deviation from the RTA.
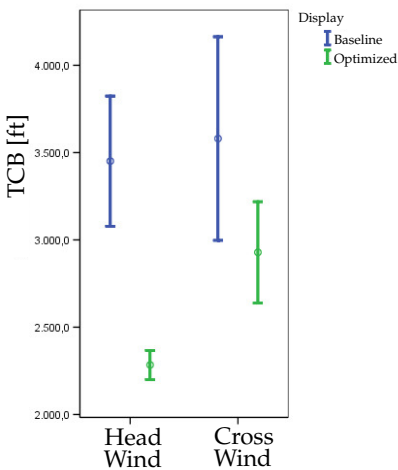
(c) The means and 95% confidence intervals for the thrust cut altitude.
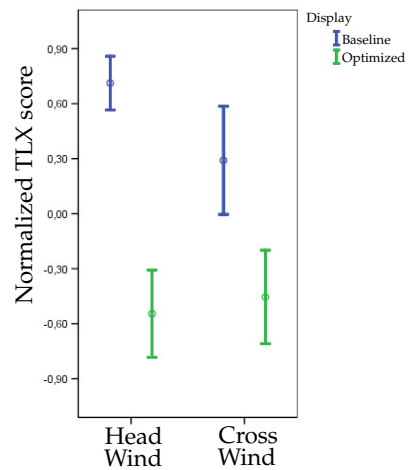
(d) The means and 95% confidence intervals for the normalized NASA Task Load Index (TLX) scores.

Figure 6-7: CDA performance scores.

error is introduced: the algorithm assumes a near-zero headwind component, while in reality the aircraft needs to compensate for the crosswind in order to stay on its ground track. As this is done by 'crabbing' the aircraft, the actual ground speed will be lower than the predicted ground speed. For the case of the 44 kts crosswind this estimation error can be as much as 4%. As a consequence, the airplane starts

lagging behind the original predicted time profile, which in turn causes pilots to delay flap selection in order to maintain a higher airspeed. In many cases, the deviation from V_{APP} suffers from this decision, with the average approach speed going up from little over 151 kts to 156 kts. For the baseline condition, the data on the cue cards is based on trial runs, instead of predictor data. Since the wind information on the cards (based on logarithmic profiles) does not take the effect of 'crabbing' into account, the deviation from V_{APP} is not influenced in the crosswind scenario.

The fact that speed performance goes down when the track prediction is less accurate (in the crosswind condition) suggests that pilots closely followed the cues presented on the displays. At the same time, the large spread in speed performance in the baseline condition indicates significant differences between the different strategies adopted by each pilot. This is confirmed by the pilots' answers to a questionnaire, which showed that they used the CDA-parameter cue card mostly to determine the thrust cut altitude, but thereafter relied more on their pilot experience to determine flap selection. In the optimized display configuration, the need to look away from the instruments to check the cue cards is eliminated, and pilots use the displayed instructions.

Deviation from RTA The main check on the time performance is the deviation from the RTA at the reference window. The means and 95% Confidence Intervals for this parameter are shown in Figure 6.7(b). Clearly, the average time performance is better with the aid of display optimization. An ANOVA shows that this influence is indeed significant ($F_{1,6}$ = 7.368, p = 0.033). Average time performance is within 4 seconds of the RTA. This is definitely accurate enough to guarantee safe separation. This result would allow air traffic controllers to space incoming traffic more tightly, increasing runway throughput capacity. The addition of the proposed automation to existing cockpit displays enables pilots to fly a time based CDA.

The explanation for this improvement is twofold. First, by providing the pilot with continuously updated information on his status, he is able to very accurately adjust the aircraft's speed profile to minimize ΔT. In the baseline, the number of intermediate time gates is limited to four (for conditions C and D in Table 6-2) or five (for conditions A and B). Second, the more accurate wind prediction that is available in the enhanced display condition yields a better estimate of the optimal altitude for thrust reduction. This can be seen in Figure 6.7(c), showing the altitude where pilots cut back on thrust to decelerate the aircraft to 150 kts. Regardless of wind direction, this altitude is significantly lower in the optimized display condition than in the baseline condition ($F_{1,6}$ = 3.560, p = 0.098). With the used wind profile class in mind (see Figure 6-4), it becomes clear that the logarithmic profile prediction is not able to deal with the increase in wind speed around 3,500 ft. The aircraft encounters more (head)wind than expected, so its thrust cut altitude should be lowered. The track prediction and optimization routines take this effect into account.

Although the automation provided a major improvement in time performance, speed performance (deviation from V_{APP}) was still in the same range as in the

baseline situation. This might be due to the fact that the the automation mainly focused on achieving the time goal. To strike a better balance between the two performance criteria, and to provide a more logical lay out of the presented clues, it is recommended to let the cues on the Primary Flight Display focus on CDA performance (arrive stabilized at the reference window), while the cues on the Navigation Display (ghost and ΔT) focus on the time goal. Another improvement would be to integrate the cues more tightly with current procedures. For example, in many aircraft the landing gear should be lowered between two fixed consecutive flap settings. To incorporate such information in the pilot support system would ease implementation and increase acceptability by airlines and flight crew.

6-7-2   Pilot workload

The results for the subjective workload measurements are represented by the normalized NASA TLX rating scores in Figure 6.7(d). Workload experienced by the pilots is lower for the optimized display condition, in all wind conditions. This effect is highly significant ($F_{1,6} = 50.390$, $p < 0.001$), an observation that is confirmed by the questionnaire answers with all pilots indicating a higher workload in the baseline condition. In contrast, the workload in this type of noise abatement procedure with the optimization present was considered comparable to that of a conventional ILS approach.

Furthermore, it can be seen that for the baseline condition, the workload score also depends on the wind direction. The score is significantly lower in crosswind conditions on Final ($F_{1,6} = 12.797$, $p = 0.012$). Several factors could influence this phenomenon. First, in a headwind condition, the full force of the sharp changes in wind speed along the altitude profile is felt. In a crosswind, only one component of the wind is of influence, so the absolute change in wind speed is smaller. Another factor might be that the crosswind condition on Final means a headwind condition between waypoints TILDA and EH608 (see Figure 6-1). In many cases, this is the phase where pilots reach the on-time schedule ($\Delta T = 0$ and reduce speed from 250 or 270 kts to the nominal speed of 220 kts. This is not always an easy task, since a B747 in this situation (Flaps 1°, gear up, 3° glide path, no speed breaks) has a low deceleration rate. A headwind in this situation reduces the kinematic flight path angle, which makes it easier for the pilot to decelerate the aircraft. This increases the chances of a stabilized approach and hence reduces pilot workload.

Flying a CDA already puts more demand on the flight crew than a regular arrival, where the basic control task is following ATC vectors. Although the tasks of flying and navigation are normally shared between the Pilot Flying and the Pilot Not Flying, the pilots interviewed indicated that they would find the sharp increase in workload as experienced in the base-line scenario unacceptable.

6-8   Conclusions

This paper investigated the feasibility of introducing time based spacing in realistic, three dimensional continuous descent approaches under actual wind conditions. For reasons of safety, it is important that first, the continuous descent ends in a stabilized approach configuration and speed some distance before the runway and second, pilots are able to meet the required arrival times instructed by ATC, in order to maintain safe separation throughout the approach.

The development of an FMS based prediction and optimization system combined with a pilot support interface enables the flight crew to reach these two goals. A wind prediction algorithm that makes use of weather information broadcast by other aircraft in the TMA makes accurate wind profile prediction along the approach trajectory possible. Wind speed prediction error along a 30-45 nm approach trajectory is 2 kts. An accurate knowledge of the wind ahead makes sure an optimal thrust cut altitude and flap speed schedule can be selected. The piloted experiments show a strong improvement in time performance when continuously updated information on this goal is present on the display. Pilots are able to reach their RTAs within an average margin of 4 seconds, regardless of wind conditions. The average speed performance (being stabilized at a reference window) is unaffected by display optimization, although the presence of automation reduces the spread in this performance criterion. The addition of time constraints without extra aids would result in an unacceptable increase in workload, due to the continuous calculation and interpolation the pilots have to perform. Workload is significantly lower with the display optimization present, and at the same level as in current ILS approach procedures.

6-9   Recommendations

The piloted experiment shows the feasibility of time-based continuous descent approach procedures under realistic wind conditions, along a fixed trajectory. The pilot's control space to reach an RTA could be greatly enlarged by adopting a more flexible approach route. Shortening or extending the length of the track to fly, similar to the 'tromboning' technique currently used by ATC, should reduce the need for speed changes, thereby improving predictability of the speed profile during the approach.

References

[1] Assembly Resolution A33-7: Consolidated Statement of Continuing ICAO Policies and Practices Related to Environmental Protection. International Civil

Aviation Organization (ICAO), 2001.

[2] Outlook for Air Transport to the Year 2015. Technical Report AT-127, International Civil Aviation Organization (ICAO), Sep 2004.

[3] Aeronautical Information Publication AIP. Air Traffic Control The Netherlands, 2006.

[4] Sourdine II, Final Report. Technical Report D9-1, National Aerospace Laboratory (NLR), Aug 31 2006.

[5] E. H. Bolz and L. M. Reuss. System Study of Advanced Operational Procedures for Noise Reduction. Technical Report NASA (Task Order (TO) 56), National Aeronautics and Space Administration NASA, Oct 2001.

[6] J.-P. Clarke. Systems Analysis of Noise Abatement Procedures Enabled by Advanced Flight Guidance Technology. *Journal of Aircraft*, 37(2), Mar-Apr 2000.

[7] J.-P. Clarke, N. T. Ho, L. Ren, J. A. Brown, K. R. Elmer, K. Tong, and J. K. Wat. Continuous Descent Approach: Design and Flight Test for Louisville International Airport. *AIAA Journal of Aircraft*, 41(5):1054–1066, 2004.

[8] R. A. Coppenbarger, R. W. Mead, and D. N. Sweet. Field Evaluation of the Tailored Arrivals Concept for Datalink-Enabled Continuous Descent Approach. *AIAA Journal of Aircraft*, 46(4):1200–1209, 2009.

[9] L. J. J. Erkelens. Research into New Noise Abatement Procedures for the 21st Century. Number AIAA 2000-4474, pages 1–10, Denver (CO), USA, Aug 14-17 2001.

[10] W. F. de Gaay Fortman, M. M. van Paassen, M. Mulder, A. C. in 't Veld, and J.-P. Clarke. Implementing Time-Based Spacing for Decelerating Approaches. *AIAA Journal of Aircraft*, 44(1):106–118, Jan-Feb 2007.

[11] P. Frenzen and C. A. Vogel. On the Magnitude and Apparent Range of Variation of the Von Karman Constant in the Atmospheric Surface Layer. *Boundary-Layer Meteorology*, 72:371–392, 1995.

[12] S. G. Hart and L. E. Staveland. Development of NASA-TLX (Task Load Index): Results of Emperical and Theoretical Research. In *Human Mental Workload*, pages 239–250. Elsevier Science Publishers, Amsterdam, The Netherlands, 1988.

[13] N. T. Ho. *Design of Aircraft Noise Abatement Approach Procedures for Near-Term Implementation*. PhD thesis, Massachusetts Institute of Technology, Cambridge (MA), USA, 2005.

[14] N. T. Ho and J.-P. Clarke. Methodology for Optimizing Parameters of Noise Abatement Approach Procedures. *AIAA Journal of Aircraft*, 44(4):1168–1176, 2007.

[15] N. T. Ho, J.-P. Clarke, R. Riedel, and C. Oman. Cueing System for Near-Term Implementation of Aircraft Noise Abatement Approach Procedures. *AIAA Journal of Aircraft*, 44(3):718–725, 2007.

[16] A. D. Kershaw, D. P. Rhodes, and N. A. Smith. The Influence of ATC in Approach Noise Abatement. Napoli, Italy, Jun 13-16 2000.

[17] M. F. Koeslag. Advanced Continuous Descent Approaches, an Algorithm Design for the FMS. MSc. Thesis, Faculty of Aerospace Engineering, Delft University of Technology, 2001.

[18] A. M. P. de Leege, A. C. in 't Veld, M. Mulder, and M. M. van Paassen. Three-Degree Decelerating Approaches in High-Density Arrival Streams. *AIAA Journal of Aircraft*, 46(5):1681–1691, Oct 2009.

[19] P. S. Maybeck. *Stochastic Models, Estimation and Control*, volume 1. Academic Press, 1979.

[20] D. Painting. AMDAR Reference Manual. Technical report, World Meteorological Organization-AMDAR Panel, 2001.

[21] J. L. de Prins, K. F. M. Schippers, M. Mulder, M. M. van Paassen, A. C. in 't Veld, and J.-P. Clarke. Enhanced Self-Spacing Algorithm for Three-Degree Decelerating Approaches. *AIAA Journal of Aircraft*, 30(2):576–590, Mar 2007.

[22] L. Ren and J.-P. Clarke. Flight-Test Evaluation of the Tool for Analysis of Separation and Throughput. *AIAA Journal of Aircraft*, 45(1):323–332, Jan-Feb 2008.

[23] L. Ren, J.-P. Clarke, and N. T. Ho. Achieving Low Approach Noise without Sacrificing Capacity. In *22nd Digital Avionics Systems Conference*, number AIAA-2001-5239, pages 1–9, Indianapolis (IN), USA, Oct 12-16 2003.

[24] A. C. in 't Veld, M. M. van Paassen, M. Mulder, and J.-P. Clarke. Pilot Support Interface for Three-Degree Decelerating Approach Procedures. *The International Journal of Aviation Psychology*, 19(3):287–308, Jul 2009.

[25] F. Wubben and J. Busink. Night Time Restrictions at Amsterdam-Schiphol, an International Comparison. Technical report, to70 Aviation and Environment, under Contract of the Ministry of Transport, Public Works and Water Affairs, 2004.

7

Self-spacing in High-Density Arrival Streams

A.M.P. de Leege, A.C. in 't Veld, M. Mulder and M.M. van Paassen

7-1   Abstract

Trajectory unpredictability of aircraft performing continuous descent approaches results in reduced runway capacity, because more spacing is applied. A possible solution to this problem is self-spacing - the transfer of the spacing task from the controller to the pilot. Using a fast-time simulation tool the performance differences between distance- and time based self-spacing in high-density traffic in terms of runway capacity and separation are quantified for the Three-Degree Decelerating Approach. Distance based self-spacing is the most promising concept. The average runway capacity is 39 aircraft per hour (40% heavy, 60% medium aircraft). Runway capacity in case of time based self-spacing is 3 aircraft per hour lower, due to spacing margins applied to lower the separation violation rate to the level of distance based spacing. A sensitivity analysis was carried out for distance based self-spacing. One of the results is that accurately determining the starting time and subsequently arriving at this time benefits the TDDA performance. TDDA performance is also affected by the initial speed and altitude as they affect the TDDA's control space.

7-2   Introduction

Continuous Descent Approach (CDA) is a cost effective mean to reduce aircraft noise, emissions, flight time, and fuel burn.[5,10,17,18] Aircraft continuously decelerate while on these approaches, which leads to trajectory unpredictability from the standpoint of a controller who is monitoring inter-aircraft spacing based on periodic radar updates of aircraft position. As such, controllers apply larger spacing to prevent vectoring instructions that would conflict with the CDA. Larger spacing between aircraft reduces runway capacity down to 50% when compared to conventional approaches.[3,11,13,14]

A possible solution to this problem is the use of in-trail self-spacing.[3,14] The spacing task is transferred from the controller to the pilot. Self-spacing is proposed because of the availability of precise aircraft performance information and the control strategy onboard the aircraft. The maneuverability of an aircraft while executing a CDA is limited and driven by the aircraft performance, the control strategy, and wind conditions. Information about wind conditions the aircraft is likely to encounter during descent can be made available as described in.[7] The flight crew can plan and execute, with the help of onboard systems, a CDA to remain safely separated.[6,9,12]

This paper discusses research into the performance of the Three-Degree Decelerating Approach (TDDA) in high-density arrival streams in a distance- or time based self-spacing environment. The TDDA is a CDA that lies within the boundaries of present approach procedure limitations and gives the pilot control over the descent path to fulfill the spacing task.[4,6,7,9,12,14] In a distance based self-spacing environment the aircraft actively adapts its speed profile to the speed profile of the aircraft flying directly in front. This requires that the aircraft predicts the trajectory of this leading aircraft. Using the relative state of the leading aircraft to predict the trajectory can give rise to transient motions in the arrival stream, hereafter referred to as the 'slinky effect', resulting in spacing problems.[15] In this research intent-based trajectory prediction is introduced for the TDDA to prevent the slinky effect in case of distance based self-spacing. Another solution to circumvent the slinky effect is a time based self-spacing procedure, which does not require trajectory prediction of the leading aircraft during the TDDA. Its performance was compared with the more common distance based procedure. In the time based environment the aircraft receive a Required Time of Arrival (RTA) for the runway threshold point. The RTAs are set prior to the start of the TDDA with the aim to keep the aircraft safely separated during approach. A fast-time simulation tool was developed to investigate the differences in performance between distance- and time based self-spacing in terms of capacity, and loss of separation.
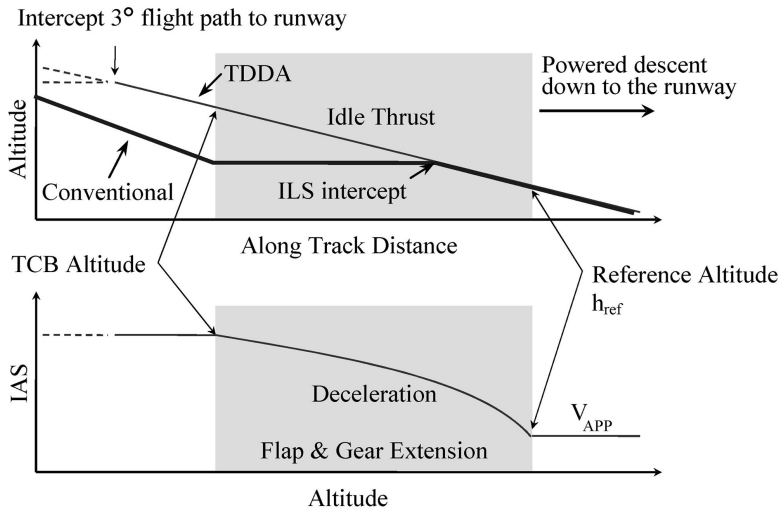
Figure 7-1: The Three-Degree Decelerating Approach profile

7-3   Three-Degree Decelerating Approach

7-3-1   Description of the Procedure

The TDDA is a straight-in approach, with a constant $3°$ geometrical path angle.[4] Figure 7-1 illustrates the TDDA together with a conventional step-down approach. The approach procedure starts when the aircraft intercepts the fixed descent path at an altitude (7,000-10,000 ft) well above the altitude the aircraft intercepts the instrument landing system's glide slope. Initially the aircraft maintains a constant Indicated Airspeed (IAS).

To perform the spacing task, control over the descent is required. The TDDA gives the pilot two controls. The first control option is the thrust cutback (TCB) altitude, where engine thrust is set to idle and the aircraft starts to decelerate. Moving the TCB altitude up results in a slower descent and moving the TCB altitude down speeds up the descent. Second control option available after the TCB is flap scheduling. After the TCB the aircraft starts to decelerate. By changing flaps speeds the pilot controls the deceleration of the aircraft along the flight path. During the TDDA the pilot performs two tasks. One task is the spacing task in a distance based or time based self-spacing environment. Second task is to bring the aircraft in a stabilized landing configuration at the 1,000 ft reference altitude, h_{ref}, at approach speed V_{APP} for safety reasons. Below h_{ref} the aircraft maintains V_{APP}. Reaching V_{APP} above h_{ref} is not desired because engine thrust has to be reapplied, negating noise and fuel benefits.

Weight Cat.	Trailing Aircraft		
Leading Aircraft	Heavy	Medium	Light
Heavy	4	5	6
Medium	4	4	5
Light	2.5	2.5	2.5

Table 7-1: Separation minima in nm

7-3-2   Self-Spacing Task

The aim of the self-spacing task is to control the aircraft such that the minimum distance to the leading aircraft equals the minimum safe separation. In this situation the highest runway capacity is achieved for a fixed sequence. The separation minima used in this research are listed in Table 7-1. The self-spacing tasks in a distance based and time based self-spacing environment are different.

Distance based Self-Spacing   Input for the self-spacing task in distance based self-spacing is the predicted minimum distance between the own aircraft and the leading aircraft and the separation minimum. If this prediction indicates that the separation minima will be violated, the approach of the own aircraft has to be slowed down such that the minimum distance between the aircraft equals the separation minimum. If necessary the aircraft may decelerate to V_{APP} before reaching h_{ref}. If the predicted minimum exceeds the separation minimum, a faster approach profile should be selected if available. From a safety point of view no approach should be selected where V_{APP} is reached below h_{ref}, even if this would close the spacing gap between the aircraft. In a distance based self-spacing environment the pilot has two performance goals: First, the minimum distance to preceding aircraft should equal the applicable separation minimum, hereafter referred to as the separation goal. Second, the aircraft should reach to V_{APP} when at h_{ref} hereafter referred to as the noise goal.

Time Based Self-Spacing   In the time based self-spacing environment the aircraft in the arrival stream adhere to a RTA for the runway threshold point. The RTA is computed before the aircraft starts the TDDA and is based on early predictions of the TDDA trajectories of the own aircraft and leading aircraft. The RTA is fixed during the TDDA. The RTA can be provided by the air traffic service provider but could also be calculated on-board the aircraft. Section 7-6-3 describes the methodology used in the simulations to compute the RTA. In the time based concept the pilot has two performance goals. First, to cross the runway threshold at the RTA (time goal) and second the noise goal that is also applies in the distance based environment. Figure 7-2 compares the self-spacing concepts.

TDDA Pilot Support Algorithms   Previous research showed that it is difficult for pilots to determine the correct TCB altitude and flap schedule.[9,12]   Therefore the
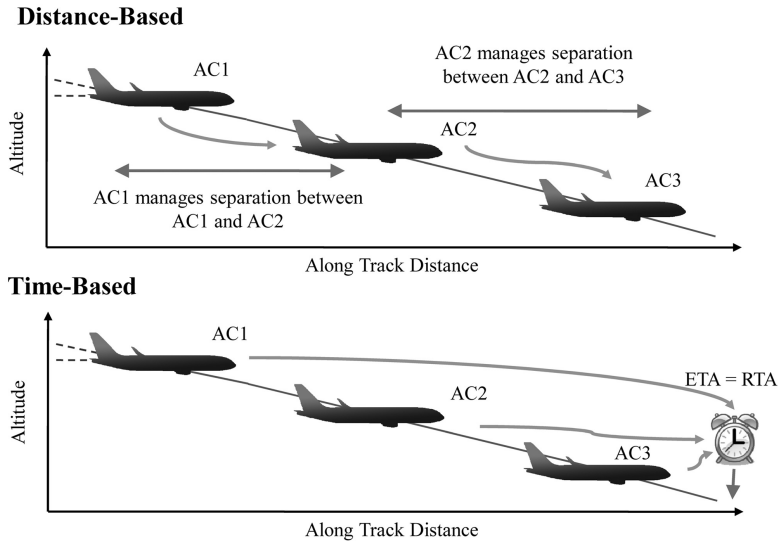
Figure 7-2: Time- and distance based self-spacing compared.

pilot is supported by TCB altitude and flap scheduling optimization algorithms fed by wind and trajectory predictions to meet the noise goal, and separation or time goal.[7,9,12] Figure 7-3 gives an overview of the algorithms used to provide the pilot with a TCB altitude and flap schedule in the distance based self-spacing environment.

Shown on the left are the three algorithms that provide the input for the TCB altitude and flap schedule optimization algorithms at the right. The wind prediction algorithm used in this research is the Advanced Wind Prediction Algorithm described in.[7] The output is a wind profile the aircraft is likely to encounter during descent. The algorithm is driven by Automated Meteorological Data Relay (AMDAR) observations received from aircraft in the vicinity. The observations are stored, ordered, and filtered to obtain a wind prediction. Trajectory prediction of the own aircraft uses an onboard performance model. Inputs are the current state of the aircraft, planned TCB altitude, flap schedule, and the wind prediction. Trajectory prediction of the leading aircraft uses an aircraft intent based prediction model that is addressed in Section 7-4. In addition to an aircraft intent description of the leading aircraft, the wind prediction is used. From the trajectory predictions the minimum distance between the aircraft is derived.

The minimum distance is compared with separation goal (the separation minimum). The trajectory prediction of own the aircraft is also used to determine the altitude where V_{APP} is reached to check against the noise goal. When the aircraft position is still above the last computed TCB altitude, TCB optimization continues until all performance goals are met. The separation goal has priority over the noise goal when the minimum separation between the aircraft is less than the separation
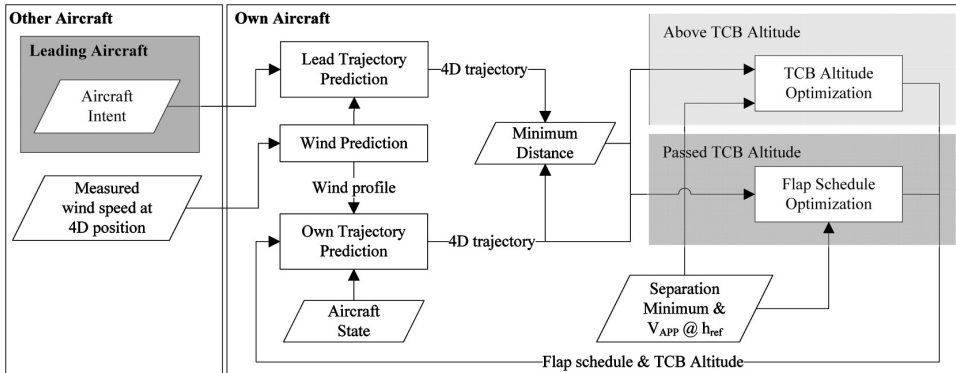
Figure 7-3: Structure of TDDA algorithm for distance based self-spacing.

minimum. The noise goal has priority over the separation goal when the minimum separation between the aircraft exceeds the separation minimum. Once below the TCB altitude, flap schedule optimization is started. The flap scheduler is based on the scheduler developed by de Prins et al.[9] The flap scheduler uses a binary search algorithm to determine the optimal schedule. The scheduler only optimizes for the noise goal is only if the separation goal is met, thus giving priority to the separation task.

The TDDA algorithm structure for time based self-spacing is similar to the structure used for distance based spacing, see Figure 7-4. The minimum distance between the aircraft is no longer computed and is replaced by the Estimated Time of Arrival (ETA), which is checked against the RTA. In the TCB altitude and flap schedule optimization algorithms the time goal is treated in a similar way as the separation goal.

7-4   Aircraft Intent-Based Trajectory Prediction

To prevent the slinky effect during of distance based self-spacing aircraft intent is used to predict the trajectory of the leading aircraft. Captured in the intent is the outcome of optimization of the trajectory by the TDDA algorithms on-board the leading aircraft. If an aircraft descent profile is disturbed, for instance by a wind change or delayed pilot action, the TDDA algorithm optimizes the trajectory. The new trajectory is described in aircraft intent that may be different from the previous intent information, because of the optimization process. The intent is exchanged using a data-link. Predictions only based on previous states do not account for the ongoing optimization process. This can cause unnecessary control actions from the trailing aircraft that can propagate through the arrival stream resulting in the slinky effect.
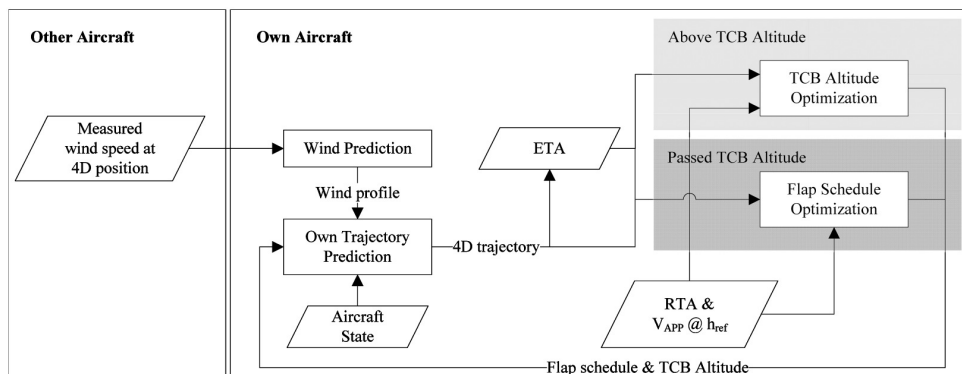
Figure 7-4: Structure of TDDA algorithm for time based self-spacing.

7-4-1 Aircraft Intent Description of the TDDA

Aircraft intent is an unambiguous description of how the aircraft is to be operated within a timeframe. The intent information is the input to a trajectory predictor.[16] The TDDA procedure can be expressed in terms of aircraft intent and consists of three segments:

- Descent along the glide slope with constant IAS down to the TCB altitude.

- Descent and deceleration along the glide slope down to the altitude where V_{APP} is reached, normally 1,000 ft above the runway. During this segment the flaps and landing gear are extended.

- Descent along the glide slope with constant IAS (V_{APP}) down to the runway threshold.

Before continuing with the design of the trajectory predictor based on aircraft intent, the relevance of the leading aircraft prediction has to be analyzed.

7-4-2 Point of Minimum Separation

When the relative ground speed of the trailing aircraft is higher than the leading aircraft, the separation reduces. For two aircraft on CDA this is generally the case and minimum separation takes place when the leading aircraft passes the runway threshold. One exception is when the leading aircraft is locked into its own approach speed while the trailing aircraft is still decelerating to meet its approach speed and the ground speed of the trailing aircraft has dropped below the leading aircraft. A headwind component that increases with altitude can have the same effect. Simulations of arrival streams of aircraft performing a TDDA under actual wind conditions indicated that the minimum separation takes places when the leading aircraft has passed h_{ref} and maintains a constant IAS.[8]
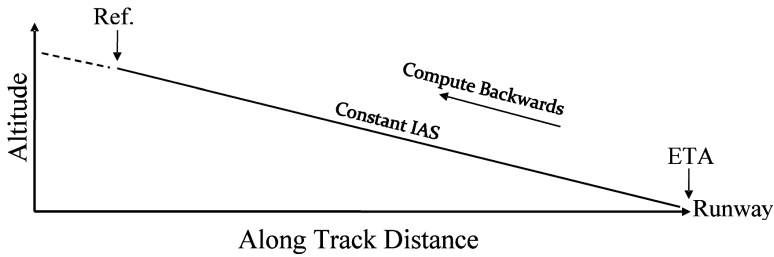
Figure 7-5: Intent-based trajectory prediction.

7-4-3   Intent-Based Trajectory Prediction

A prediction of the last constant speed segment is sufficient to determine the minimum separation. This segment can be predicted independent of the other segments using the leading aircraft ETA, V_{APP}, and descent path angle as illustrated in Figure 7-5.

The speed and flight path angle are constant during the last stage of the final approach. Only aircraft intent information is needed for the prediction. The predictor starts at the runway threshold where the aircraft is at the ETA with speed V_{APP} and computes the trajectory up to the reference altitude. Because the aircraft maintains a constant IAS, no aerodynamic performance model of the leading aircraft is required. A wind prediction is supplied by the wind predictor.

7-5   TDDAs in Arrival Streams

An arrival stream consists of aircraft aligned to land on the same runway. The aircraft in the stream vary in type and weight and have different aircraft performance characteristics. This imposes constraints on the initial separation between aircraft at the start of the TDDA. These constraints are determined by size of the TDDA control space and the separation minimum or RTA. The control space is defined as the time interval between the earliest and latest possible arrival for a given starting time.

7-5-1   Factors that Affect the TDDA Control Space

The boundaries of the TDDA's control space are a function of the aircraft type, weight and wind conditions. Figure 7-6 gives the control spaces under three wind conditions for a Boeing 737NG-like aircraft. The boundaries are the TDDA with the shortest and longest duration. To get the shortest duration all flaps are extended at their maximum speed, resulting in a fast but late deceleration and the lowest possible TCB altitude. The longest duration is achieved by extending flaps at their
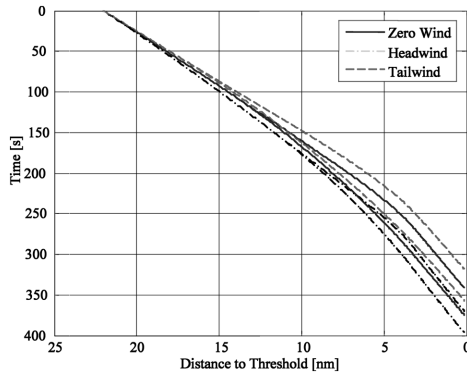
Figure 7-6: Control space time vs. distance for three wind conditions.
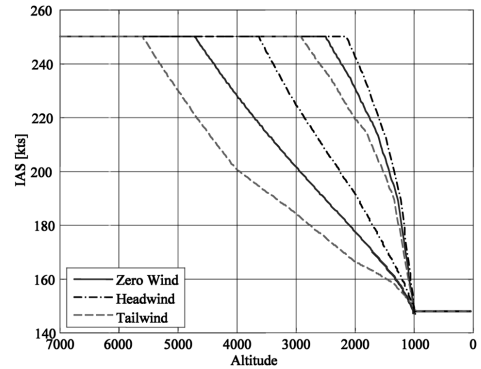
Figure 7-7: Control space IAS vs. altitude for three wind conditions.

minimum speed resulting in a gradual and early deceleration and the highest possible TCB altitude.

From Figure 7-6 the minimum and maximum time-to-fly can be derived. Alternatively the control space can be expressed in terms of the TCB altitude, as shown in Figure 7-7. The figure shows the range of TCB altitudes for which the noise goal can be met. A headwind increases the duration of the TDDA and lowers the TCB altitudes, but also makes the control space smaller. A tailwind has the opposite effect.

7-5-2 Effect of Initial Separation on TDDA

Figure 7-8 shows a TDDA control space for three different initial separations behind a leading aircraft in a distance based self-spacing environment. The separation goal is visualized by offsetting the leading aircraft trajectory prediction over the required separation away from the runway (separation boundary). The separation boundary gives the minimum allowable distance to the runway threshold.

For the upper control space the initial separation is too small. The separation boundary crosses the full control space. The aircraft must reduce speed to V_{APP} before the aircraft passes h_{ref} otherwise there will be a loss of separation. If the separation boundary does not cross the control space, which is the case for the lower control space, there will be spacing gap with a negative effect on the runway capacity. The aircraft is not able to fly the TDDA fast enough to close this gap.

Only when the separation boundary ends in the control space a TDDA is possible that meets the performance goals. Figure 7-9 and Figure 7-10 show two possible trajectories for TDDAs with the highest and lowest possible TCB that meet the performance goals. A high TCB altitude is preferred because of the positive effect on
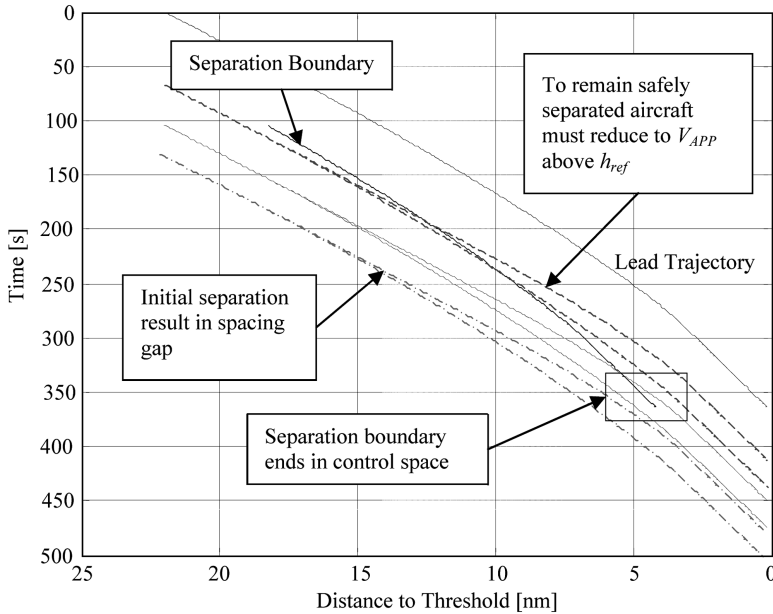
Figure 7-8: Effect of Initial Separation on TDDA Performance

the aircraft noise, fuel use, and less flap wear. For time based self-spacing the separation is replaced by the RTA.

7-5-3   Initial Separation Constraints - Distance Based Self-Spacing

Using the control space and separation boundary the initial separation constraints can be determined. Figure 7-11 illustrates how these constraints are determined for distance based self-spacing. The control space boundaries are positioned such that the minimum separation equals the minimum safe separation; hence the minimum and maximum initial separation are visible.

7-5-4   Initial Separation Constraints - Time Based Self-Spacing

The initial separation constraints in case of time based spacing are determined in a similar way. The arrival time of the control space boundaries is set equal to the RTA from where the entry time interval is determined, see Figure 7-12. For sake of reference the separation boundary is drawn, hence the minimum separation between the aircraft should not be violated.
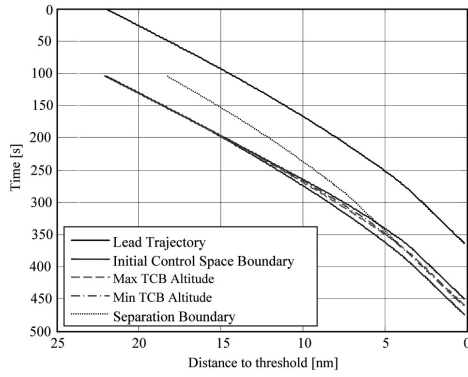
Figure 7-9: Feasible TDDA Trajectories.
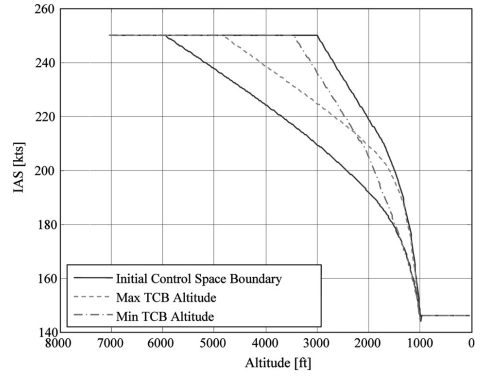
Figure 7-10: Feasible TCB Altitudes.
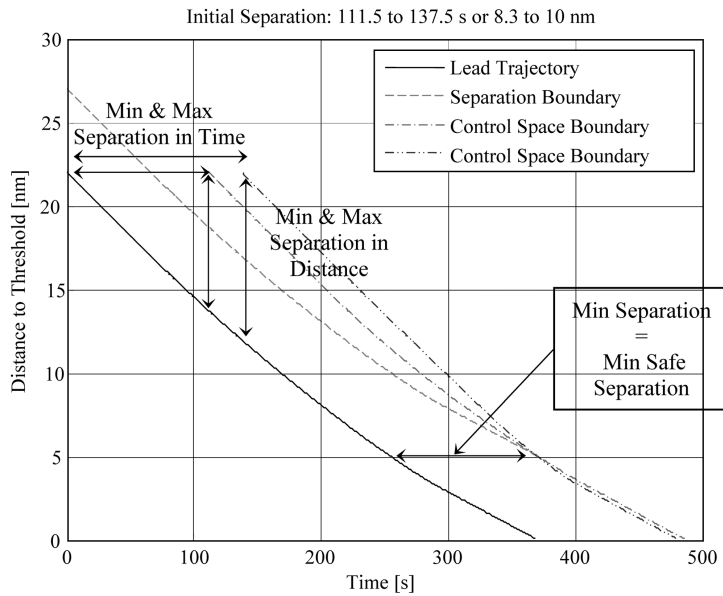
Figure 7-11: Min and max initial separation for distance based spacing.

Initial Separation: 116 to 148.5 s or 8.6 to 11 nm
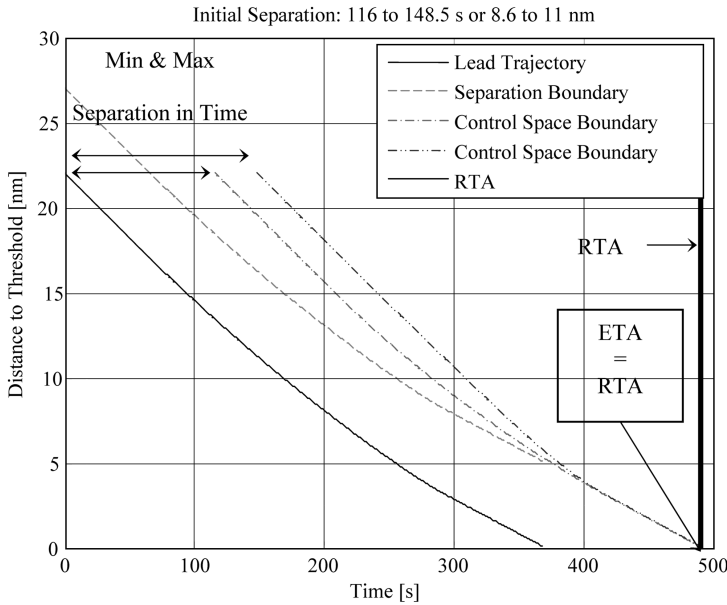
Figure 7-12: Min and max initial separation for time based spacing.

7-6   Fast-Time TDDA Simulation Tool

The fast-time simulation tool simulates arrival streams of aircraft executing the TDDA in a distance- or time based self-spacing environment under actual wind conditions. Implemented in the simulator is the TDDA with the optimization and scheduling algorithms depicted in Figure 7-3 and Figure 7-4.

7-6-1   Aircraft Model

For the aircraft trajectory simulation and trajectory prediction, point mass models are used that approximate the following aircraft: Boeing 747-400, 777-300, 737-400, 737-800, and the Airbus 321. The models resemble the performance differences between different aircraft types and sizes, which for this research is more important than a very precise modeling of the aircraft performance. The equations of motion are derived using Figures 7-13 and 7-14.

For small angles of attack (α) and assuming that the geometric path angle equals the aerodynamic path angle ($\gamma_k = \gamma_a$) the equations of motion in the kinematic reference frame F_k, along the fixed flight path are:

$$\sum F_Z : 0 = L - mg \cos \gamma_k \tag{7-1}$$

$$\sum F_X : 0 = m\ddot{x}_k = T - D + mg \sin \gamma_k \tag{7-2}$$
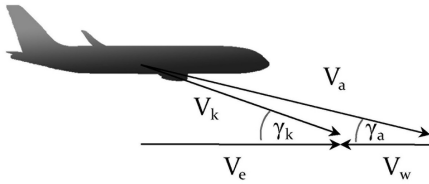
Figure 7-13: Kinetic Diagram
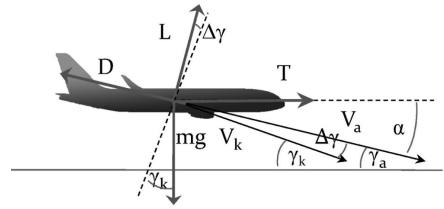
Figure 7-14: Force Diagram

The mass is assumed to remain constant during the simulation and is used to determine the required lift force L and resulting drag. Subsequently the aerodynamic coefficients C_L and C_D and thrust are computed. The approach speed V_{APP} is 1.3 times the stall speed in the landing configuration plus 10 kts. Maximum flap extension speeds are obtained from the aircraft manufacturer or operator. Minimum speed for an aircraft configuration is 1.3 times the stall speed for that configuration.

7-6-2   Pilot Response Time and Wind

The pilot response time for flap and gear deployment is modeled using the Pilot Response Delay Model described in.[11] The model consists of a normal distribution fitted to pilot response time data collected during an experiment to investigate the variables that influence the performance of noise abatement procedures. AMDAR observations have been used to create 54 time-varying wind profiles of approximately one hour. For simulation of the aircraft trajectory the observations are used. For the wind prediction algorithm noise is superimposed on the observations to simulate measurement errors.

7-6-3   Setting the RTA and Initial Separation

The RTA and starting time for an aircraft are set 600 s before the leading aircraft starts the TDDA. Use is made of the prediction algorithms described in Section 7-3 to compute the control space boundaries and initial separation constraints. A 0.2 nm buffer is added to the separation minima to account for uncertainties in the predictions, wind changes. The size of the buffer was determined using trial and error. To set the RTA the procedure to determine the initial separation constraints for distance based self-spacing is followed. The RTA is set to the latest crossing of the control space boundaries with the time axis to account for trajectory deviations. The starting times position the aircraft exactly in between the initial separation constraints.

7-7   Distance- and Time Based Self-Spacing Performance

Using the simulation tool 5,000 arrival streams consisting of eight aircraft have been simulated for both self-spacing environments. The aircraft type was selected randomly from the five available aircraft models. Per aircraft type three different weights were assigned randomly to the aircraft: the Operating Empty Weight (OEW), the Maximum Landing Weight (MLW), and mean of the OEW and MLW. The TDDA starts at 7,000 ft with 230 kts IAS. The performance of the TDDA in high traffic density arrival streams in the two self-spacing environments was assessed using the formulated noise, separation, time goal, and the runway capacity.

7-7-1   Noise Goal

The noise goal is met if V_{APP} is reached at h_{ref}. Figure 7-15 shows the average altitude where V_{APP} was reached, hereafter referred to as $h_{V_{APP}}$, per position in the arrival stream. As expected for time based self-spacing no trend between the position of the aircraft and $h_{V_{APP}}$ could be identified ($R = 0.006, p = 0.287$, *Pearson 2-tailed*). On average $h_{V_{APP}}$ lies 20 ft above h_{ref}. When taking tolerances used by algorithms into account it is concluded that on average the noise goal is met. For the distance based scenario a positive correlation between $h_{V_{APP}}$ and the position in the stream can be identified ($R = 0.145, p < 0.001$, *Pearson 2-tailed*). The noise reduction deteriorates towards the end of the arrival stream. From the median and 5th to 95th percentiles it can be concluded that the number of aircraft that fail the noise goal remains almost constant but that the deviation from h_{ref} increases, see Figure 7-16.

Deterioration of the noise reduction is caused by accumulation of delays (slow-down effect) in the arrival stream. If there is delay in the arrival stream all trailing aircraft in the stream are affected by this delay. Aircraft in the end of arrival stream are confronted with longer delays than the aircraft in the beginning of the arrival stream. To remain safely separated, aircraft increase the TCB altitude to the upper bound of their control space. If this is not sufficient, flap extension is advanced but this will result in failure to meet the noise goal. In case of a delayed arrival there is a significant correlation between h_{ref} and the magnitude of the delay ($R = 0.672, p < 0.001$, *Pearson 2-tailed*). When an aircraft arrives earlier than initially planned, no effect on the noise goal can be identified ($= 0.057, p < 0.001$, *Pearson 2-tailed*).

Deterioration of the noise reduction due to accumulating time delays was suppressed by increasing the initial separation between the aircraft in the end of the arrival stream. The 0.2 nm buffer was increased for the last four aircraft to 0.5 nm. The aircraft first use the additional spacing when confronted with a delay before starting to move the TCB. The result is that the aircraft still reach V_{APP} at h_{ref},
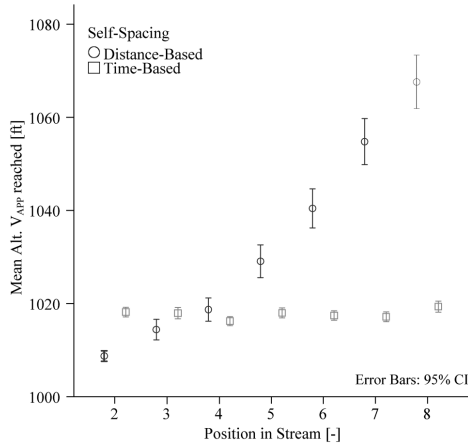
Figure 7-15: Altitude V_{APP} reached.
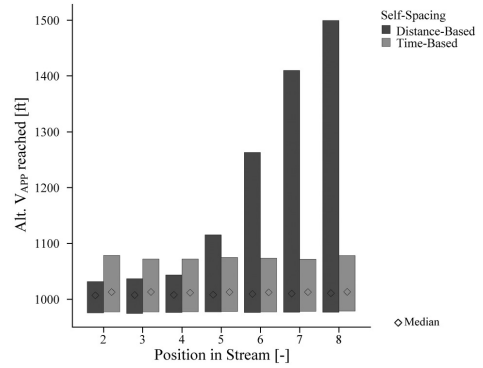
Figure 7-16: Median and 5th to 95th percentile of Altitude V_{APP} reached.

	Percentile					
	1	25	50	75	99	100
Deviation [s]	0.0	0.0	0.5	1.0	6.5	49.5

Table 7-2: Absolute Deviation from the RTA in Percentiles

see Figure 7-17. A positive correlation between $h_{V_{APP}}$ and the position can not be identified ($R = 0.040, p < 0.001$, *Pearson 2-tailed*).

7-7-2 Separation

Table 7-2 shows the deviation of the RTA for time based self-spacing. All aircraft arrived within 49.5 s from the RTA and 99% of the aircraft arrived within 6.5 s of the RTA.

The two self-spacing concepts are compared using the separation margin. The separation margin is defined as the actual minimum separation minus the minimum allowable separation; hence a positive margin yields a spacing gap and a negative margin a separation loss. Visible in the histograms in Fig. 18 are the 0.2 nm buffer applied in case of time based self-spacing and the 0.2 nm and 0.5 nm buffers for the distance based scenario. In both self-spacing environments separation violations do occur, see Table 7-3. Under distance based self-spacing there was a separation loss between 0.32% of the aircraft pairs. This percentage is comparable to go-around percentages reported by two major UK airports: London Heathrow 0.24% and London Gatwick 0.31% of the total annual arrivals.[1,2] At this stage of the research this is deemed to be an acceptable reference level. Furthermore, other
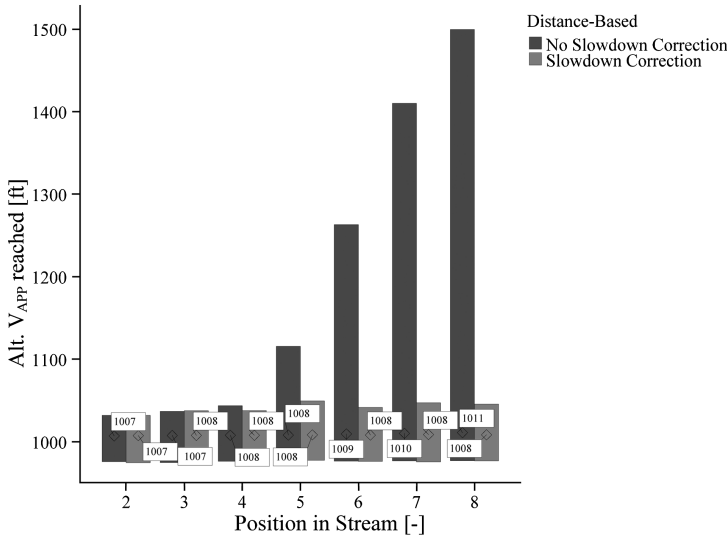
Figure 7-17: Effect of slowdown correction on median and 5th to 95th percentile of altitude V_{APP}

Self-Spacing	Mean	Median	Separation Violations
Time Based	0.47	0.22	1.42%
Distance based	0.37	0.31	0.32%
Time Based (0.5 nm buffer)	0.76	0.52	0.27%

Table 7-3: Separation Violations Compared

possible measures to bring this percentage down (e.g. the use of speed brakes) have not been evaluated because of limitations of the fast time simulator.

In case of time based self-spacing the separation violation percentage is 1.42%. To lower the violation rate for time based spacing to the level of distance based spacing, the separation buffer was extended by 0.3 nm to 0.5 nm. As a result, the separation violation percentage dropped to 0.27% and the separation margin increased, see Table 7-3.

7-7-3   Capacity

For evaluation of the runway capacity the time based scenario with the extended separation buffer is used, such that the separation violation percentage is similar. For the distance based self-spacing use is made of the arrival stream initially described in Section 7-7 with the slowdown correction. The capacity figures are based on 5,000 randomly created arrival streams per self-spacing concept. Figure 7-19 shows the histograms of the capacity expressed in aircraft per hour (AC/H) for
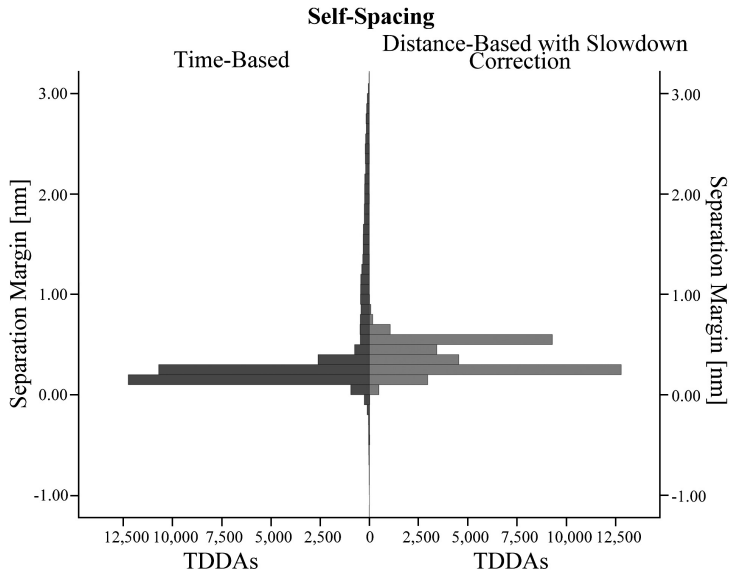
Figure 7-18: Separation margin

Self-Spacing	Mean	Median	Std.	Min	Max	Range
Time Based	35.7	35.3	3.3	26.7	49.7	23.0
Distance based	39.2	38.8	3.6	30.9	53.3	22.3

Table 7-4: Capacity descriptive statistics in AC/H

both forms of self-spacing. Independent of the self-spacing concept there is some spread in the runway capacity, because the traffic mix (on average: 40% heavy, 60% large) is determined randomly, variation in the runway capacity can be expected.

Use of distance based spacing results in a higher runway capacity than time based spacing; as expected due to the 0.5 nm separation buffer used for time based spacing. For distance based self-spacing the separation buffer was also extended to 0.5 nm, but only for the last four aircraft. Furthermore, this buffer is used to absorb delays. For the time based scenario the average runway capacity is 35.7 aircraft per hour (s = 3.3 AC/H); when using distance based spacing for eight aircraft in the arrival stream the average capacity is 39.2 aircraft per hour (s = 3.6 AC/H). More descriptive statistics are summarized in Table 4. To determine significance of the difference in runway capacity, an Analysis of Variance test (ANOVA) is used ($F = 2560.04, p < 0.001$).

A simulation tool for arrival streams executing a conventional approach is not available; this makes an exact capacity comparison impossible. The runway capacity figures are analyzed using a packing factor. The packing factor PF is defined
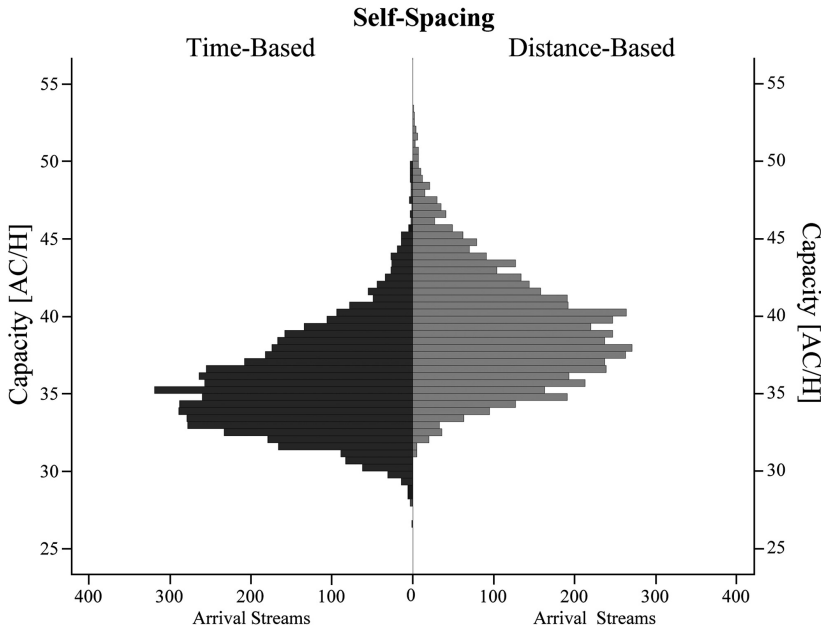
Figure 7-19: Runway capacity

as:

$$PF = \frac{\sum_{i=2}^{k} S_{allowed}}{\sum_{i=2}^{k} S_{actual}} \forall S_{actual} \geq S_{allowed} \qquad (7\text{-}3)$$

where k is the number the aircraft in the arrival stream, S_{actual} is the actual separation minimum between two aircraft, and $S_{allowed}$ the minimum safe separation. Separation violations are not included in the PF calculation. If $PF = 1$ the runway capacity equals the theoretical maximum. As expected from results discussed earlier the PF for distance based spacing is higher than for time based spacing: 0.90 and 0.81, respectively. Both self-spacing scenarios increase runway capacity significantly when compared to runway capacity figures for current CDA operations.[14, 18]

Using conventional approach procedures the PF will also be less than 1. The runway capacity observed in the distance based simulations is a least 90% of the runway capacity when using conventional approach procedures.

7-8   Sensitivity Analysis

Time based and distance based self-spacing perform comparable except for the runway capacity where the distance based scenario has a three AC/H advantage. Runway capacity is one of the major issues with CDAs in high-density traffic; in that
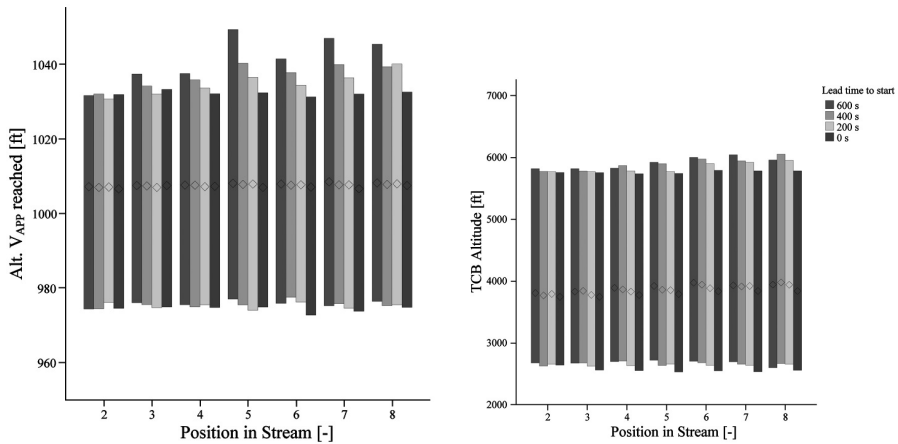
Figure 7-20: Median and 5th to 95th percentile of 7.20(a) altitude V_{APP} and 7.20(b) TCB altitude.

respect distance based self-spacing is the most promising option. Therefore a sensitivity analysis was carried out for the distance based self-spacing scenario with the slowdown correction. The goal of this study was to investigate the effects of ATM performance, top of descent altitude, predictions based on erroneous weight information, and initial speed on the TDDA performance. The main effects are described; possible interactions are the subject of ongoing research.

7-8-1   Initial Control Space Prediction

In the simulations the starting time of the TDDA for an aircraft was set 600 s before the preceding aircraft starts the TDDA to give the controller and the aircraft sufficient time to let the aircraft arrive at the computed entry time. The required time is subject of ongoing research. To assess the effect of this time period (lead time to start) on the TDDA performance, the lead time to start is reduced to 0 s in 3 equal steps of 200 s. In case the lead time to start is 0 s, the control space used to determine the starting times for the trailing aircraft are computed when the leading aircraft start the TDDA.

From Figure 7-20 it is concluded that the lead time to start affects the TDDA noise goal performance and TCB altitude, especially those of the last four aircraft in the arrival stream. The noise goal performance and TCB altitude become less dependent on the position of the aircraft in the arrival stream. The Predictions over a shorter time horizon benefit the performance of the TDDA. The number of separation violations and the runway capacity (39.1 AC/H±0.1, PF = 0.90) are not affected.

The slowdown effect is not visible when the lead time to entry is 0 s, hence the cor-
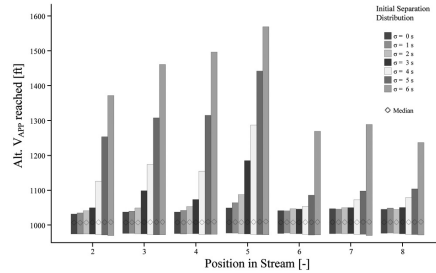
Figure 7-21: Median and 5th to 95th percentile of altitude V_{APP}

rection is no longer needed. Without the slowdown correction, the capacity would increase to 40.6 AC/H (0.34% separation violations) and only a 5 ft deterioration of the noise goal is visible. Time based spacing is still being outperformed by distance based spacing in case the shortest time period would be feasible, both in terms of capacity (-2.4 AC/H) and separation violations (+1.38%).

7-8-2   Initial Separation Distribution

In the previous sets of simulations the TDDA starting time was such that the aircraft were positioned in the middle of their control space. It is expected that in reality a distribution will be observed around the computed starting time. A new set of simulations was made in which the aircraft were initially positioned around computed starting time using a normal distribution with the standard deviations s ranging from 1 to 6 s.

Noise Goal   Figure 7-21 shows the median and 5th to 95th percentile of hV_{APP} per position for each initial separation distribution. The noise reduction deteriorates with the increase of the standard deviation s, but the impact is limited when the standard deviation is below or equal to 3 s. The 3 s standard deviation means that 95% of the aircraft are positioned within 6 s of the middle of the control space, creating a 12 s interval. This interval is equivalent to the smaller control spaces. A bigger standard deviation causes aircraft to be positioned outside the initial separation constrains, making it impossible to fly a TDDA and remain safely separated as was shown in Figure 7-8. Because of the additional initial separation applied in the end of the arrival stream, the effect is less strong there.

Separation Violations and Capacity   The separation violation percentage increases almost exponentially with the standard deviation, see Figure 7-22. No significant effect on the runway capacity could be identified ($F = 1.859, p = 0.084$).
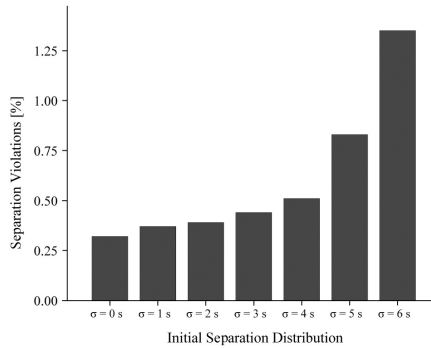
Figure 7-22: Effect of initial separation on separation violations

Starting Altitude	Separation Violations [%]
8,000 ft	0.48%
7,000 ft	0.32%
6,000 ft	0.26%

Table 7-5: Effect of starting altitude on % of arrivals with separation violation

Thrust Cutback Altitude The initial separation distribution affects the TCB altitude. This is logical because TCB altitude is related to the control space and initial separation. The mean of the TCB altitude shows a negative trend. The TCB altitude lies approximately 100 ft lower for s = 6 s when compared to s = 0 s. An ANOVA confirms the effect of the initial separation on the TCB Altitude ($F = 9.847, p < 0.001$). The effect depends on the position of the aircraft in the stream ($F = 104.548, p < 0.001$).

7-8-3 Starting Altitude

The starting altitude of the TDDA procedure sets the length of the TDDA and the maximum achievable TCB altitude. A higher altitude allows for higher TCB altitudes, see Figure 7.23(b). The median of TCB altitude increases slightly. The increase of the 95th percentile indicates that only a number of flights with a TCB altitude above the median benefit from the increased starting altitude. The median altitude where V_{APP} is reached remains constant, but the 95th percentile increases indicating that the deviations from the reference altitude become bigger. A higher starting altitude and thus a longer TDDA leads to an increase of the number separation violations, see Table 7-5.
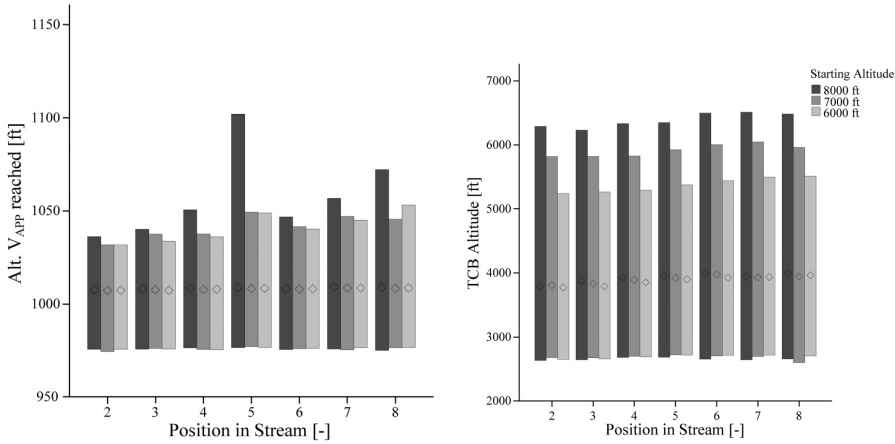
Figure 7-23: Median and 5th to 95th percentile of 7.23(a) altitude V_{APP} and 7.23(b) Median and 5th to 95th percentile of TCB altitude.

Initial Speed	Separation Violations [%]
230 kts	0.32%
220 kts	0.53%
210 kts	1.26%
200 kts	2.00%

Table 7-6: Effect of initial speed on separation violations

7-8-4   Initial Speed

Figure 7-24 shows the effect of the initial speed on the noise goal performance and the TCB altitude. A lower speed results in a lower TCB altitude but also shrinks the control space. The smaller control space limits the aircraft in their power to account for the slowdown effect. A speed of 230 kts IAS is the maximum possible speed; beyond 230 kts the acceleration along the glide path cannot be stopped for all aircraft types due to flap limits (speed brakes are not included in the simulation).

Separation Violations and Runway Capacity   No effect on the runway capacity was expected because the approach speeds were unchanged, this is confirmed by an ANOVA ($F = 0.627, p < 0.645$). The lower IAS has a negative effect on the control space of the aircraft with a negative effect on the number of separation violations, see Table 7-6.
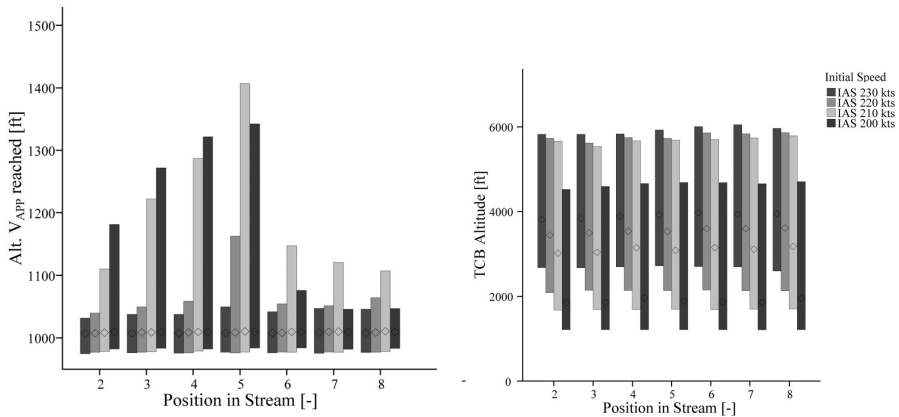
Figure 7-24: Effect of the initial speed on the median and 5th to 95th percentile of of 7.24(a) altitude V_{APP} and 7.24(b) TCB altitude.

7-8-5   Aircraft Weight

The aircraft weight is one of the factors that determines the aircraft performance. In the simulations performed thus far it was assumed that the weight of the aircraft used by the TDDA algorithms equals the actual weight of the aircraft. Because of the use of standard passenger and baggage weights, it is expected that the computed weight and the actual weight differ. To investigate the effect of differences between the computed and actual weight on the TDDA performance an error as percentage of the payload was introduced. Three simulations were set up with payload errors up to 0%, $\pm 5\%$, $\pm 10\%$. The actual percentage per aircraft in the arrival stream was selected using a uniform distribution. No significant effects on the TDDA performance could be identified.

7-9   Discussion

The aim of this research was to evaluate the performance of the TDDA in high-density traffic arrival streams in a distance- and time based self-spacing environment. Distance based self-spacing concepts may suffer from instability of arrival streams, if predictions of the leading aircraft trajectory are based on previous aircraft states. In this research prediction of the leading aircraft trajectory solely based on intent was introduced in the TDDA. No signs of the slinky effect have been found in the simulated arrival streams. In case of time based spacing the trailing aircraft trajectory is not adjusted as a reaction to changes in the leading aircraft trajectory, hence the slinky effect is by definition not possible.

Application of the TDDA in arrival streams imposes constraints on the initial separation between aircraft. The initial separation interval expressed in time or distance

follows from the control space that is a function of the aircraft type and weight, and the wind conditions.

Under distance based self-spacing there was a separation loss between 0.32% of the aircraft pairs. To lower the violation rate for time based spacing to the level of distance based spacing, the separation buffer to set the RTA was extended by 0.3 nm to 0.5 nm. For the time based scenario the average runway capacity is 35.7 AC/H, when using distance based spacing the average capacity is 39.2 AC/H. The runway capacity under distance based self-spacing is 90% of the theoretical maximum capacity. Because distance based self-spacing outperformed time based self-spacing in terms of runway capacity, distance based self-spacing is considered to be the most promising option.

To further evaluate the performance of the TDDA in a distance based self-spacing environment a sensitivity study was carried out. Reducing the time between computing the TDDA starting time and the actual starting time improves the performance of the TDDA. However, this also gives the pilot and controller less time to take actions to let the TDDA start on time. The sensitivity analysis also shows that it is crucial for the aircraft arrive to start the TDDA at the set starting time. When aircraft are positioned outside their control space, the performance degrades. The initial conditions of the TDDA affect the performance. A higher initial speed results in a larger control space, which benefits performance. A higher starting altitude results in higher TCB altitude but also increases the number separation violation. The trajectory becomes longer, which increases the uncertainties. Trajectory predictions based on erroneous aircraft weight with errors up to 10% of the payload did not have a significant effect on the performance.

7-10 Conclusion

Distance based self-spacing has a three AC/H runway capacity advantage over time based self-spacing when the number of separation violations between aircraft is comparable. Runway capacity is one of the major factors limiting the use CDAs; in that respect distance based self-spacing is the most promising option. The observed runway capacity is 90% of the theoretical maximum. A sensitivity analysis for distance based self-spacing showed that accurately determining the starting time and the ability to arrive at the starting time with great precision benefits the TDDA performance.

References

[1] BAA London Gatwick, Flight Evaluation Report 2001/02. Technical report, British Airports Authority BAA Gatwick, 2002.

[2] BAA Heathrow, Flight Evaluation Report 2007. Technical report, Heathrow Flight Evaluation Unit (FEU), 2007.

[3] T. S. Abbott. Speed Control Law for Precision Terminal Area In-Trail Self-Spacing. Technical Report NASA/TM-2002-211742, NASA Langley Research Center, Hampton (VA), USA, Jul 2002.

[4] J.-P. Clarke. *A Systems Analysis Methodology for Developing Single Event Noise Abatement Procedures*. Sc.D. Dissertation, Massachusetts Institute of Technology, 1997.

[5] R. A. Coppenbarger, R. W. Mead, and D. N. Sweet. Field Evaluation of the Tailored Arrivals Concept for Datalink-Enabled Continuous Descent Approaches. In *7th AIAA Aviation Technology, Integration and Operations Conference (ATIO)*, number AIAA-2007-7778, Belfast, Northern Ireland, Sep 18-20 2007.

[6] B. A. F. de Beer, M. Mulder, M. M. van Paassen, and A. C. in 't Veld. Development of an Ecological Interface for the Three-Degree Decelerating Approach. In *AIAA Guidance, Navigation, and Control Conference & Exhibit*, number AIAA-2008-7108, Honolulu (HI), USA, Aug 18-21 2008.

[7] W. F. de Gaay Fortman, M. M. van Paassen, M. Mulder, A. C. in 't Veld, and J.-P. Clarke. Implementing Time-Based Spacing for Decelerating Approaches. *AIAA Journal of Aircraft*, 44(1):106–118, Jan-Feb 2007.

[8] A. M. P. de Leege. *Three-Degree Decelerating Approaches in Arrival Streams*. Msc. thesis, Faculty of Aerospace Engineering, Delft University of Technology, Sep 2007.

[9] J. L. de Prins, K. F. M. Schippers, M. Mulder, M. M. van Paassen, A. C. in 't Veld, and J.-P. Clarke. Enhanced Self-Spacing Algorithm for Three-Degree Decelerating Approaches. *AIAA Journal of Guidance, Control & Dynamics*, 30(5):576–590, Mar-Apr 2007.

[10] E. Dinges. Determining the Environmental Benefit of Implementing Continuous Descent Approach Procedures. In *7th USA/Europe Air Traffic Management R&D Seminar (ATM 2007)*, Barcelona, Spain, Jul 2-5 2007.

[11] N. T. Ho and J.-P Clarke. Mitigating Operational Aircraft Noise Impact by Leveraging on Automation Capability. In *AIAA 1st Aircraft, Technology, Integration, and Operations Forum (ATIO)*, number AIAA-2001-5239, Los Angeles (CA), USA, Oct 16-18 2001.

[12] A. C. in 't Veld, M. M. van Paassen, M. Mulder, and J.-P. Clarke. Pilot Support for Separation Assurance during Decelerated Approaches. In *Proceedings of the AIAA Guidance, Navigation, and Control Conference & Exhibit*, number AIAA-2004-5102, pages 1–13, Providence (RI), USA, Aug 16-19 2004.

[13] L. Ren and J.-P. Clarke. Flight-Test Evaluation of the Tool for Analysis of Separation and Throughput. *AIAA Journal of Aircraft*, 45(1):323–332, Jan-Feb 2008.

[14] L. Ren, J.-P. Clarke, and N. T. Ho. Achieving Low Approach Noise without Sacrifying Capacity. In 22nd *Digital Avionics Systems Conference*, volume 1, pages 1–9, Indianapolis (IN), USA, Oct 12-16 2003.

[15] G. L. Slater. Dynamics of Self-Spacing in a Stream of In-Trail Aircraft. In *Proceedings of the AIAA Guidance, Navigation, and Control Conference & Exhibit*, number 2002-4927, Monterey (CA), USA, Aug 11-14 2002.

[16] M. A. Vilaplana, E. Gallo, F. A. Navarro, and S. Swierstra. Towards a Formal Language for the Common Description of Aircraft Intent. In *Digital Avionics Systems Conference*, volume 1, pages 3.C.5–3.1–9, Washington DC, USA, Oct 30-Nov 3 2005.

[17] I. Wilson and F. Hafner. Benefit Assessment of Using Continuous Descent Approaches at Atlanta. In *Digital Avionics Systems Conference*, volume 1, pages 2.B.2– 2.1–7, Washington DC, USA, Oct 30-Nov 3 2005.

[18] F. J. M. Wubben and J. J. Bussink. Environmental Benefits of Continuous Descent Approaches at Schiphol Airport Compared with Conventional Approach Procedures. Technical Report NLR-TP-2000-275, National Aerospace Laboratory (NLR), Amsterdam, The Netherlands, May 2000.

8

Conclusions and recommendations

The fundamental question that started the research presented in this thesis is whether or not it is possible to implement continuous descent approach procedures without sacrificing landing runway throughput capability.

Continuous Descent Approaches in various forms have shown to result in significant reductions in aircraft noise impact and as they require less fuel in comparison to conventional step-down approaches, the implementation of these procedures is highly desirable. As the required speed and altitude profiles during a CDA vary greatly amongst different aircraft, the task of closely spacing the aircraft is very difficult for the air traffic controller, however. This is the root cause for the capacity reductions typically found when implementing CDA procedures.

CDA is a generic term, basically covering all approach procedures that have no level flight segments. A useful distinction can be made between CDAs that require a fixes lateral path, RNAV-CDAs, and CDAs where ATC can issue vectors as long as the aircraft remain in a continuous descent, vectored CDAs. A good example of a vectored CDA is the procedure in use at London Heathrow airport. Generally, vectored CDAs do not suffer from capacity loss because the air traffic controller can still issue speed and heading commands to closely space the aircraft.

Current developments in the SESAR program emphasize the development of fixed lateral approach trajectories, and fixed trajectories in general which is why this research focuses on the RNAV CDA and its associated capacity problems. The solution investigated in this thesis is to delegate the task of in-trail spacing to the flight deck on the notion that better information on the speed and altitude profile will be more readily available on the flight deck. Furthermore, the flight crew is in a better position to actively control their trajectory behind a preceding aircraft.

Two scenarios have been investigated, one where aircraft are instructed to regulate the distance behind the preceding aircraft, and one scenario where ATC issues a

required time of arrival and aircraft are instructed to manage their approach profile to meet that time. Both scenarios relieve the controller of the control task, at the cost of increased workload for the flight crew. The results presented in Chapters 3, 4 and 6 show that not only is the workload still acceptable, but also that pilots are indeed capable of accurately achieving the self-spacing or the time-goal, given an adequate flight deck support interface.

8-1   Key factors

Using the flight deck support interfaces presented in this work, it was shown that pilots are able to robustly handle both distance based self-spacing and time based spacing. During the development of these flight deck support interfaces, a number of factors were identified that are of key importance for the accuracy of the generated solutions.

8-1-1   Procedure constraints

The CDA-procedure used throughout this work is the Three Degree Decelerating Approach, which is defined by a constant three degree descending path from the initiation point all the way to the runway, flown at idle thrust. This procedure was chosen because it represents the ultimate solution for a single aircraft in terms of noise impact. Due to the steep approach angle and the fact that the entire procedure is flown at idle thrust, the available control space is quite small and completing the procedure while controlling the spacing interval with the preceding aircraft has proven to be a difficult task.

Because of these drawbacks it is not very likely that the TDDA will ever be implemented in its current form, however, it provides a very interesting research case. If it can be shown that it is possible to preserve runway capacity with the TDDA, it follows that other CDA procedures with less stringent operational constraints should be feasible as well.

8-1-2   Aircraft drag and thrust data

At the core of the self-spacing algorithm lies the trajectory prediction algorithm. The trajectory predictions require accurate knowledge of the lift-drag polar and the engine thrust as illustrated by the flight test preparations in Chapter 4. Models currently in use by ATC such as BADA [1] do not possess the necessary accuracy to generate the required speed- and distance profiles. Current state of the art FMS installations are capable of accurate trajectory estimations, however this information is not normally available to ATC. In general aircraft manufacturers are very reluctant to share this information for economical reasons.

In order to implement the spacing concepts as proposed in this work, exchange of information is vital and a number of scenarios can be envisaged to accomplish this. On the one end, a ground based database could be used by a central computer to generate all trajectories, on the other end a situation can be envisaged where each aircraft calculates its own trajectory and down-links this to ATC or directly to nearby aircraft.

Developments in the field of System Wide Information Management (SWIM) by both SESAR and NextGen already move towards a system where 4D-trajectories can be shared by different users of the air traffic system.

8-1-3 Aircraft operating mass

Closely related to the requirement of accurate lift and drag data is the requirement of knowledge of the current operating mass of the aircraft. Availability of this information is normally not an issue on board the aircraft as the aircraft's FMS keeps track of this figure for its performance calculations. If the trajectory prediction is generated outside the aircraft, however, information on the current mass must be made available through other means.

8-1-4 Wind data

It was shown that an accurate wind estimate is necessary to assure performance. The AMDAR Wind Prediction Algorithm (AWPA) presented in Chapter 5 performs well, providing real-time accurate wind estimates as was demonstrated on a set of AMDAR data for Chicago O'Hare. The AWPA has the benefit of becoming more accurate as more data is available, i.e., in high traffic densities, where its accuracy is needed most.

8-1-5 Pilot technique

In current implementations of continuous decent approaches, such as the RNAV night transition at Amsterdam Schiphol Airport, a lot of freedom is left to the flight crew to execute the procedure in terms of altitude and speed management. This is the main reason for the capacity loss associated with this procedure. Also the early research presented in Chapter 3 showed that flight crews were able to fly the idle thrust approach without help form the cockpit interface as long as the preceeding aircraft behaved predictably, but self-spacing performance was inadequate for nonnominal behavior of the preceding aircraft. The use of a suitable pilot support system such as presented in this chapter assures consistent pilot behavior both for distance based spacing and time based spacing as was shown in Chapter 6.

8-2   Results

8-2-1   Self-spacing performance

One of the main findings during the different experiments is that pilots are able to complete the procedure and space themselves safely behind the leading aircraft when the initial spacing is within the control space of the aircraft, i.e., when the aircraft are spaced in such a way that it is physically possible to control the final spacing during the TDDA by flap and gear timing alone.

The Monte Carlo simulations of Chapter 4 show that the developed algorithm is robust against errors in the wind estimation, aircraft mass estimate and accuracy of the drag-coefficient. Errors in the estimates of the headwind component of up to ±20 kts, estimate errors of aircraft mass of $\pm10\%$ and errors in the drag-coefficient of $\pm10\%$ showed no loss of separation at all and only a degradation of the noise impact due to re-applying thrust on short final of ±100 feet maximum.

8-2-2   Pilot workload

As expected, the pilot workload does increase due to the added task of self-separation. The different piloted experiments all showed, however, that the overall workload was still considered acceptable by the pilots, a fact corroborated by the TLX-scores.

8-2-3   Landing runway capacity

When the key uncertainties mentioned in the previous sections are adequately addressed, the TDDA can be flown in a high traffic density environment. In Chapter 7 extensive Monte Carlo simulations showed that in both time based and distance based scenarios runway throughput numbers that are very close to current peak capacity numbers are achievable. Figure 8-1 shows the throughput results for Monte Carlo simulations of strings of 8 different aircraft, operating at random flight mass. An average of 35.7 aircraft per hour on a single runway was found for the time based scenario, while the distance based scenario showed 39.2 aircraft per hour on a single landing runway. Compared to the absolute maximum possible throughput for the given traffic stream, expressed as a *packing factor*, average landing runway throughput capacities of 81% and 90% were found for time based and distance based spacing, respectively.

This shows that the problems encountered when implementing Continuous Descent Approaches in high traffic densities can indeed be solved, paving the way for actual implementation.
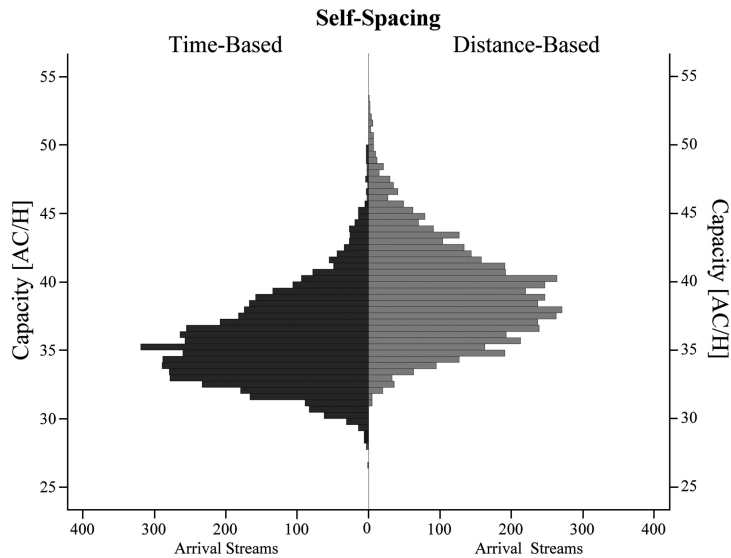
Figure 8-1: Landing runway capacity for distance based and time based separation, result of Monte Carlo simulations with strings of eight aircraft.[source: Chapter 7]

8-3   Recommendations

8-3-1   Developments in ATM research

Current developments in air traffic management in the form of the European Single European Sky ATM Research (SESAR) and the Federal Aviation Administration's NextGen program, lead to a new ATM environment where digital information exchange will be possible between aircraft and controllers, air traffic clearances will be issued as four-dimensional business trajectories.

Air traffic management is foreseen to shift from tactical short term control, to a more strategic scenario, where trajectories are negotiated and deconflicted long before the aircraft get their route clearance. This way there should be less potential conflicts when the aircraft are airborne, allowing for a sustained growth in air traffic.

8-3-2   Pilot support interface

The pilot-support interface as developed and used during the various experiments was never the main goal of the research and as such it was designed in a quick and ready fashion, without too much concern for ergonomics or ecology. As a result the display of flap and gear cues work in the way a flight director does, they prompt action when needed, without relaying much information about the

urgency of required actions or the size of the control space. The ghost symbol in combination with TCAS-symbology does provide some overview over the situation, and the experimental results show that situation awareness is enhanced by it, but a more thorough theoretical basis should be explored.

Further research is required to optimize the cockpit interface. Currently, interesting work is being done on energy-based displays. Controlling an aircraft approaching to land can be seen as an energy management problem, starting high and fast in a clean configuration and finishing low and slow and configured for landing. There are different strategies to dissipate the excess energy, but the begin and required end states are constant, which seems very suitable for an interface that conveys he aircraft's energy state and energy goals.

Within the scheme of SESAR and NextGen, new tasks and more complex trajectories will be possible. Research evaluating the impact of these developments on the flight deck and designing new interfaces to make full use of the new possibilities will be necessary.

8-3-3   Air traffic controller support

The air traffic controller workstation has been completely neglected in the work presented. If the controller is to remain responsible for aircraft flying complex, decelerating profiles, some assistance needs to be offered. In fact, the runway throughput numbers found during the Monte Carlo simulations presented in Chapter 7 could only be obtained by assuring that the initial spacing of the arrival stream was within the control space of each aircraft.

In future scenarios, the interaction between controllers and pilots will probably change dramatically with less use of voice communications and an emphasis of data-link clearance delivery and aircraft down-linking their own predicted trajectories. To cope in such a different environment, new support systems need to be developed in order to maintain the level of safety we enjoy today.

Already work is being done to develop new controller displays to assist in the de-conflicting and spacing of continuous descent approaches.[2,5,6] A good example is the development of the Time-Space Diagram (TSD) , a display that can be used to merge and correctly space different arrival streams of aircraft performing a CDA. The TSD can be used to space *any* type of CDA, as long as the estimated trajectories are known.[4] Another example is the development of the Speed and Route Advisor-tool (SARA) by Luchtverkeersleiding Nederland (LVNL), the Dutch air traffic control organization . The SARA-tool allows controllers to sequence aircraft inbound to Amsterdam Schiphol Airport in such a way that they meet an RTA over the initial approach fix and can follow a fixed RNAV trajectory to the landing runway.

8-3-4 Procedure design

This thesis focused on the Three-Degree Decelerating Approach as an extreme example of continuous descent approach, being flown completely at flight idle. As a research case this makes sense, as the speed profiles vary significantly between aircraft types. However, fixing the entire procedure at a three degree flight path makes for a difficult procedure to fly, because most aircraft are not able to decelerate in a clean configuration when flying such a steep flight path angle.

Further research should focus on designing more convenient procedures while leveraging on the results found for the TDDA. A number of research efforts can already be seen in this area, such as the continuous descent trials in Louisville Aiport executed by United Parcel Service's fleet of Boeings 767.[3] Also within the scheme of the NextGen program, Continuous Descent Operations are being implemented at Los Angeles International Airport.

References

[1] User Manual for the Base of Aircraft Data (BADA) Revision 3.7. Technical Report No. 2009-003, Eurocontrol EEC, 2009.

[2] S. M. B Abdul Rahman, M. Mulder, and M. M. van Paassen. The Effects of Air Traffic Control Sector Design on the Solution Space Diagram. In *Proceedings of the European Association of Cognitive Ergonomics (ECCE) Conference*, pages 261–268, Delft, Aug 25-27 2010.

[3] J.-P Clarke, N. T. Ho, L. Ren, J. A. Brown, K. R. Elmer, K. Tong, and J. K. Wat. Continuous Descent Approach: Design and Flight Test for Louisville International Airport. *AIAA Journal of Aircraft*, 41(5):1054–1066, 2004.

[4] A. M. P. de Leege, A. C. in 't Veld, M. M. van Paassen, and M. Mulder. A Time-Space Diagram as Controller Support Tool for Advanced Continuous Descent Approach Operations. In *Proceedings of the International Air Transport and Operations Symposium (ATOS 2010)*, Delft, The Netherlands, Apr 14-15 2010.

[5] J. G. d'Engelbronner, M. Mulder, M. M. van Paassen, S. de Stigter, and H. Huisman. The Use of a Dynamic Solution Space to Predict Air Traffic Controller Workload. In *Proceedings of the International Air Transport and Operations Symposium (ATOS)*, Delft, The Netherlands, Apr 14-15 2010.

[6] G. A. Mercado Velasco, M. Mulder, and M. M. van Paassen. Analysis of Air Traffic Controller Workload Reduction Based on the Solution Space for the Merging Task. In *Proceedings of the AIAA Guidance, Navigation, and Control Conference*, number AIAA-2010-7541, Toronto, Canada, Aug 2-5 2010.

Samenvatting

Algoritmes voor het Regelen van de Onderlinge Afstand tijdens Geluidsarme Naderingsprocedures

Alexander in 't Veld

Bij de ontwikkelingen op het gebied van beperking van geluidsoverlast door vliegtuigen is de aandacht verschoven van zuiver technische maatregelen, zoals het ontwikkelen van stillere motoren, naar meer operationele maatregelen. Deze kunnen van politieke aard zijn, zoals het verminderen van het aantal nachtvluchten, of het instellen van een maximum jaarlijks aantal vliegbewegingen per vliegveld, maar ook procedurele maatregelen zijn mogelijk in de vorm van geluidsbeperkende vertrek- en naderingsprocedures. Als gevolg van deze verschuiving is ook de focus van het luchtvaartonderzoek verschoven naar het ontwerpen van vliegprocedures die minder geluidsimpact hebben op de omgeving. Daarbij is ook het milieu-aspect in de vorm van het verminderen van de uitstoot van uitlaatgassen en het verlagen van het brandstofverbruik een steeds grotere rol gaan spelen.

Onderzoek naar het beperken van geluidsoverlast heeft zich van nature gericht op de naderings- en vertrekprocedures van luchthavens, aangezien geluid pas overlast wordt wanneer deze als negatief wordt ervaren door mensen op de grond, oftewel tijdens die fasen van de vlucht die op lage hoogte of op de grond

plaatsvinden. Internationaal onderzoek naar het verminderen van geluidsoverlast tijdens de start van vliegtuigen heeft geresulteerd in een beperkt aantal effectieve vertrekprocedures. Deze procedures zijn overgenomen door de International Civil Aviation Organization (ICAO) en inmiddels wereldwijd op verschillende luchthavens ingevoerd. Het ontwerpen van standaard naderingsprocedures die de geluidsoverlast beperken is echter veel lastiger gebleken. De implementatie van geluidsarme naderingsprocedures blijkt over het algemeen te resulteren in een onacceptabele afname van het aantal vliegtuigen dat per uur op een landingsbaan kan worden verwerkt, waardoor de meeste procedures ongeschikt blijken te zijn voor toepassing op vliegvelden met een groot verkeersaanbod.

Dit proefschrift beperkt zich derhalve tot naderingsprocedures. Bij het ontwerpen van een optimaal naderingsprofiel gaat het om het verminderen van de hoeveelheid geluid van een bron die de ontvanger bereikt. Er zijn in de basis twee manieren om die geluidsimpact te reduceren:

- het beperken van het brongeluid, en

- het vergroten van de afstand tussen de bron en de ontvanger.

Vanuit een procedureel oogpunt kan het brongeluid beperkt worden door een lager motorvermogen te selecteren maar ook door het uitklappen van het landingsgestel en de liftverhogende vleugelkleppen uit te stellen, aangezien de verstoorde luchtstroom die deze veroorzaken het geluidsniveau aanzienlijk verhoogt. Het vergroten van de afstand tussen de bron en de ontvanger wordt doorgaans bereikt door de aanvliegroutes zo te kiezen dat steden en woonkernen vermeden worden, maar ook door een continue daalvlucht uit te voeren waardoor de gemiddelde hoogte tijdens de nadering toeneemt. Uit verschillende onderzoeken blijkt dat een Continuous Descent Approach (CDA), een procedure die in het geheel geen horizontale segmenten kent, de beste geluidsreductie bewerkstelligt.

Het merendeel van het werk in dit proefschrift bevat onderzoek naar een bijzondere implementatie van de Continuous Descent Approach, de zogenaamde Three-Degree Decelerating Approach (TDDA). Deze procedure wordt gevlogen met minimaal motorvermogen, langs een relatief steil glijpad van drie graden naar de landingsbaan. Dit resulteert in een nadering waarbij het vliegtuig continu vertraagt, met als doel om zonder gas bij te geven pas op het normale stabilisatiepunt vlak voor de landingsbaan volledig geconfigureerd te zijn voor de landing. Hierbij wordt de vliegsnelheid uitsluitend geregeld door het op het juiste moment selecteren van de opvolgende flap-standen en het op het juiste moment neerlaten van het landingsgestel.

Het probleem met deze en vergelijkbare procedures waar met minimaal motorvermogen gevlogen wordt, is dat verschillende vliegtuigtypen door het verschil

in aerodynamische eigenschappen ook verschillende snelheidsprofielen hebben. Tevens worden deze profielen beïnvloed door de verschillen in vliegtuigmassa en de besturingsstrategie van de bemanning. Bij elkaar opgeteld zorgen deze factoren ervoor dat het voor de luchtverkeersleider zeer lastig wordt de verschillende vliegtuigen op een veilige manier kort achter elkaar op te lijnen voor de baan, met als gevolg dat zij noodgedwongen meer afstand tussen opeenvolgende vliegtuigen moeten aanhouden. Het aantal vliegtuigen dat per uur op een gegeven landingsbaan kan landen wordt hierdoor sterk gereduceerd.

Doordat de snelheid van de vliegtuigen tijdens deze procedure continu afneemt, wordt de verkeersleider geconfronteerd met een rij vliegtuigen die allemaal langzaam inlopen op hun voorganger, waarbij het de taak van de verkeersleider is te beoordelen of de uiteindelijke separatie tussen de vliegtuigen volgens de veiligheidseisen voldoende zal zijn. Dit staat in scherp contrast met de huidige manier van werken waarbij de vliegtuigen koers-, hoogte- en snelheidsinstructies ontvangen van de verkeersleider. Dit resulteert in minder optimale naderingen vanuit geluids- en emissieoogpunt, maar levert wel een situatie op waarin op een efficiënte en veilige wijze grote verkeersvolumes afgehandeld kunnen worden.

Om dit probleem op te lossen liggen twee strategiën voor de hand, namelijk 1) een systeem ontwikkelen om de verkeersleider te ondersteunen bij het oplijnen van decelererende vliegtuigen, en/of 2) een systeem ontwikkelen waarmee de cockpitbemanning zelf de afstand achter hun directe voorganger kan regelen.

Het onderzoek gepresenteerd in dit proefschrift richt zich op de tweede strategie door het probleem om dicht achter elkaar Continuous Descent Approaches te vliegen te benaderen vanuit de cockpit. Het ligt overigens voor de hand dat een daadwerkelijke implementatie van een dergelijke naderingsprocedure aanpassingen aan zowel de cockpit als de werkplek van de verkeersleider met zich mee zal brengen.

In dit proefschrift is algemeen aangenomen dat er een vorm van dataverbinding beschikbaar is die het mogelijk maakt gegevens uit te wisselen zowel tussen de vliegtuigen en de luchtverkeersleiding als tussen vliegtuigen onderling. Dit is volledig in lijn met de visie van SESAR, die voorziet in de introductie van *System Wide Information Management* (SWIM) als onderdeel van het toekomstige luchtverkeersleidingssysteem. De exacte implementatie doet voor dit onderzoek niet ter zake, maar er is van uitgegaan dat de vliegtuigen zijn voorzien van Automatic Dependent Surveillance - Broadcast (ADS-B). Twee mogelijke scenario's zijn onderzocht: de eerste is een vorm van *self-spacing* waarbij de vliegtuigen hun deceleratie dusdanig moeten regelen dat ze zelf zorg dragen voor het handhaven van een veilige afstand achter hun voorganger. Bij de tweede methode draagt de luchtverkeersleiding de vliegtuigbemanning een zogenaamde *Required Time of Arrival (RTA)* op, oftewel een tijdstip waarop het vliegtuig boven de baandrempel moet zijn. Hierbij is de bemanning zelf verantwoordelijk voor het exact behalen van de RTA. In beide scenario's verschuift de verantwoordelijkheid voor het bereiken van de juiste

separatie naar de vliegtuigbemanning onder de hypothese dat aan boord van het vliegtuig de beste informatie en controle over de door het vliegtuig gevolgde baan beschikbaar is.

Voor distance-based self-spacing is het noodzakelijk dat naast het eigen vliegpad ook het vliegpad van het te volgen vliegtuig nauwkeurig geschat kan worden. Om een voldoende nauwkeurige schatting te kunnen maken blijkt gedetailleerde kennis van de vliegtuigpolaire in alle verschillende vliegtuigconfiguraties noodzakelijk, alsook een goede schatting van de momentane massa van het vliegtuig. Het is voorstelbaar dat deze informatie over het eigen vliegtuig aanwezig is, maar deze informatie up-to-date beschikbaar hebben van alle andere vliegtuigen lijkt lastiger te bewerkstelligen. In dit proefschrift zijn goede resultaten behaald door het extrapoleren van gemeten positie-, hoogte- en snelheidsdata, welke geacht worden beschikbaar te zijn via ADS-B. Hiervoor zijn wel gegevens nodig over de *final approach speed* van de voorganger en de hoogte waarop deze bereikt zal worden. Gemakshalve is aangenomen dat deze informatie deel uitmaakt van de 'intent information'-data die via ADS-B wordt uitgezonden.

Gebruikmakend van de schattingen van het eigen traject en dat van de voorganger is een algoritme ontwikkeld dat continu het juiste moment om het vermogen te reduceren, de momenten van flap-selectie en het juiste moment om het landingsgestel te selecteren uitrekent. Dit algoritme optimaliseert het flap-schema zodanig, dat het vliegtuig de gehele TDDA kan uitvoeren en gelijktijdig een veilige afstand achter de voorganger handhaaft. Monte Carlo simulaties hebben aangetoond dat dit algoritme robuust is tegen fouten in de schatting van de windsnelheid, de massa van het vliegtuig en de vliegtuigpolaire. Onnauwkeurigheden in de windsnelheid tot ± 20 kts, de vliegtuigmassa tot $\pm 10\%$ en fouten in de grootte van de weerstandscoëfficiënt tot $\pm 10\%$ leverden geen separatieverlies op en zorgden slechts voor een kleine verslechtering van de geluidsimpact doordat de vliegtuigen eerder moesten vertragen en daardoor ± 0.3 NM verder voor de baan al het vermogen moesten verhogen om de final approach speed vast te houden.

Vervolgens is er een cockpit interface ontwikkeld die dit algoritme gebruikt om een aantal cues aan te sturen op het primary flight display en het navigation display in de cockpit. Deze cues geven aan de vlieger het beste moment aan om naar de volgende vliegtuigconfiguratie te gaan en laten zien hoe de huidige onderlinge afstand en de uiteindelijke separatie zich ontwikkelen.

Deze interface is getest in de SIMONA onderzoekssimulator en tijdens testvluchten met het Citation II laboratoriumvliegtuig van de TU Delft en het NLR om de bruikbaarheid van het display en de haalbaarheid van het self-spacing concept te onderzoeken. Uit de resultaten blijkt dat de vliegers in staat zijn om zelf de TDDA te vliegen, zonder gebruik te maken van de cues, zolang de voorganger zich aan het nominale profiel houdt en de initiële onderlinge afstand klopt. Zodra aan deze voorwaarden niet werd voldaan, bleek het zelf regelen van de onderlinge afstand

en het gelijktijdig vliegen van de TDDA een te moeilijke taak. In deze gevallen verbeterde het gebruik van de aangepaste displays het resultaat aanzienlijk, terwijl de werkdruk van de vliegers omlaag ging. Hiermee is de haalbaarheid van het concept van distance-based self-spacing aangetoond.

Het alternatief voor distance-based self-spacing, het zogenaamde *time-based self-spacing*, heeft het grote voordeel dat geen enkele informatie van het voorgaande vliegtuig noodzakelijk is. Een veilige separatie wordt gewaarborgd doordat alle vliegtuigen zich houden aan een required time of arrival (RTA) die door de luchtverkeersleiding wordt toegekend. Het algoritme is aangepast zodat deze het flap-schema optimaliseert voor het gelijktijdig vliegen van de TDDA en het bereiken van de landingsbaan op de opgedragen RTA. De resultaten van experimenten met vliegers in de simulator waren vergelijkbaar die van de distance-based proeven. De prestaties waren beter als de aangepaste displays gebruikt werden, met name in die situaties waarin grote fouten in de windschatting werden geïntroduceerd, of wanneer de RTA zo gekozen was dat deze zeer moeilijk haalbaar was. In alle gevallen liet het gebruik van de interface in vergelijking met tests zonder de aangepaste displays een significante afname van de werkdruk van de piloten zien.

Nu is vastgesteld dat zowel de distance-based als de time-based scenario's een werkbare oplossing opleveren, is er een experiment opgezet om beide methodes te vergelijken, met als voornaamste doel de effecten op verkeerscapaciteit te onderzoeken. Tot dat moment was alleen nog gekeken naar combinaties van twee vliegtuigen en waren er nog geen gegevens beschikbaar over de stabiliteitseffecten van langere reeksen vliegtuigen. Voor dit vergelijkend onderzoek werden Monte Carlo simulaties uitgevoerd met willekeurige reeksen van vijf verschillende vliegtuigtypen, met massa's variërend tussen de *maximum take-off mass* en de *dry operating mass*. Uit deze vliegtuigtypen werden willekeurige reeksen van acht vliegtuigen opgebouwd die allen een TDDA uitvoeren, de helft van de reeksen volgens het distance-based en de andere helft volgens het time-based principe. Verder werd het gedrag van de vliegers gevarieerd, evenals de gebruikte wind-profielen en de initiële onderlinge afstand tussen de vliegtuigen.

Wanneer distance-based self-spacing wordt gebruikt, reageert ieder vliegtuig op het gedrag van zijn voorganger, wat kan leiden tot een instabiele reeks. Gedurende de Monte Carlo simulaties werden deze effecten echter niet gevonden. Time-based self-spacing heeft het voordeel dat deze effecten niet kunnen optreden omdat de interactie tusssen de vliegtuigen ontbreekt. In termen van landingscapaciteit was het met beide methoden mogelijk circa 39 vliegtuigen per uur op een landingsbaan te laten landen, oftewel circa 90% van de theoretisch maximale capaciteit van dezelfde combinatie van vliegtuigen. Distance-based self-spacing leverde iets betere resultaten op, doordat een onverhoopte toename in de onderlinge afstand tussen twee vliegtuigen door het algoritme wordt geabsorbeerd, aangezien het al-

goritme naar de minimale separatie probeert te regelen. Bij de time-based methode wordt een dergelijk verlies aan capaciteit niet weggeregeld aangezien de RTA's niet werden aangepast tijdens een run. Dat de RTA's niet worden bijgewerkt tijdens de vlucht heeft tevens als effect dat er geen actie wordt ondernomen door de vliegers wanneer de voorganger onverhoopt te vroeg afremt en een veilige separatie in gevaar komt. In dit geval zal de luchtverkeersleider of een *Airborne Separation Assurance System* moeten ingrijpen, terwijl in een distance-based scenario deze situatie duidelijk wordt weergegeven op het display en er direct door het algoritme op wordt gereageerd door het flap-schema aan te passen.

Concluderend kan worden vastgesteld dat beide methoden een werkbare strategie bieden voor het capaciteitsprobleem bij Continuous Descent Approaches. Het toepassen van self-spacing ontheft de verkeersleider van zijn taak om de onderlinge afstand te regelen, zodat de werklast van de verkeersleider zou kunnen afnemen, terwijl de huidige capaciteit gehandhaafd kan blijven. Voor beide scenario's is het echter nog wel noodzakelijk dat de reeks vliegtuigen van tevoren op de juiste manier wordt opgelijnd door de luchtverkeersleider. Voor distance-based self-spacing geldt dat de benodigde initiële afstand tussen twee opeenvolgende vliegtuigen afhangt van de beide typen en hun massa op dat moment. Hetzelfde geldt voor het vaststellen van de RTA's voor elk vliegtuig. Op dit moment wordt dan ook op uitgebreide schaal onderzoek gedaan hoe de verkeersleider ondersteund kan worden bij het vaststellen van de benodigde separatie en de Required Time of Arrival, maar zal verder niet in dit proefschrift worden behandeld. De resultaten geven aan dat het mogelijk is vergelijkbare aantallen vliegtuigen per landingsbaan af te handelen met wat in de huidige operatie het geval is, zonder instabiliteitseffecten in de stroom naderende vliegtuigen.

Het is duidelijk dat het volgende probleem dat moet worden opgelost het correct oplijnen van de vliegtuigen is, voordat zij aan de eindnadering beginnen, waarbij elke combinatie van vliegtuigen een andere optimale initiële afstand heeft. Hoewel het niet erg waarschijnlijk is dat de TDDA in de vorm zoals gepresenteerd in dit onderzoek geïmplementeerd zal worden, zijn de gevonden resultaten zeker bruikbaar voor de verdere ontwikkeling van *advanced arrival procedures* binnen de kaders van de SESAR en NextGen programma's.

Curriculum vitae

Alexander Christiaan in 't Veld was born on a sunny morning on March 2, 1976 in Rotterdam. At a very young age he was exposed to aviation as he was frequently taken on family trips with a Cessna 172 by his father who was a flight instructor. Shortly after finishing his high-school education at the Erasmiaans Gymnasium in Rotterdam he got his private pilot license.

In 1994 he enrolled in the Aerospace Engineering program at the Delft University of Technology, where he joined the Control & Simulation group in 2000. By that time he had already acquired his commercial pilot license which later proved beneficial during his research as it allowed him to combine academic knowledge with real world aviation experience. It will come as no surprise that for his M.Sc. thesis project he researched the very practical problem of performing noise abatement approach procedures. A project that came into existence as the result of a successful internship in Cambridge, Massachusetts, where he worked on this issue at the Massachusetts Institute of Technology.

After finishing his M.Sc. thesis in 2003 he was offered a job at the Control & Simulation group as a research test pilot and researcher. Part of the job offer included the opportunity to continue the work of the M.Sc. thesis project and let it mature into a Ph.D. project, the result of which lies before you.

Around the same time that Xander graduated, one of the few girls who choose to pursue an aerospace engineering degree also graduated, also with the Control & Simulation group. Merlijne and Xander got married in October 2010.

Currently Xander holds the position of chief research test pilot at the faculty of Aerospace Engineering and he continues to work on the research of trajectory based air traffic management.

Acknowledgments

As anyone who has ever tried to pursue a Ph.D. will tell you, it can be a seemingly endless period of seclusion. Family and friends are kept at arms length, as all attention is focused on the research project. My situation was somewhat non-typical, as I did not get a four year grant to work on a specific project, rather I was offered the possibility to pursue a Ph.D. as part of my full time job as a research test pilot/researcher. This basically meant doing all the Ph.D. stuff outside office hours. On the one hand this construction had the benefit of not having a solid deadline after four years, so I was allowed more time to finish the work. On the other hand not having this deadline held the risk of day-to-day tasks and projects diverting my attention away from the research.

I would like to thank Max Mulder and René van Paassen for their support and motivation. On numerous occasions Max had to remind me that what seem to be the most urgent matters are seldom the most important matters, and more than once he was able to get my nose pointed in the right direction again. René always amazed me with his ability to instantly come up with a solution to the problem you have been pondering over for a week. Without his insights none of my algorithms would ever made it to any of the simulators, or the airplane for that matter.

Furthermore I thank Bob Mulder for offering me the opportunity to start working on my Ph.D. and introducing me to the wonderful combination of academic research and the operational world of research flying.

This whole line of research would probably never have started at the Control & Simulation group if it were not for John-Paul Clarke, J-P to his friends, who in 2002 took me under his wing during my internship at the Massachusetts Institute of Technology. At that time J-P was researching the Three-Degree Decelerating Approach that forms the basis for this thesis. His enthusiasm and endless energy (does he ever sleep?) made it possible for me to extend the internship project from three

to seven months, and thereafter to continue the research as a thesis project in Delft, which has resulted in a number of joint publications.

Much of the research presented in this thesis was accomplished in close collaboration with graduate students. The simulator-experiments directly leading to the test flights at Soesterberg would not have been possible without the hard work and dedication of Johan de Prins and Kristof Schippers. Rob Groenouwe and Rick de Gaay-Fortman contributed greatly to the development of the wind prediction algorithm. Thanks to hard work of Arjen de Leege, who ran the Monte Carlo simulations that provide the first runway throughput estimates, we have been able to make the first real comparisons between the new procedures and current day operation.

The largest sacrifices are often made by people not directly in the spotlight, and I cannot appreciate enough, the love and support I received from Merlijne. She is the love of my life, and the fact that even though I was already working on my Ph.D. before we even met and that she was still willing to marry me before it was finished six years later, is testimony to her unconditional dedication. With her cheerful presence and solid determination she was always able to show me a way out when I was stuck, and convince me to continue writing when I was facing one of the many writer's blocks that seem to be an inevitable part of the process. This thesis would never have been completed without her.